Title
PRODUCTION AND DECAY OF CASCADE HYPERONS

Authors
Dauber, Philip M.
Berge, J. Peter.
Hubbard, J. Richard
et al.

Publication Date
1968-11-01

UCRL-18388

cy. 2

PRODUCTION AND DECAY OF CASCADE HYPERONS

Philip M. Dauber, J. Peter Berge,
J. Richard Hubbard, Deane W. Merrill,
and Richard A. Muller

November 1968

E

LAWRENCE RADIATION LABORATORY
UNIVERSITY of CALIFORNIA BERKELEY

UCRL-18388

cy. 2

DISCLAIMER

RECALL NOTICE

PLEASE RETURN THE PUBLICATION LISTED BELOW.
It should be returned to the Library as soon as possible, since another reader is waiting for it.

AUTHOR: DAUBER et al.

TITLE: PRODUCTION & DECAY OF CASCADE HYPERONS . . .

CALL NO.: UCRL-18388 c.2

Thank you.
Lawrence Berkeley Laboratory
Library
Bldg. 50, Room 134, Berkeley

Date:

RL-3188 (Rev. 9/71)

HAUPTMAN
508-2266

Submitted to Physical Review

UCRL-18388
Preprint

UNIVERSITY OF CALIFORNIA

Lawrence Radiation Laboratory
Berkeley, California

AEC Contract No. W-7405-eng-48

PRODUCTION AND DECAY OF CASCADE HYPERONS

Philip M. Dauber, J. Peter Berge, J. Richard Hubbard,
Deane W. Merrill, and Richard A. Muller

November 1968

Contents

PRODUCTION AND DECAY OF CASCADE HYPERONS*

Philip M. Dauber, J. Peter Berge,† J. Richard Hubbard,‡
Deane W. Merrill,‡ and Richard A. Muller**

Lawrence Radiation Laboratory
University of California
Berkeley, California

November 1968

ABSTRACT

The production of cascade hyperons by K^- incident on hydrogen has been studied at beam momenta of 1.7, 2.1, and 2.4 to 2.7 GeV/c. A sample of 3028 Ξ^- and 934 Ξ^0 was obtained. Cross sections and polarization for $\Xi^- K^+$ and $\Xi^0 K^0$ production are presented. The data are compatible with dominance by I = 0 baryon exchange in $\Xi^- K^+$ production, but also provide strong evidence for resonance formation in the s-channel compatible with $Y_0^*(2100)$. Copious production of $\Xi^*(1530)$ and $K^*(890)$ is observed in the three- and four-body final states. A broad $\Xi\pi$ enhancement is observed in the $\Xi^- K^+ \pi^0$ and $\Xi^0 K^+ \pi^-$ final states at a mass near 1894 MeV/c^2 and with a width about 98 MeV/c^2. This enhancement is identified with the $\Xi^*(1930)$ first observed by Badier et al. Lifetime measurements give $\tau_{\Xi^-} = (1.61 \pm 0.04) \times 10^{-10}$ sec and $\tau_{\Xi^0} = (3.07 \,^{+.22}_{-.20}) \times 10^{-10}$ sec. A decay parameter analysis assuming spin 1/2 yields $\alpha_{\Xi^-} = -0.391 \pm 0.045$, $\alpha_{\Xi^0} = -0.43 \pm 0.09$, $\Phi_{\Xi^-} \equiv \tan^{-1}(\beta/\gamma)_{\Xi^-} = -14 \pm 11$ deg, $\Phi_{\Xi^0} = 38 \pm 19$ deg if $\alpha_\Lambda = 0.647$ is used. These results are in agreement with T invariance and the $|\Delta I| = 1/2$ rule. A compilation of LRL results for

Ξ^- and Ξ^0 yields $\alpha_{\Xi} = -0.380 \pm 0.034$ and $\Phi_{\Xi} = -1 \pm 7$ deg, implying $\Delta = \tan^{-1}(-\beta/\alpha)_{\Xi} = 178 \pm 16$ deg. Hence the final-state $\Lambda\pi$ phase difference $(\delta_s - \delta_p) = -2 \pm 16$ deg if T is strictly conserved in the decay. Two examples of $\Xi^- \rightarrow \Lambda e^- \bar{\nu}$ were observed. Upper limits $\approx 1 \times 10^{-3}$ have been set for the branching fractions of other $|\Delta S| = 1$ and $|\Delta S| = 2$ leptonic and nonleptonic decays of Ξ^- and Ξ^0.

I. INTRODUCTION

Production and decay properties of Ξ^- and Ξ^0 hyperons have been studied in an exposure of the 72-inch hydrogen bubble chamber of the Lawrence Radiation Laboratory to a separated K^- beam.[1] The data were taken at incident K^- momentum settings of 1.70, 2.10, 2.47, 2.59, 2.64, and 2.73 GeV/c. Preliminary results have been reported previously.[2-5]

Total and differential cross sections and Ξ polarization data have been obtained for the $K^-p \to \Xi K$ reaction. The data have been qualitatively analyzed in terms of a baryon exchange model. Strong evidence exists for s-channel resonance formation near 2100 MeV, with subsequent decay into ΞK. Additional s-channel structure is also indicated by the data.

An analysis of resonance production in the $K^-p \to \Xi K\pi$ reactions is presented. The familiar $\Xi^*(1530)$ and $K^*(890)$ dominate the production at our energies. Both the Ξ^{*-} and Ξ^{*0} production angular distributions above 2 GeV/c have backward (baryon exchange) peaks with pronounced dips in the extreme backward direction. A forward peak of comparable size is present in the Ξ^{*-}. The production and decay distributions are discussed in terms of baryon exchange and possible s-channel effects. A $\Xi\pi$ enhancement identified with $\Xi^*(1930)$ is observed in $K^-p \to \Xi^- K^+ \pi^0$ and $\Xi^0 K^+ \pi^-$.

The $\Xi K\pi\pi$ reactions have been analyzed and are also dominated by production of $\Xi^*(1530)$ and $K^*(890)$. There is some indication of a $\Xi^*(1815) \to \Xi^*\pi$ contribution in these data.

The Ξ^- lifetime and decay asymmetry parameters have been determined in several prior experiments[6-13] by use of a total of 2600 events. The experiment presented here, with 2800 Ξ^- events, has yielded a life-

time somewhat smaller than the earlier measurements and decay parameters in good agreement with previous results except for those of the UCLA experiment. A new technique was employed in the decay-parameter analysis to make use of the smooth variation of Ξ polarization with production angle.

Previous results on Ξ^0 decays were based on ≈200 events. We have analyzed nearly 1000 Ξ^0 events, of which 340 were used for the lifetime measurement and 739 for the decay parameter measurement. Results for Ξ^- and Ξ^0 are compared as a check of the $|\Delta I| = 1/2$ rule for weak decays.

A search for unusual Ξ decay modes has yielded two examples of $\Xi^- \rightarrow \Lambda e^- \bar{\nu}$. Upper limits have been set for other $|\Delta S| = 1$ and 2 leptonic and nonleptonic decays of Ξ^- and Ξ^0.

II. EXPERIMENTAL PROCEDURE

A. Selection of Events

The events were produced in the reactions

$$K^- p \rightarrow \Xi^- K^+, \tag{2.1}$$

$$\Xi^0 K^0, \tag{2.2}$$

$$\Xi^- K^+ \pi^0, \tag{2.3}$$

$$\Xi^- K^0 \pi^+, \tag{2.4}$$

$$\Xi^0 K^+ \pi^-, \tag{2.5}$$

$$\Xi^- K^+ \pi^+ \pi^-, \tag{2.6}$$

$$\Xi^- K^0 \pi^+ \pi^0, \tag{2.7}$$

$$\Xi^0 K^0 \pi^+ \pi^-. \tag{2.8}$$

Two-thirds of the film was double scanned for the relevant topologies; the remaining third was scanned only once. Scanning efficiencies were 85 to 97% on each scan for fitted events within our cutoffs; the loss of useful events due to incompletion of the second scan is estimated to be about 2%. The event measurements were kinematically analyzed by using the LRL PACKAGE program. The event selection for the normal decay sequence is described below; selection criteria for unusual decay modes are discussed in Sec. VII.

Selection of Ξ^- events was entirely straightforward. All candidates for Ξ^- were required to have a visible Ξ^- decay kink and a visible Λ^0 decay, except that events with visible K^0 only were also accepted for reaction (2.4). Separate fits with satisfactory χ^2 were required for the decay sequence

$$\Lambda^0 \rightarrow p\pi^-, \tag{2.9a}$$

$$\Xi^- \rightarrow \Lambda^0\pi^-, \tag{2.9b}$$

as well as a fit to one of the Ξ^- production hypotheses listed above. The χ^2 cutoffs were chosen to correspond to a confidence level of approximately 0.5%. Events with K^0 decays too short for the gap between the production and decay vertices to be seen were recovered by fitting four-prong events with visible Ξ^- and Λ. Visible K^0 decay was required for the $\Xi^-K^0\pi^+\pi^0$ events.

There is essentially no confusion between Ξ^- reactions in our topologies and non-Ξ^- reactions. The only significant ambiguity among the Ξ^- hypotheses is that between $\Xi^-K^+\pi^0$ and $\Xi^-K^0\pi^+$ when the K^0 is unseen. Most of these ambiguities were resolved by visual inspection of the bubble density of the positive track. However, the K^+ or π^+ momentum was too

large to permit such resolution for 27 events in a total sample of 1189 events with no observed K^0. In these cases the hypothesis with smaller χ^2 (one constraint) was chosen; 18 of the 27 events were assigned to $\Xi^- K^+ \pi^0$ and 9 to $\Xi^- K^0 \pi^+$. Even assuming that half of the 27 events were misassigned leads to $< 2\%$ contamination of the former reaction and $< 0.5\%$ contamination of the latter. The numbers of $\Xi^- K^0 \pi^+$ events observed with either K^0 or Λ decay visible, or both visible, are consistent with the experimentally well-known[14] decay branching fractions of Λ and K^0 into $p\pi^-$ and $\pi^+\pi^-$.

In contrast to the Ξ^- reactions, which provide nearly all the events in their topologies, the Ξ^0 reactions contribute only a small fraction of the events in their respective topologies. Consequently, one encounters substantial difficulties in their separation. Since purity of the sample is crucial in the Ξ^0 lifetime and decay parameter determinations, we discuss the Ξ^0 separation procedure in detail. The Ξ^0 direction is not known (unless the decay π^0 decays via $e^+e^-\gamma$), so reactions with a missing neutral at production are not overconstrained. Thus, $\Xi^0 K^0 \pi^0$ and $\Xi^0 K^+ \pi^- \pi^0$ production cannot be fitted. Only $\Xi^0 K^0$, $\Xi^0 K^+ \pi^-$, and $\Xi^0 K^0 \pi^+ \pi^-$ productions were considered as sources of Ξ^0, and only when the Λ from Ξ decay and, if appropriate, the K^0 were observed to decay in the chamber. The Λ was required to pass a one-constraint (1C) Λ decay fit with unspecified incident Λ momentum and direction; the Λ momentum vector from this fit was used in a 3C, two-vertex fit to the production reaction followed by $\Xi^0 \rightarrow \Lambda \pi^0$ decay. (The extra constraint is obtained by requiring the Ξ^0, Λ, and π^0 momentum vectors to lie in a plane.) This fitting procedure was checked by putting $\Xi^0 K^+ \pi^-$ events generated by the Monte Carlo program

FAKE[15] through PACKAGE; the FAKE events were useful in calibrating the separation of $\Xi^0 K^+ \pi^-$ events as well as in the Ξ^0 decay analysis. The 3C fit of the Λ to the production vertex was also performed; at our momenta the Λ from Ξ^0 decay frequently (about 25% of the time) acceptably fits to the production vertex due to a small laboratory-system angle between the Ξ^0 and Λ directions.

1. Reaction $K^- p \to \Xi^0 K^0$

Each of the 1900 observed 0-prong two-V events was checked on the scanning table and the assignment of each "V" as Λ or K^0 was required to be consistent with the bubble density of the decay tracks as estimated from visual comparison with the minimum-ionizing beam tracks. Some 204 events had consistent $\Xi^0 K^0$ fits. None of these fit $K^- p \to \Lambda(\Sigma^0) K^0 \overline{K}^0$. However, there is substantial pion contamination in the beam, especially at the upper beam momenta. Many of the $\Xi^0 K^0$ candidates fit hypotheses involving incident π^-. In particular, the reaction channels

$$\pi^- p \to \Lambda K^0, \tag{2.10a}$$

$$\Lambda K^0 \pi^0, \tag{2.10b}$$

$$\Sigma^0 K^0 \tag{2.10c}$$

feed the 0-prong two-V topology and can be kinematically ambiguous with $\Xi^0 K^0$ production. Fits to reaction (2.10a) are 4C at production and were accepted as unambiguous evidence that the event is pion-induced. This assignment was confirmed by study of the χ^2 distributions for the 32 events fitting both $K^- p \to \Xi^0 K^0$ (flattish distribution with some peaking at high χ^2) and $\pi^- p \to \Lambda K^0$ (normal 4C χ^2 distribution). Using measured cross sections[16] for $\pi^- p \to \Lambda K^0$ in our momentum region and the number of our events fitting ΛK^0 at each beam momentum, we have obtained the

path length of π^- in the beam. This path length, based on 81 total $\pi^- p \to \Lambda K^0$ events, was used to determine the contamination of π^- in the beam (Table I).

There are 25 events that fit only $\Sigma^0 K^0$ production (2.10c). An additional 29 events fit (2.10c) better than $\Xi^0 K^0$ production. These events were removed from the Ξ^0 sample, together with five other events fitting $\Lambda K^0 \pi^0$ (2.10b) better than $\Xi^0 K^0$. Thus we have 54 $\pi^- p \to \Sigma^0 K^0$ events in the final assignment, consistent with the 56 events expected on the basis of the observed number of ΛK^0 events and the known cross sections.[16] We were left with 138 Ξ^0 events, of which two, having a missing mass above K^0 consistent with $\Xi^0 K^0 \pi^0$ production, were removed. Of the 136 events in the final sample, five fit $\Lambda K^0 \pi^0$ or $\Sigma^0 K^0$ production with confidence level $> 1/3$ of the confidence level for $\Xi^0 K^0$ and are considered ambiguous. We estimate the contamination in the sample as 2^{+3}_{-2} events. Of the events removed from the original sample fitting $\Xi^0 K^0$, we estimate that 5 ± 3 really are $\Xi^0 K^0$ events.

2. Reaction $K^- p \to \Xi^0 K^+ \pi^-$

The $\Xi^0 K^+ \pi^-$ events form a tiny fraction of the more than 120 000 two-prong V events in our experiment. Most of the background was eliminated by the following procedure:

(a) All events fitting $K^- p \to \Xi^0 K^+ \pi^-$ (2.5) were inspected on the scanning table and the consistency of the fitted momenta of each track with bubble density was checked.

(b) The fit to $\Xi^0 K^+ \pi^-$ was required to be the best fit among hypotheses involving an incident K^-.

(c) Events consistent (on the basis of χ^2 and ionization) with the 4C hypotheses $K^- p \to \Lambda K^+ K^-$, $\Lambda \pi^+ \pi^-$, $\bar{K}^0 p \pi^-$, and $\pi^- p \to \Lambda K^+ \pi^-$ were rejected.

(d) Events consistent with $K^- p \rightarrow \Lambda \pi^+ \pi^- \pi^0$ were rejected.

(e) Events consistent with $\pi^- p \rightarrow \Sigma^0 K^+ \pi^-$ were rejected if the confidence level for $\Xi^0 K^+ \pi^-$ production was < 5%.

After the imposition of criteria (a) through (e), 971 events remained. FAKE events were generated with a realistic beam momentum distribution, Ξ^0 and Λ lifetimes $\tau_{\Xi^0} = 3.2 \times 10^{-10}$ sec and $\tau_\Lambda = 2.5 \times 10^{-10}$ sec, and a constant matrix element for production and decay. Fitting of these FAKE-generated events showed that about 8% of real $\Xi^0 K^+ \pi^-$ events fit $K^- p \rightarrow \Lambda \pi^+ \pi^- \pi^0$; only 1% fit other K^--induced reactions with Λ in the final state or $\pi^- p \rightarrow \Lambda K^+ \pi^-$. Their χ^2 distribution for the fit to $\Xi^0 K^+ \pi^-$ closely approximates that of the 1.7- and 2.1-GeV/c $\Xi^0 K^+ \pi^-$ candidates with $\Xi^0 \pi^-$ effective masses in the $\Xi^*(1530)$ region, which is a highly purified subsample (see Fig. 6). Thus, only $\approx$ 1% of the real events are lost through the imposition of (b) and (c) and $\approx$ 8% through (d). Only 36 events were removed by the imposition of (e), so that $\approx$2 $\Xi^0 K^+ \pi^-$ events were lost. The sample of 971 events is still contaminated due to unfittable reactions such as $K^- p \rightarrow \Lambda \pi^+ \pi^- \pi^0 \pi^0$ and $K^- p \rightarrow \Sigma^0 \pi^+ \pi^- \pi^0$, as well as reactions such as $\pi^- p \rightarrow \Lambda K^+ \pi^- \pi^0$ at the upper momenta where the pion contamination in the beam is large. The further purification of the sample was carried out as appropriate to the particular measurement to be made.

For the purpose of measuring the Ξ^0 lifetime, a sample is required which is not only pure but also free from length-dependent biases. Rejection of events fitting non-Ξ^0 hypotheses (events with the Λ pointing back to the productive vertex) is therefore not suitable, as this criterion discriminates against events with short Ξ^0. Study of the FAKE events has shown that this effect is large and that the Ξ^0 lifetime, measured by using

the calculated Ξ^0 lengths, is found to increase in direct proportion to the number of events eliminated. The Ξ^0 length, as calculated by intersecting the fitted Ξ^0 and Λ momentum vectors, is a useful quantity in performing the separation, since contamination events (i. e., without real Ξ^0) should yield equal numbers of positive and negative Ξ^0 lengths. (Negative lengths occur when the calculated Λ line of flight intersects the Ξ^0 line of flight before, rather than after, the production point.) This follows from the symmetry of the fitted Ξ^0 and Λ directions about the beam direction, and has been checked with a sample of events (mostly $\Lambda\pi^+\pi^-\pi^0$) known to be largely free of Ξ^0. It also follows that the Ξ^0 lifetime calculated from non-Ξ^0 events is zero. Real Ξ^0 events may also yield negative calculated Ξ^0 lengths because of angle uncertainties. The FAKE events indicate that negative lengths occur in $\approx$ 4% of real Ξ^0 events. We note that only four of the 136 Ξ^0K^0 events have negative Ξ^0 lengths; this result is consistent with zero contamination or with the estimate of $2\ ^{+3}_{-2}$ contamination events obtained from consideration of the fits.

The $\Xi^0K^+\pi^-$ sample for the Ξ^0 lifetime determination was defined by accepting events only at the 1.7- and 2.1-GeV/c momentum settings and by requiring that the K^+ have laboratory momentum < 600 MeV/c (relative ionization $\gtrsim$ 1.7) or be otherwise identifiable by virtue of a characteristic decay or interaction. (Events with higher beam momentum could not be used due to the pion contamination in the beam.) This sample, containing 215 events, should be nearly free of contamination and bias; the number of events with negative Ξ^0 length is 12, compared with the eight expected if the sample were pure. We estimate the contamination to be 8 ± 8 events. None of the events has a missing mass above the

measured charged tracks consistent with the $\Xi^0 K^+ \pi^- \pi^0$ hypothesis.

The $\Xi^0 K^+ \pi^-$ sample for the decay parameter analysis was defined by accepting only events for which the Λ did not point back to the production vertex, as determined by failure to fit the 3C Λ-decay fit. This definition causes a slight bias of the decay-parameter analysis, but the effect is negligible at our level of precision. (See note 42.) The sample contains 603 events; a significantly larger sample of nearly pure Ξ^0 cannot be defined. Unfortunately, the sample contains $(7 \pm 2)\%$ contamination, estimated from the presence of 44 events with negative calculated Ξ^0 lengths, where 24 such events are expected. By comparison, the complete 971-event sample contains $(26 \pm 4)\%$ contamination.

We have verified the completeness of the $\Xi^0 K^+ \pi^-$ sample in an approximate way by comparing the rates for $K^- p \rightarrow \Xi^*(1530) K^+$ with decay into $\Xi^0 \pi^-$ and $\Xi^- \pi^0$. On the basis of the fits to the mass spectra in Section V, and after correction for the different detection efficiencies of the two topologies, a ratio $\Xi^0 \pi^- / \Xi^- \pi^0 = 2.3 \pm 0.2$ was obtained, in comparison with the ratio of 2 expected from isospin conservation.

3. Reaction $K^- p \rightarrow \Xi^0 K^0 \pi^+ \pi^-$

A total of 34 events is consistent with interpretation as reaction (2.8), but of these nine are also consistent with hypotheses such as $\pi^- p \rightarrow (\Lambda, \Sigma^0) K^0 \pi^+ \pi^- (\pi^0)$.

B. Scanning Losses and Corrections

Events were missed in scanning if a Ξ^-, Λ, or K^0 track was too short to be distinguished as such or if the decay occurred outside the chamber. Events were also lost if the projected laboratory-system angle of

the $\Xi^- \rightarrow \Lambda$ decay was too small for the decay kink to be observed. In the calculation of total and differential cross sections and in the lifetime analysis, minimum acceptance lengths were imposed. These were 0.5 cm for Ξ^-, K^0, and Λ from Ξ^0 decay, and 0.3 cm for Λ from Ξ^- decay. Decays were accepted only if they took place within a volume whose boundaries are sufficiently removed from the chamber walls to ensure measurability of the decay. Probabilities $P_{\Xi, \Lambda}$ and P_{K^0} for decay within these cutoffs and inside the decay volume were calculated; for the Ξ decay sequence these are the normalization integrals used in the likelihood determination of the Ξ lifetime (see VI A). The losses affect the angular distributions through their dependence on the lab momentum of the missed particles. The loss at small Ξ^- decay angles is most serious when the Λ is emitted in the Ξ rest frame in a direction opposite to the Ξ momentum (forward π^-), but also occurs when the Λ is emitted in the Ξ^- direction, and at all emission angles when the normal to the decay plane is nearly perpendicular to the camera axes.[17] The probability P_D for recognition of the Ξ^- decay was estimated as a function of Ξ momentum and decay angle by a Monte Carlo technique, as described in the Appendix.

For each event, the reciprocal product[18] of the detection probabilities $P_{\Xi, \Lambda}$, P_D, and P_{K^0} (if observation of the K^0 was required) was assigned as a weight $W = 1/P_{\Xi, \Lambda} P_D P_{K^0}$. For Ξ^0 events $P_D = 1$; the observed Ξ^0 decay distribution (Fig. 20) shows no loss of small-angle decays. Average values of $P_{\Xi, \Lambda}$ were 82% for Ξ^- events and 90% for Ξ^0 events. The average P_D and P_{K^0} are also about 90%.

III. TOTAL CROSS SECTIONS

The path length $\mathcal{L}_{K^-}$ of the beam was determined by a count of three-prong K^- decays. We have used a branching ratio for all K^- decays giving a three-prong configuration, $B = 0.059 \pm 0.001$,[14] and $\rho = (0.0593 \pm 0.0006)\ g/cm^3$ for the density of liquid hydrogen in the chamber.[19] The path length for π^- was obtained from the number of two- V events fitting $\pi^- p \rightarrow \Lambda^0 K^0$ as described above. Table I lists $\mathcal{L}_{K^-}$ in a restricted fiducial volume with the pion contamination $\mathcal{L}_{\pi^-}/(\mathcal{L}_{\pi^-} + \mathcal{L}_{K^-})$. The beam momentum distributions centered at 1.70, 2.10, and 2.47 GeV/c are relatively sharp, and Gaussian with full width at half maximum (FWHM) of 40, 60, and 50 MeV/c respectively. On the other hand, the 2.64-GeV/c distribution is made up of three distinct momentum settings, but is roughly flat with a width of 160 MeV/c.

Table II contains the numbers of events and cross sections for each reaction channel. The numbers of events listed are the total number available for analysis. Only events produced in a highly restricted fiducial volume were used for calculation of the total cross section, and only those in a somewhat less restricted volume were used for differential cross sections. The cross sections have been corrected for decay losses by the weighting procedure described above. In addition, we have corrected for scanning efficiency, measuring efficiency, and the decay of Λ and K^0 into neutrals. The uncertainties are mainly due to the statistical uncertainty in the number of events, estimated as the square root of the sum of the squares of the weights W. A contribution of ±3% for Ξ^- reactions and ±5% for Ξ^0 has been <u>added</u> (rather than folded) to the

errors to account for systematic uncertainties. Thus, our errors are more conservatively estimated than those quoted in most bubble chamber experiments.

The variation of total cross section for Ξ^-K^+ and Ξ^0K^0 production is illustrated in Fig. 1 for the beam momentum interval 1.2 to 3.0 GeV/c.[7,9,10,20,21] The cross sections have been divided by the factor $4\pi\lambda^2$ to facilitate a search for resonant enhancements in distinct partial waves. Both reaction cross sections peak near 1.7 GeV/c. In particular, the peak in Ξ^0K^0 is consistent in mass and width with the well-established $Y_0^*(2100)$ resonance.[22] This Y^* has $J^P = 7/2^-$, $M \approx 2100$ MeV, and $\Gamma \approx 140$ MeV. Although the cross-section data alone are insufficient to confirm the existence of a ΞK decay made for $Y_0^*(2100)$, we have drawn a curve for Ξ^0K^0 production with $\approx 50\%$ $Y_0^*(2100)$ and $\approx 50\%$ nonresonant background at the peak. The curve for Ξ^-K^+ assumes $\approx 25\%$ $Y_0^*(2100)$. These curves are intended to guide the eye; no fitting has been carried out. We postpone further discussion of possible $Y^* \rightarrow \Xi K$ effects until the differential cross section and polarization data have been presented.

Above our range the Ξ^-K^+ cross section continues to fall off rapidly, reaching 0.6 μb by 10 GeV/c.[23]

Approximate total Ξ^- production cross sections can be obtained by adding the entries in Table II. At 1.7 and 2.1 GeV/c no correction is required; at 2.47 and 2.64 GeV/c a correction $\approx 5\%$ is adequate to account for $\Xi^-K^+\pi^0\pi^0$. (A search for examples of $\Xi K3\pi$ production yielded only one event of this type).

IV. Ξ K PRODUCTION

A. Presentation of Data

The differential cross section and Ξ polarization data in Ξ^-K^+ and Ξ^0K^0 production are shown as a function of $\cos\Theta = \hat{K}_{in} \cdot \hat{K}_{out}$ in Figs. 2 and 3. The events have been weighted as described above. Our choice of production plane normal, $\hat{n} = (\hat{K}_{in} \times \hat{K}_{out})/|\hat{K}_{in} \times \hat{K}_{out}|$, conforms with convention in analyzing meson-nucleon scattering; however, it is opposite to that used in previous work[7] by the LRL group. We have expanded in Legendre functions

$$\frac{d\sigma}{d\Omega} = \frac{\sigma}{4\pi} \sum_{\ell=0} \left(\frac{A_\ell}{A_0} \right) P_\ell(\cos\Theta), \tag{4.1}$$

$$P_\Xi \frac{d\sigma}{d\Omega} = \frac{\sigma}{4\pi} \sum_{\ell=1} \left(\frac{B_\ell}{A_0} \right) P_\ell^1(\cos\Theta), \tag{4.2}$$

where

$$P_\ell^1(\cos\Theta) = \sin\Theta \, [dP_\ell/d\cos\Theta],$$

$A_0 = \sigma/4\pi\lambda^2$, and λ is $\hbar$ divided by the initial-state c.m. momentum. The expansion coefficients (A_ℓ/A_0) and (B_ℓ/A_0) were computed as moments of the distribution function (6.2). Table III lists $\langle P_\Xi \rangle$ at each momentum in representative bins of $\cos\Theta$. Decay parameters $\alpha_\Xi = -0.38$ and $\Phi_\Xi = 0$ deg were used. Footnote 41 describes the method for computation of $\langle P_\Xi \rangle$ and the (B_ℓ/A_0). Coefficients (A_ℓ/A_0) are given in Table IV for Ξ^-K^+ and plotted in Fig. 4 along with those for experiments at other momenta. Data were obtained from the authors of Refs. 7, 9, and 20; the moments were calculated as for our own data.

Coefficients for $\Xi^0 K^0$ are given in Table V.

The solid curves in Figs. 2 and 3 correspond to an expansion of the maximum required complexity; the dashed curves show the $\ell \leq 3$ fits. (The cutoff in ℓ is the order at which χ^2 for a fit to the experimental points shown decreased by less than two for each additional order.) Below 1.7 GeV/c in $\Xi^- K^+$, $\ell = 3$ is adequate,[7] corresponding to partial waves up to D_3. At 1.7 and 2.1 GeV/c, terms up to third order reproduce the cross section, including the prominent backward peak, but qualitatively do not fit the variation of polarization with $\cos\Theta$; in particular the jump in polarization near $\cos\Theta = 0.3$, which is present at all our momenta, requires $\ell > 3$. Inclusion of terms up to $\ell = 7$ at 1.7 GeV/c and $\ell = 6$ at 2.1 GeV/c yields adequate fits to $P_\Xi \, d\sigma/d\Omega$. At 2.64 GeV/c, partial waves requiring $\ell = 4$ through 8 are present and inclusion of $\ell = 9$ improves the fit slightly. The higher partial waves are required both by the sharpness of the backward peak and by the presence of undulations in $d\sigma/d\Omega$.

The $\Xi^0 K^0$ data differ from the $\Xi^- K^+$ data in several respects. At all momenta, the concentration of events in the backward peak is less pronounced than in $\Xi^- K^+$ production. In addition, a forward peak seems to be present at all our momenta. The production cross section varies more rapidly with energy than does that for $\Xi^- K^+$; the changes in A_1, A_2, and A_4 are particularly striking. Best fits are obtained with a maximum $\ell = 5$. The sign of $\langle P_{\Xi^0} \rangle$ changes between 1.7 and 2.1 GeV/c. By contrast, $\langle P_{\Xi^-} \rangle$ is consistently negative or ≈ 0, and varies slowly with momentum at a given $\cos\Theta$.

B. Interpretation

The pronounced backward peak in ΞK production may be simply explained as the result of exchange of one or more strangeness-carrying baryons in the u channel. The undulations in $d\sigma/d\Omega$ may be ascribed to structure in the s channel and possibly also to interference between s- and u channel amplitudes. Meson exchange may be neglected, since there is no known meson with strangeness 2. The persistently low cross section near 90 deg may have a simple interpretation in terms of a zero in the trajectory function for a Reggeized baryon exchange. The presence of significant Ξ polarization varying rapidly with $\cos\Theta$ rules out a simple model of single baryon exchange in which the amplitudes are relatively real. The polarization may arise from the interference of different u-channel amplitudes, or may be due mainly to s-channel contributions.

The production mechanism for Ξ^0K^0 is quite different from that for Ξ^-K^+, since exchange of a neutral baryon is forbidden for Ξ^0K^0 but allowed for Ξ^-K^+. The ratio of total cross sections for the two cases indicates that $I=0$ exchange is dominant in Ξ^-K^+ production. We obtain $\sigma_{\Xi^0K^0}/\sigma_{\Xi^-K^+} = (0.55\pm0.13)$, (0.22 ± 0.06), and (0.24 ± 0.07) at 1.7, 2.1, and 2.64 GeV/c respectively, in contrast to the ratio of 4 expected from $I=1$ exchange. A partial-wave analysis of the 2.0-GeV/c data by Trippe and Schlein[20] and calculations by Donohue[24] indicate a preference for $1/2^-$ and $3/2^+$ exchange. Since there is no known $I=0$ hyperon state with $J^P = 3/2^+$, the most likely candidate for the exchanged baryon is $Y_0^*(1405)$ with $J^P = 1/2^-$.[25] Only S_1, P_1, P_3 and D_3 waves were required by Trippe and Schlein to fit the backward peak, although one additional small partial wave with $J \geq 9/2$ seems to be required to fit the full angular distribution. The

forward peak in $\Xi^0 K^0$ production might be due to an interference involving s-channel resonances in one or more partial waves.

The evidence for s-channel resonances decaying to ΞK may be summarized as follows:

(a) The peak in A_0 for both $\Xi^0 K^0$ and $\Xi^- K^+$ near 1.7 GeV/c (2100 MeV total c.m. energy) (see Fig. 1).

(b) An increase in the magnitude of A_1 near 2100 MeV, and in A_2 near 2150 MeV in $\Xi^- K^+$ (see Fig. 4).

(c) The large variation of the A_ℓ and $\langle P_{\Xi 0} \rangle$ between 1.7 and 2.1 GeV/c in $\Xi^0 K^0$ (see Tables III, V).

If $Y_0^*(2100)$ were causing all or some of these effects, we might expect to see some A_4 and A_6 near 2100 MeV. A decaying $J = 7/2$ resonance contributes (neglecting interferences) to A_0, A_2, A_4, and A_6 in the ratios 1.00: 1.14: 1.05: 0.76. The bump in A_0 for $\Xi^- K^+$ (Fig. 1) is about 25% of the peak. If we associate this bump with a resonance, we have $A_0^{res}/A_0 = 0.25$. The bump in A_2/A_0 (Fig. 4) is roughly 0.4±0.2 in height. Thus the observed ratios A_0^{res}/A_0: A_2^{res}/A_0: A_4/A_0: $A_6/A_0 = (\approx 1.0 \pm 0.3)$: (1.6 ± 0.9): (1.48 ± 0.84): (0.64 ± 1.04) are compatible with the $Y_0^*(2100)$ hypothesis. The small observed A_7 at 1.7 GeV/c might be due to an $F_7 G_7$ interference with $Y_1^*(2030)$; this Y_1^* may also account for the shoulder in A_0 for $\Xi^- K^+$ near 1.5 GeV/c. The negative sign of the A_7 at 1.7 GeV/c is consistent with the assignment of $Y_1^*(2030)$ to a decuplet [as a recurrence of $Y_1^*(1385)$] and $Y_0^*(2100)$ to a unitary singlet [as a recurrence of $Y_0^*(1520)$].[22] The positive A_7 in $\Xi^0 K^0$ (Table V) provides further support for this interpretation. The increase in the magnitude of A_1, which can come only from an interference between the G_7 and a positive parity partial wave having $J \geq 5/2$, is most simply understood by assuming an $F_5 G_7$

interference with $Y_1^*(1910)$. Neither the F_7G_7 nor the F_5G_7 term requires much amplitude for the interfering resonance, since the relevant partial-wave expansion coefficients are large. We conclude that the data near 1.7 GeV/c are qualitatively consistent with

(a) $\Xi^- K^+$ production largely from I = 0 baryon exchange, and

(b) $\Xi^0 K^0$ production primarily ($\approx 50\%$) from $Y_0^*(2100)$ formation. The $Y_0^*(2100)$ production, which contributes in roughly equal parts to the Ξ^0K^0 and Ξ^-K^+ amplitudes, contributes about 100 μb total ΞK cross section. Cool et al.[26] report a total cross section for $Y_0^*(2100)$ of 10 mb, of which 5 mb is K^-p. Thus the branching ratio into ΞK is about $2 \pm 1\%$.

It is noteworthy that recent Saclay data on $K^-p \to \Xi K$ between 1.2 and 1.8 GeV/c have been interpreted as suggesting a new Y^* near 2070 MeV with little $Y_1^*(2030)$ or $Y_0^*(2100)$.[27] The spin of the new resonance would be 3/2 or 5/2. Our data are also consistent with such an interpretation.

The increase in the higher coefficients above 2.1 GeV/c may also have an explanation in terms of s-channel resonances. At 2.4 GeV/c (2480 MeV c.m. energy) the highest-order significant coefficient is A_8; thus one or more $J \geq 9/2$ waves are present. The large negative A_7 could not come from a G_9H_9 interference, since A_9 is small. Thus, if there are several $J \geq 9/2$ resonances in this region, they must have the same parity. An $F_7\,G_9$ or $G_7\,H_9$ term would give ratios for A_3: A_5: A_7 close to the observed values. The observed A_4 and A_6 could arise from a J = 9/2 resonance and its interference with the S-, P-, and D-wave "background" from the baryon exchange. Recent measurements[28] of K^-p and K^-d total cross sections have provided evidence for I = 1 resonances at 2455±10 and 2595±10 MeV with widths ≈ 140 MeV. The lower-mass state could be accommodated as a Regge recurrence of $Y_1^*(1385)$ with

spin-parity $11/2^+$ or as a $9/2^+$ recurrence of the Σ. Our data support the latter assignment.

We are now carrying out a partial-wave analysis of the $K^-N \rightarrow \Xi K$ reaction from threshold to 2.7 GeV/c, using UCLA and LRL data, including $K^-d \rightarrow \Xi^- K^0(p)$ events at 1.5, 2.1, and 2.6 GeV/c. An attempt will be made to determine the isotopic spin composition of the u-channel exchange amplitudes as well as to tie down the structure in the s channel. If a resonance of known spin and parity, such as $Y_0^*(2100)$, is largely responsible for the Ξ polarization, the fits may distinguish between positive and negative KN Ξ parity and therefore afford a determination of the Ξ parity.

V. MULTIBODY PRODUCTION

A. $\Xi K\pi$ Mass Spectra

In this section, we present an analysis of the reactions

$$K^-p \rightarrow \Xi^- K^+ \pi^0, \tag{2.3}$$

$$\Xi^- K^0 \pi^+, \tag{2.4}$$

$$\Xi^0 K^+ \pi^-, \tag{2.5}$$

with emphasis on production of the well-known $\Xi^*(1530)$ and $K^*(890)$ resonances. The evidence for higher-mass Ξ^* production in these reactions is considered; substantial production of $\Xi^*(1930)$ is observed. $\Xi^*(1705)$ and $\Xi^*(1815)$ are not resolved if they are present at all. There is no evidence for $K^-p \rightarrow Y^*K$ with $Y^* \rightarrow \Xi K$. We find no evidence for a low-mass $K\pi$ resonance.

Figure 5 contains Dalitz plots of $M^2(K\pi)$ vs $M^2(\Xi\pi)$ for the combined reactions (2.3) through (2.5) at each of three incident K^- momenta, 1.7, 2.1, and 2.6 GeV/c. All the data above 2.4 GeV/c have been combined in

the 2.6-GeV/c sample. Inspection of the Dalitz plots and projections (Figs. 5 through 8) shows enhancements corresponding to $\Xi^*(1530)$ for each momentum and reaction. $K^*(890)$ is observed at 2.1 and 2.6 GeV/c; threshold is 1.93 GeV/c.

For the Ξ^0 events we have plotted the complete data sample of reaction (2.5), which includes 5%, 15%, and 32% non-Ξ^0 contamination at the 1.7-, 2.1-, and 2.6-GeV/c momenta respectively. We have shaded in Fig. 6 through 8 the purified sample which includes only events with Λ which do not fit with the production vertex taken as the origin. We have checked that the small bias in the Ξ^0 momentum spectrum introduced by this selection does not significantly affect the mass plots.

Maximum-likelihood fits[29] to the Dalitz plots have been performed for each final state and momentum. The fits assume p-wave Breit-Wigner resonant amplitudes plus a phase-space-like background. Interference between the amplitudes, and angular correlations in the production and decay of the resonant states, were neglected in constructing the likelihood function. A Gaussian approximation to the $M(\Xi\pi)$ experimental resolution function was folded with the Ξ^* Breit-Wigner line shape. The width (FWHM) of the Gaussian function varied from ≈ 7 MeV/c^2 at the lowest beam momentum for $\Xi^- K^0 \pi^+$ production to ≈ 14 MeV/c^2 for $\Xi^0 K^+ \pi^-$ production at the highest beam momentum. For the Breit-Wigner width of the Ξ^*, we used $\Gamma_0 = 7.3$ MeV/c^2 and $M_0 = 1534$ MeV/c^2 for the Ξ^{*-}, and 1531 MeV/c^2 for the Ξ^{*0}.[4] For K^* we used $\Gamma_0 = 49$ MeV/c^2, $M_0 = 893$ MeV/c^2.[14] The production fractions of Ξ^* and K^* and their cross sections are presented in Table VI. Figure 9 shows the variation of these production cross sections from threshold to 3 GeV/c.[7,10,30,31] The Ξ^* cross sections rise smoothly from threshold, reach a maximum near 2.1 GeV/c,

and then fall off.

Curves calculated from the Ξ^* and K^* production fractions obtained in the fits are included in Figs. 6 through 8. The curves under the peaks indicate the calculated background levels. The curves are generally adequate representations of the data, but some discrepancies are discussed below.

2. Ξ^* Other than $\Xi^*(1530)$

There is an excess of high-mass events in Fig. 6 (c), (f), and (i). In order to examine this effect we have plotted $M^2(\Xi\pi)$ for the highest-energy events separately in Fig. 10. (Only purified Ξ^0 events have been used.) The effect is greatest for $(\Xi\pi)^-$, as shown in Fig. 10(d); here the curve based only on the $\Xi^*(1530)$ and K^* resonances is too low by ≈ 3.5 standard deviations for $3.35 < M^2(\Xi\pi) < 3.75$ $(\mathrm{GeV}/c^2)^2$. This excess is most easily interpreted as a single broad $\Xi\pi$ resonance in the region of 1900 MeV/c^2. Assuming a single resonance, we obtain a good fit to the combined $\Xi^0 K^+\pi^0$ data with a Ξ^{*-} mass of 1894±18, width 98±23 MeV/c^2, and production cross section of 24 ± 7 μb, when a simple Breit-Wigner distribution is assumed. Using the same mass and width, we obtain a cross section of 4 ± 4 μb for Ξ^{*0}. Separate fits to the $\Xi^-\pi^0$ and $\Xi^0\pi^-$ events yield a branching ratio $\Xi^0\pi^-/\Xi^-\pi^0 = 1.4 \pm 0.7$ where a ratio of 2 or 1/2 is expected for I = 1/2 or 3/2. The large uncertainty, which is partly due to uncertainties in the Ξ^0 purification, prevents a clear-cut rejection of I = 3/2. The production favors low momentum transfer between K^- and this Ξ^*. Evidence for such a Ξ^* (in the neutral charge state) was first obtained by Badier et al.[21] in the $\Xi^- K^0\pi^+$ final state at 3.0 GeV/c; the reported mass was 1933 ± 16 and the width 140 ± 35 MeV/c^2. Smith

and Lindsey[32] presented evidence supporting $\Xi^*(1930)$ in a preliminary analysis of the data of this work. It may be possible to explain the lowering of our peak position with respect to that reported by Badier et al. as an effect of the more severely limited phase space for Ξ^*K production at our momentum.

There is no significant evidence for other Ξ^* resonances in the $\Xi K\pi$ data. A small bump is present at $M^2(\Xi\pi) \approx (1700\ \mathrm{MeV}/c^2)^2$ in $\Xi^0 K^+\pi^0$ (Fig. 10 d). Smith and Lindsey[32] combined the bump in these data with a similar enhancement observed in the $\Lambda\bar{K}$ spectrum to suggest a $\Xi^*(1705)$. Similarly, our data provide no support for a $\Xi\pi$ decay mode of $\Xi^*(1815)$, which is believed[14] to have $\Gamma \leq 30\ \mathrm{MeV}/c^2$. Our data provide upper limits of $\approx 10\ \mu b$ for production of Ξ^* other than $\Xi^*(1530)$ and $\Xi^*(1930)$ with decay into $\Xi\pi$.

3. Search for $Y^* \rightarrow \Xi K$ Enhancements

We have attempted to examine possible resonant effects in the ΞK distributions by combining reactions and removing events in the $\Xi^*(1530)$ and $K^*(890)$ bands (Fig. 11). At 2.1 GeV/c there are no significant discrepancies from the fit. At 2.6 GeV/c, the fit including $\Xi^*(1930)$ (using our values for the mass and width and shown dashed) is adequate. Thus, we have no evidence for $K^- p \rightarrow Y^* \pi$ with Y^* decay into ΞK.

4. Low-Mass $K\pi$ Enhancement

Previous experiments have produced evidence for a narrow, low-mass, $(K\pi)$ enhancement in the $\Xi K\pi$ system. The peak is centered at 730 MeV/c^2 at 2.24 GeV/c[10] and at 710 MeV/c^2 in work by Trippe at 2.0 GeV/c.[31] The widths are consistent with the now-discredited[33] κ meson. In the experiment at 2.24 GeV/c the $K\pi$ peak is seen both inside and outside the

Ξ^* band on the Dalitz plot, while at 2.0 GeV/c it is present only outside the Ξ^* band. Indications of similar enhancements are also seen in experiments at 1.8 to 1.95 GeV/c[9] and at 4.25 GeV/c.[34]

Figure 8 shows the (Kπ) mass spectra for our experiment with fitted curves based on $\Xi^*(1530)$ and $K^*(890)$ production. Figures 12(a) and (b) present (Kπ) mass distributions for events inside and outside the Ξ^* band, for all charge states combined and for incident momenta 2.1 GeV/c and above. Events at 2.1 GeV/c are cross-hatched.

Inside the Ξ^* band, at 2.1 GeV/c, there is a three-standard-deviation departure from the fitted curves near $M(K\pi) = 710$ MeV/c^2 [$M^2 = 0.5$ $(GeV/c^2)^2$], with width ≈ 50 MeV/c^2. However, effects inside the Ξ^* band could result from interference between the $\Xi^*(1530)$ amplitude and other amplitudes. Interference was ignored in the fits, which also assume isotropy for the Ξ^* decay.

We see no (Kπ) enhancement near 710 MeV/c^2 for the events outside the Ξ^* band. Thus we have no evidence for a kappa-like effect in this experiment.

B. Reaction $K^-p \to \Xi^*(1530)K$

Production of $\Xi^*(1530)$ is observed in the reactions

$$K^-p \to \Xi^{*0}K^0, \tag{5.1}$$

$$\Xi^{*-}K^+. \tag{5.2}$$

The cross sections and production and decay distributions are shown in Figs. 9, 13, and 14. The events were selected by $\Xi\pi$ mass cuts and are weighted according to the detection probability of the Ξ in Fig. 13 only. No background subtraction has been performed. The events in bins below and

above the Ξ^* have more isotropic production distributions than those in the Ξ^* bins. The $\Xi^- K^+ \pi^0$ and $\Xi^0 K^+ \pi^-$ events, which yield consistent distributions and numbers of events consistent with I = 1/2 for the Ξ^*, have been combined in treating Ξ^{*-}. Figure 14 displays the polar decay distribution of Ξ^* in its own rest frame, with the beam direction used as the Z axis. We have folded about $(\hat{\Xi} \cdot \hat{K}^-)_{\Xi^*} = 0$ after verifying the symmetry of each distribution. The unshaded histograms correspond to the complete Ξ^* samples; the shaded portions contain only Ξ^* produced forward in the c.m., $(K_{in} \cdot K_{out}) < 0$. The curves plotted are normalized to the full samples; they assume $J_{\Xi^*} = 3/2$ and either pure $m = \pm 3/2$ or $m = \pm 1/2$ population of the spin states.

Inclusion of K^* events is a potential source of bias for the Ξ^* decay distributions, particularly at the highest beam momenta. Figure 14(c) and (f) contains about 10% K^* events, which bias the distributions towards $m = \pm 3/2$. The distributions for events inside and outside the $K^* - \Xi^*$ crossing region of the Dalitz plot indicate that the bias is too small to affect the qualitative conclusions below.

The $\Xi^{*0} K^0$ and $\Xi^{*-} K^+$ production are strikingly different from each other in their gross features, strongly energy-dependent in our range, and also striking in their difference from the $\Xi^0 K^0$ and $\Xi^- K^+$ production properties discussed in Sec. IV. The following remarks summarize the situation, and qualitatively compare the data to various baryon-exchange models:

(a) The Ξ^* production angular distributions are both flat at 1.7 GeV/c (threshold is 1.51 GeV/c). At 2.1 and 2.6 GeV/c the Ξ^{*0} distributions have large backward peaks, which, however, have very pronounced dips

in the extreme backward direction. The Ξ^{*-} production is roughly fore-aft symmetric at the higher momenta, with slight peaking at 2.1 GeV/c which becomes very pronounced at 2.6 GeV/c. Again the backward peak dips for $\hat{K}_{in} \cdot \hat{K}_{out} < -0.8$. The forward peak in the 2.6-GeV/c Ξ^{*-} is probably the most striking feature of these data. It cannot be explained as being due to K^* (890) background, as is shown by the darkened histograms (purified Ξ^0 events only, with the K^* band cut out) and cross-hatched histograms ($\Xi^- K^+ \pi^0$ events with K^* cut out) in Fig. 13(f).

(b) The features mentioned in (a) contrast with those of ΞK production, which exhibits double peaking in the $\underline{\Xi^0 K^0}$ case and for which the backward peak shows no sign of a dip in any case.

(c) The decay data indicate preference for $m = \pm 3/2$ alignment in the Ξ^{*0} case and preference for $m = \pm 1/2$ in the Ξ^{*-} case. This effect was previously noted by Schlein[30] in the 1.8- and 1.95-GeV/c UCLA data. Schlein also pointed out that the $m = \pm 3/2$ alignment of the Ξ^{*0} rules out production via simple $J = 1/2$ baryon exchange, whereas the $m = \pm 1/2$ preference of the Ξ^{*-} is consistent with such a mechanism. However, the $m = \pm 1/2$ alignment of Ξ^{*-} is not particularly associated with events in the backward (baryon exchange) peak, as shown by the shaded histograms in Fig. 14(d), (e), and (f). A single-baryon-exchange model would also be difficult to reconcile with the dip in the extreme backward direction.

A model involving exchange of several baryons with different spin and isospin could presumably be constructed to explain most of the features of the Ξ^* data, including the ratio of total cross sections, the dip in the backward peak, and the mixture of spin substates.[35] Such a model would also have to account for the large forward peak in Ξ^{*-} production. In the

absence of a meson with strangeness 2, the forward peak must be explained by interference among s-channel resonance amplitudes and possibly the baryon exchange amplitudes as well. A purely s-channel explanation requires at least two resonances with different isospin to account for the absence of a peak in Ξ^{*0} production. An explanation involving baryon exchange alone would require a very large change in the relative phase of the several exchange amplitudes between small and large u. In Regge model terms this means radically different trajectories for the exchanged Regge poles in the u channel.

A more detailed and quantitative treatment of the data, necessary to distinguish between complicated u-channel models, is presently under way. That analysis will be published separately.

C. Reaction $K^- p \to \Xi K^*(890)$

Production of K^* is observed via the reactions

$$K^- p \to \Xi^0 K^{*0}, \tag{5.3}$$

$$\to \Xi^- K^{*+}. \tag{5.4}$$

Figure 9(a) shows the variation of $\sigma/4\pi\lambda^2$ from threshold to 2.6 GeV/c for these reactions. Production angular distributions are shown in Fig. 15. A K^* mass cut, $0.86 < M(K\pi) < 0.93$ GeV/c^2, was used to select events; the resulting samples contain roughly 50% background events. The $\Xi^- K^+ \pi^0$ and $\Xi^- K^0 \pi^+$ events were combined in making the K^{*+} plots. Only purified $\Xi^0 K^+ \pi^-$ events were used in the K^{*0} plots.

The production plots show backward peaking, particularly at 2.6 GeV/c in $\Xi^- K^{*+}$ [Fig. 15(d)]. There is no evidence for any forward peaking comparable to that seen in $\Xi^{*-} K^+$ production.

D. $\Xi K\pi\pi$ Production

We observe the following four-body final states at an average beam momentum of 2.6 GeV/c:

$$K^- p \rightarrow \Xi^- K^+ \pi^+ \pi^-, \quad 87 \text{ events}, \tag{2.6}$$

$$\Xi^- K^0 \pi^+ \pi^0, \quad 42 \text{ events}, \tag{2.7}$$

$$\Xi^0 K^0 \pi^+ \pi^-, \quad 24 \text{ events} \tag{2.8}$$

Events were accepted only if the Λ decay and the K^0 decay (when appropriate) were observed. Scatter plots of $M(\Xi\pi)$ vs $M(K\pi)$ and $M(\Xi\pi\pi)$ are shown in Fig. 16(a) and (b) for the combined reactions. Only the $(\Xi\pi)$ and $(K\pi)$ charge combinations with $I_z = \pm 1/2$ have been plotted. Thus $\Xi^- K^0 \pi^+ \pi^0$ events are plotted twice.

The production is dominated by $\Xi^*(1530)$. Roughly 80% of the events have a $\Xi\pi$ combination in the 1530 region. There is also some $K^*(890)$. Maximum-likelihood fits have been performed assuming incoherent resonance production [$\Xi^*(1530)$, $K^*(890)$ and simultaneous $\Xi^* K^*$ production]. Cross sections based on these fits are given in Table VII. The mass projections and fitted curves are shown in Fig. 17. The darkened events in (c) are those inside the the Ξ^* band, $1500 < M(\Xi\pi)^{\overline{0}} < 1560$ MeV/c^2 and <u>outside</u> the K^* band, $840 < M(K\pi)^{\overset{+}{0}} < 940$ MeV/c^2; the cross-hatched events are those inside both bands. The dotted (dashed) curve represents the original fit with the same cuts applied as in the darkened (cross-hatched) histograms.

The small bump in the uncut data near 1815 MeV/c^2 contains 9 ± 5 events above the solid fitted curve. The number of darkened events

above the dotted curve is 8 ± 4. Statistically our bump is not convincing. The evidence presented previously[2, 21, 32] for $\Xi^*(1815)$ comes mostly from the $\Lambda\bar{K}$ channel. As pointed out in earlier publications,[2, 32] these data provide only very weak evidence for a possible $\Xi\pi\pi$ decay mode of the claimed resonance. The position and width of the bump in Fig. 17(c) are consistent with the values from the $\Lambda\bar{K}$ observations.[32] We estimate the upper limit for the branching fractions of $\Xi^*(1815) \rightarrow \Xi^*(1530)\pi$ to be about 25%.

VI. THE DECAY $\Xi \rightarrow \Lambda\pi$

A. Ξ Decay Rate

1. Ξ^- Lifetime

For the determination of the Ξ^- lifetime, the 2823 Ξ^- events with a visible Λ decay were considered. We imposed minimum-length cutoffs of 0.5 cm for the Ξ^- and 0.3 cm for the Λ, and a more restricted fiducial volume. These criteria reduced the sample to 2610 events.

Proper times $t_1 = (\ell M/pc)_\Xi$ and $t_2 = (\ell M/pc)_\Lambda$ were calculated for the Ξ^- and Λ in each event from the measured hyperon flight paths ℓ and fitted momenta p. The lengths and the momenta are typically determined to 1% or better. Masses of 1321.0 and 1115.6 MeV/c^2 were used for Ξ^- and Λ respectively. Figure 18 shows the distribution of Ξ^- proper time of flight, excluding Ξ^- produced less than 80 cm from the end wall of the chamber to reduce the effect of escape losses.

The lifetime τ_{Ξ^-} was obtained by maximizing the log of the likelihood function

$$W(\lambda_1, \lambda_2) = \ell n \mathcal{L}(\lambda_1, \lambda_2) = \sum_{k=1}^{N} \ell n\, P_k(t_{1k}, t_{2k};\ \lambda_1, \lambda_2),$$

where the probability P_k for observing the kth event with proper times t_{1k} and t_{2k} if the decay rates are $\lambda_1 = \tau_\Xi^{-1}$ and $\lambda_2 = \tau_\Lambda^{-1}$ is

$$P_k(t_{1k}, t_{2k}; \lambda_1, \lambda_2) = f_k(\lambda_1, \lambda_2)\lambda_1\lambda_2 \exp(-\lambda_1 t_{1k} - \lambda_2 t_{2k}).$$

The function $f_k(\lambda_1, \lambda_2)$, which is the inverse of the detection probability $P_{\Xi,\Lambda}$ referred to in Sec. II, normalizes P_k to unity. It is given by

$$\frac{1}{f_k(\lambda_1, \lambda_2)} = \int_{a_{1k}}^{b_{1k}} dt_1 \int_{a_{2k}}^{b_{2k}(t_1)} dt_2 \; \lambda_1\lambda_2 \exp(-\lambda_1 t_{1k} - \lambda_2 t_{2k}),$$

where a_{1k} and a_{2k} are the proper times corresponding to the lower-length cutoffs on Ξ^- and Λ, b_{1k} is the proper time corresponding to the maximum possible length for the Ξ^-, and $b_{2k}(t_1)$ corresponds to the maximum possible length for a Λ emitted after a Ξ^- proper flight time t_1. The maximum lengths are determined either by a simple cutoff or by the intersection of the hyperon flight paths with a wall of the restrictive fiducial volume.

With no maximum-length cutoffs imposed and with $\tau_\Lambda = 2.52 \times 10^{-10}$ sec,[36] we obtain a maximum for $W(\lambda_1, \lambda_2)$, which is parabolic near its maximum, at $\tau_{\Xi^-} = (1.600 \pm 0.033) \times 10^{-10}$ sec. The stated error refers to the shift in lifetime necessary to decrease $W(\lambda_1, \lambda_2)$ by 0.5. The value of τ_{Ξ^-} is dependent on τ_Λ only through the finite size of the chamber; a shift in τ_Λ by 0.1×10^{-10} sec produces a change in τ_{Ξ^-} of only 0.002×10^{-10} sec. Maximizing $W(\lambda_1, \lambda_2)$ also as a function of λ_2 yields $\tau_\Lambda = (2.61 \pm 0.06) \times 10^{-10}$ sec, in comparison with the world average of $(2.52 \pm 0.03) \times 10^{-10}$ sec. Variation of the length cutoffs and the acceptance volume leads to small shifts in τ_{Ξ^-}, less than $\pm 0.02 \times 10^{-10}$ sec for reasonable cutoffs, within

statistical expectations. There is no significant dependence of τ_{Ξ^-} on beam momentum, Ξ^- momentum, or the projected angle of the Ξ^- decay in the laboratory system. We have calculated the two-scan efficiency for detecting Ξ^- and find no significant correlation with length. Correction for energy loss and interactions of Ξ^- in the chamber (assuming an average $\sigma_{\Xi p} = 20$ mb)[37] increases τ_{Ξ^-} to 1.61×10^{-10} sec. Including systematic uncertainties, we obtain as our result

$$\tau_{\Xi^-} = (1.61 \pm 0.04) \times 10^{-10} \text{ sec.}$$

2. Ξ^0 Lifetime

For the determination of the Ξ^0 mean lifetime we used the $\Xi^0 K^0$ events and 215 $\Xi^0 K^+ \pi^-$ events in the highly purified and bias-free sample described in Sec. IIA.2. In four additional events the π^0 from the Ξ^0 decays into γ plus a Dalitz $e^\pm$ pair, identifying the event as an unambiguous Ξ^0.[38] After the imposition of fiducial volume criteria and the requirement that the Λ decay farther than 0.5 cm from the production vertex, 340 events remained in the sample.

The Ξ^0 and Λ momenta obtained in the kinematic fits have uncertainties of the order of 2%. The Ξ^0 flight distances were calculated from the fitted Ξ^0 and Λ directions and the measured length ℓ_3 of the join between the Ξ^0 production and Λ decay vertices. Figure 18 shows the distribution of Ξ^0 proper time of flight calculated by using a Ξ^0 mass of 1315 MeV/c^2, again including only events with Ξ^0 produced at least 80 cm from the end wall of the chamber. As noted in Sec. II A.2., 16 events have negative calculated flight times. Uncertainties of 5 to 10% are typical for the Ξ^0 length, but events in which the Ξ^0 and Λ are nearly collinear can

yield much larger uncertainties. For the events with Dalitz $e^{\pm}$ pairs, we used the accurately measured Ξ^0 lengths, which are in agreement with the calculated lengths.

The uncertainty in the Ξ^0 length was taken into account by folding a Gaussian error function Q into the probability function for each event,

$$P_k'(\ell_{1k}, \ell_{3k}; \lambda_1, \lambda_2) = \int_0^{\ell_{3k}} dx\, Q(x, \ell_{1k})\, P_k(t_1(x), t_2(x); \lambda_1, \lambda_2),$$

where $$Q(x, \ell) = \frac{1}{\sqrt{2\pi}\,\sigma_k} \exp[-(x-\ell)^2/2\sigma_k^2]$$

and $$P_k(t_1(x), t_2(x); \lambda_1, \lambda_2) = f_k(\lambda_1, \lambda_2) \exp[-\lambda_1 t_1(x) - \lambda_2 t_2(x)].$$

Here $t_1(x)$ and $t_2(x)$ are the proper times for Ξ^0 and Λ with the join length ℓ_{3k} held constant and the true Ξ^0 decay point at a distance x from the production vertex; ℓ_{1k} and σ_k are the calculated Ξ^0 length and its uncertainty.[39] The normalization integral, $[f_k(\lambda_1, \lambda_2)]^{-1}$, was performed with minimum and maximum lengths of the join ℓ_3 as limits. With 0.5 cm as the lower limit and no upper length cutoff imposed,

$$W(\lambda_1, \lambda_2) = \sum_{k=1}^{N} \ell n\, P_k'(\ell_{1k}, \ell_{3k}; \lambda_1, \lambda_2)$$

was found to be nearly parabolic in $\lambda_1 = \tau_{\Xi^0}^{-1}$ about a maximum at

$$\tau_{\Xi^0} = (2.969 \pm^{0.196}_{0.173}) \times 10^{-10} \text{ sec.}$$

The value $\tau_\Lambda = 2.52 \times 10^{-10}$ sec was used; variation of τ_Λ by 0.1×10^{-10} sec produces shifts in τ_{Ξ^0} of only 0.002×10^{-10} sec. The solution is stable

and insensitive with respect to variation of the cutoffs and the length uncertainties. Significant dependence of the two-scan efficiency on length was not observed.

It is necessary to correct τ_{Ξ^0} for two small systematic effects. The fitting program requires the decay tracks from the Λ to be long enough for accurate measurement, $dp/p < 25\%$; this discriminates against long ℓ_3. A study of FAKE events indicates that an increase in the measured lifetime of 2% compensates for this effect. Correction for interactions of Ξ^0 or Λ before they decay is also necessary. After increasing τ_{Ξ^0} by an additional 1% (assuming an average $\sigma_{\Xi^0 p} = \sigma_{\Lambda p} = 20$ mb),[37] we obtain our final result:

$$\tau_{\Xi^0} = (3.07^{+0.22}_{-0.20}) \times 10^{-10} \text{ sec.}$$

The errors have been increased by 1% of the mean life to account for possible systematic effects due to contamination and to fitting ambiguities.

3. Discussion of Lifetime Results

Our determinations are compared with those of previous experiments in Table VIII. Only measurements of τ_{Ξ^-} based on 50 events or more are included. With the exception of the EP-CERN (heavy-liquid bubble chamber) experiment,[11] our value for τ_{Ξ^-} agrees with the other measurements within a standard deviation or so. However, the previous determinations are systematically higher than the present one; their weighted average is $(1.730 \pm 0.054) \times 10^{-10}$ sec. We have no reason to suspect any systematic errors in our determination of the order of 0.1×10^{-10} sec, which would be necessary to remove the apparent discrepancy. Therefore, we assume the discrepancy to be statistical in origin. The weighted average of all the Ξ^- lifetimes in the table yields $\tau_{\Xi^-} = (1.651 \pm 0.032) \times 10^{-10}$ sec. In the

case of the Ξ^0 there is reasonable agreement of our lifetime determination with previous results. A study of the different methods used in previous determinations of τ_{Ξ^0} indicates that an average of the values in the table may not be significant.

The decay rates corresponding to our lifetime determinations are $\lambda_{\Xi^-} = (0.621 \pm 0.015) \times 10^{10}$ sec^{-1} and $\lambda_{\Xi^0} = (0.326 \pm 0.022) \times 10^{10}$ sec^{-1}. The ratio, $\lambda_{\Xi^0}/\lambda_{\Xi^-} = 0.525 \pm 0.038$, is within one standard deviation of the $|\Delta I| = 1/2$ rule prediction of 0.5 (the expected value is 0.485 if phase space is taken into account).

B. Decay Parameters of the Ξ^- and Ξ^0

In the following analysis we assume the Ξ spin to be 1/2. These Ξ^- data combined with the data of Berge et al.[7] yield a 2.5-standard-deviation preference for J = 1/2 over J = 3/2.[5] Analysis of 185 Ξ^- events by the UCLA group yields 3.1-standard-deviation discrimination against J = 3/2.[8] There has as yet been no direct determination of the Ξ^0 spin. Our $\Xi^0 K^0$ data are consistent with $J_{\Xi^0} = 1/2$ (Sec. VI B4).

1. Theory

The decay of a spin 1/2 Ξ into Λ and π may be described by two complex amplitudes A_0 and A_1, corresponding to s and p waves. With proper normalization the decay rate $\lambda_\Xi = 1/\tau_\Xi$ is given by $\lambda_\Xi = |A_0|^2 + |A_1|^2$. Since the overall phase is unmeasurable, only two other independent real parameters are necessary to characterize the decay. It is convenient to define decay parameters α_Ξ, β_Ξ, and γ_Ξ (where $\alpha_\Xi^2 + \beta_\Xi^2 + \gamma_\Xi^2 = 1$) in terms of A_0, A_1:

$$\alpha_\Xi = 2\tau_\Xi \, \mathrm{Re}\,(A_0^* A_1), \tag{6.1a}$$

$$\beta_{\Xi} = 2\tau_{\Xi} \, \mathrm{Im}(A_0^* A_1), \tag{6.1b}$$

$$\gamma_{\Xi} = \tau_{\Xi} \, (|A_0|^2 - |A_1|^2). \tag{6.1c}$$

Expression of $(\alpha, \beta, \gamma)_{\Xi}$ in terms of the spherical coordinates α_{Ξ} and $\Phi_{\Xi} = \tan^{-1}(\beta/\gamma)_{\Xi}$ yields parameters that are nearly uncorrelated (see Table IX). However, use of $(\alpha, \beta, \gamma)_{\Xi}$ facilitates comparison with predictions from invariance of the weak interactions under the transformations C, P, and T.

Existence of nonzero α_{Ξ} or β_{Ξ} implies parity nonconservation in the decay. The phase difference $\Delta = \tan^{-1}(-\beta/\alpha)_{\Xi}$ between the two observed decay amplitudes A_0 and A_1 includes a contribution from the decay and a contribution $(\delta_s - \delta_p)$ from the final-state interaction in the $\Lambda\pi$ system at the Ξ invariant mass. (δ_s and δ_p are the s-wave and p-wave $\Lambda\pi$ phase shifts.) Time-reversal invariance of the decay would require the decay amplitudes to be relatively real, giving a contribution of zero or π to Δ. The measured Δ would then be $(\delta_s - \delta_p)$ or $\pi + (\delta_s - \delta_p)$. Charge-conjugation invariance would require the decay amplitudes to be relatively imaginary, giving a contribution of $\pm \pi/2$ to Δ. There have been no relevant experiments on $\Lambda\pi$ scattering, but SU_3 considerations require the $\Lambda\pi$ phase shifts to be of the same order as the low-energy nucleon-π phase shifts, which are close to zero.[40] If the $\Lambda\pi$ phase shifts are small, T invariance requires $\beta_{\Xi} \approx 0$ and $\gamma_{\Xi} \approx \pm(1-\alpha_{\Xi}^2)^{1/2}$.

The $|\Delta I| = 1/2$ rule requires $A(\Xi^-) = \sqrt{2}\ A(\Xi^0)$ for the full decay amplitudes, so the Ξ^- and Ξ^0 decay parameters are equal. Since $\Lambda\pi$ scattering takes place in a pure isospin state, the $\Lambda\pi^-$ and $\Lambda\pi^0$ phase shifts must be equal.

2. Method and Results

The decay parameters are determined experimentally from the angular distributions of the $\Xi \to \Lambda\pi$ and subsequent $\Lambda \to p\pi^-$ decays. The distribution function describing this decay sequence is

$$\mathcal{P} = \frac{1}{8\pi\sigma}\frac{d\sigma}{d\Omega}\left[(1+\alpha_{\Xi}\vec{P}_{\Xi}\cdot\hat{\Lambda})(1+\alpha_{\Lambda}\vec{P}_{\Lambda}\cdot\hat{p})\right].$$

We express the Λ polarization $\vec{P}_{\Lambda}$ in terms of the Ξ polarization and decay parameters,

$$\vec{P}_{\Lambda} = \frac{1}{1+\alpha_{\Xi}\vec{P}_{\Xi}\cdot\Lambda}\left[(\alpha_{\Xi}+\vec{P}_{\Xi}\cdot\hat{\Lambda})\hat{\Lambda}+\beta_{\Xi}(\vec{P}_{\Xi}\times\hat{\Lambda}) - \gamma_{\Xi}\hat{\Lambda}\times(\hat{\Lambda}\times\vec{P}_{\Xi})\right].$$

Here the Ξ production and polarization distributions are functions of production variables. We take, for all production modes, only the component of the polarization $\vec{P}_{\Xi}$ along the production normal $\hat{n} = (\hat{\Xi}\times\hat{K}^-)/|\hat{\Xi}\times\hat{K}^-|$. This convention agrees with that used in the two-body production analysis. Combining the above two expressions, we write

$$\mathcal{P}(\xi,\eta,\phi;\alpha_{\Lambda},\alpha_{\Xi},\Phi_{\Xi}) = \frac{1}{8\pi\sigma}\frac{d\sigma}{d\Omega}\left[(1+\alpha_{\Lambda}\alpha_{\Xi}\hat{\Lambda}\cdot\hat{p}) + P_{\Xi}\left\{\alpha_{\Xi}\hat{\Lambda}\cdot\hat{n}+\alpha_{\Lambda}\hat{\Lambda}\cdot\hat{p}\hat{\Lambda}\cdot\hat{n} + \alpha_{\Lambda}\sin\theta\,(\beta_{\Xi}\hat{Y}\cdot\hat{p} - \gamma_{\Xi}\hat{X}\cdot\hat{p})\right\}\right]. \tag{6.2}$$

The Ξ decay is characterized by the single polar angle $\xi = \cos\theta = \hat{\Lambda}\cdot\hat{n}$ between $\hat{n}$ and the Λ direction in the Ξ rest frame. The Λ decay is characterized by the angles η, ϕ, giving the projections of $\hat{p}$, the proton direction in the Λ rest frame, on the coordinate triad

$$\hat{X} = \hat{\Lambda}\times(\hat{\Lambda}\times\hat{n})/\sin\theta,\quad \hat{Y} = (\hat{n}\times\hat{\Lambda})/\sin\theta,\quad \text{and}\quad \hat{Z} = \hat{\Lambda},$$

$$\left(\eta = \hat{\Lambda}\cdot\hat{p},\ \text{and}\ \phi = \tan^{-1}(\hat{Y}\cdot\hat{p}/\hat{X}\cdot\hat{p})\right).$$ [41]

The distribution function (6.2) yields five moments

$$\langle \hat{\Lambda}\cdot\hat{p}\rangle = \frac{1}{3}\alpha_\Lambda\alpha_{\Xi}, \quad \text{(a)}$$

$$\langle \hat{\Lambda}\cdot\hat{n}\rangle = \frac{1}{3}\alpha_{\Xi}\langle P_{\Xi}\rangle, \quad \text{(b)}$$

$$\langle (\hat{\Lambda}\cdot\hat{p})(\hat{\Lambda}\cdot\hat{n})\rangle = \frac{1}{9}\alpha_\Lambda\langle P_{\Xi}\rangle, \quad \text{(c)} \qquad 6.3$$

$$\langle (\hat{Y}\cdot\hat{p})\sin\theta\rangle = \frac{2}{9}\alpha_\Lambda\beta_{\Xi}\langle P_{\Xi}\rangle = \frac{2}{9}\alpha_\Lambda\sqrt{1-\alpha_{\Xi}^2}\,\sin\Phi_{\Xi}\langle P_{\Xi}\rangle, \quad \text{(d)}$$

$$-\langle (\hat{X}\cdot\hat{p})\cos\theta\rangle = \frac{2}{9}\alpha_\Lambda\gamma_{\Xi}\langle P_{\Xi}\rangle = \frac{2}{9}\alpha_\Lambda\sqrt{1-\alpha_{\Xi}^2}\,\cos\Phi_{\Xi}\langle P_{\Xi}\rangle. \quad \text{(e)}$$

Values of the decay parameters could be obtained from a least-square fit to (6.3), but the variation of $\langle P_{\Xi}\rangle$ and the error correlations are difficult to treat properly. Maximum likelihood is a more convenient fitting method. The fit consists of maximizing the logarithm of the likelihood

$$W = \sum_{k=1}^{N} \ell n\ \mathscr{P}_k(\xi_k\eta_k\phi_k;\ \alpha_\Lambda\alpha_{\Xi}\,\Phi_{\Xi})$$

as a function of the parameters α_Λ, α_{Ξ}, Φ_{Ξ}.

If the variation of the Ξ polarization as a function of total energy and production angle is unknown, one may maximize W also as a function of parameters $\langle P_{\Xi}\rangle$, the polarization averages in each bin of production angle and energy. At low momentum, $p_K \lesssim 1.6$ GeV/c, the variation of Ξ polarization with production angle in $K^-p \to \Xi^-K^+$ is slow enough to justify this bin method.[7] At our momenta, many partial waves are present; the bin method is inadequate for some reactions because of the resulting rapid variation of the polarization. Consequently we have assumed that the polarization varies smoothly with production angle in order to get maximum information on its variation.

The experimental variation of Ξ polarization was obtained by expanding the distributions $P_{\Xi}\, d\sigma/d\Omega$ and $d\sigma/d\Omega$ in Legendre functions and

evaluating the quotient at the production angle of each event. The expansion coefficients were estimated as moments[41] and the expansion was cut off when additional terms no longer yielded significant improvement of the fit to the data, as described in Sec. IV. The product $\hat{\Xi} \cdot \hat{K}^-$ was used as the expansion variable regardless of the number of final-state particles. Trial values $\alpha_{\Xi} = -0.40$, $\alpha_{\Lambda} = 0.647$, and $\Phi_{\Xi} = 6$ deg were used initially in expanding $P_{\Xi} \frac{d\sigma}{d\Omega}$, and the polarizations resulting from the expansion were scaled by a common factor which was a free parameter in the likelihood fit. For very large numbers of events the free parameter multiplying the polarizations would adjust itself to compensate for the arbitrariness of the trial values. This is a consequence of the independence of production and decay; the relative size of the B_ℓ's does not depend on α_{Ξ} and Φ_{Ξ} in the limit of large numbers. However, for our numbers of events it was necessary to iterate the procedure until the input and output α_{Ξ}, Φ_{Ξ} were equal. Convergence was attained in a few iterations. Roughly 7% of the events yielded $|P_{\Xi}| > 1$ due to statistical fluctuations of the expansion coefficients. For such events, P_{Ξ} was set equal to -1 or +1. The method outlined here is essentially equivalent to a simultaneous fit to the decay distribution of the Ξ and the variation of polarization in the Ξ production. However, the method avoids the difficulties that would arise from the very large number of free parameters required to do a simultaneous fit for several reactions at a number of energies.

The likelihood function was constructed by using the complete sample of Ξ^- events with visible Λ decays, all the $\Xi^0 K^0$ events, and those $\Xi^0 K^+ \pi^-$ events for which Λ decay did not fit with the production vertex as the origin.[42] Table IX summarizes the likelihood fits. Fits using the two-body final states

alone were also carried out; the two-body and multibody events give consistent results. Fits have been performed with the Ξ^- and Ξ^0 parameters independently varied as well as with $\alpha_{\Xi^-} = \alpha_{\Xi^0}$ and $\Phi_{\Xi^-} = \Phi_{\Xi^0}$, as predicted by the $|\Delta I| = 1/2$ rule. For the most part, we have constrained α_Λ to be close to the accepted[14] value by including a term

$$-1/2\left(\frac{\alpha_\Lambda - 0.647}{0.020}\right)^2$$

in the logarithm of the likelihood function. However, α_Λ was left free in some of the fits for the purpose of determining α_Λ independently.

The polarization-independent term $1 + \alpha_\Lambda \alpha_{\Xi^-} \hat{\Lambda} \cdot \hat{p}$ has also been fitted separately and best values of $\alpha_\Lambda \alpha_{\Xi^-}$ tabulated. The additional precision in determining α_{Ξ^-} obtained from the polarization-dependent terms of the distribution function reduces the uncertainty by 20%, under the assumption $\alpha_\Lambda = 0.647 \pm 0.020$. Distributions of $\hat{\Lambda} \cdot \hat{p}$ are plotted in Fig. 19 for all Ξ^- and Ξ^0 (shaded), along with the results of the fit to $\hat{\Lambda} \cdot \hat{p}$ alone.

Our results are, after corrections described below,

$$\alpha_{\Xi^-} = -0.391 \pm 0.045, \tag{6.4a}$$

$$\Phi_{\Xi^-} = -14 \pm 11 \text{ deg}, \tag{6.4b}$$

$$\alpha_{\Xi^0} = -0.43 \pm 0.09, \tag{6.5a}$$

$$\Phi_{\Xi^0} = 38 \pm 19 \text{ deg}, \tag{6.5b}$$

with $\alpha_\Lambda = 0.650 \pm 0.019$. With the $|\Delta I| = 1/2$ assumption we obtain

$$\alpha_{\Xi} = -0.400 \pm 0.040, \tag{6.6a}$$

$$\Phi_{\Xi} = -5 \pm 10 \text{ deg}. \tag{6.6b}$$

Our best independent value for α_Λ (determined in a fit to the Ξ^- and Ξ^0 events with the resulting $\alpha_{\Xi^-} = -0.393 \pm 0.042$, $\phi_{\Xi^-} = -5 \pm 10$ deg) is

$$\alpha_\Lambda = 0.67 \pm 0.06. \tag{6.7}$$

In an earlier Ξ decay-parameter analysis,[7] solutions with $\gamma_{\Xi^-} < 0$ ($\phi_{\Xi^-} \approx \pi$) were found to exist, although the likelihood in the Ξ^- case was much smaller than that for $\gamma_{\Xi^-} > 0$. For the Ξ^0, we have found $15 < \ell n \mathcal{L} < 19$ in the region $\phi_{\Xi^0} \approx \pi$, compared with $\ell n \mathcal{L} = 25.5$ for the $\gamma_{\Xi^0} > 0$ solution. The iteration procedure described above did not converge for these fits. Thus $\gamma_{\Xi^0} < 0$ appears highly unlikely.

The Ξ^0 sample is slightly biased by the presence of contamination by non-Ξ^0 events (see Sec. II. A) and by the loss of $\Xi^0 K^+ \pi^-$ events when the Λ points to the primary vertex.[42] We have corrected α_{Ξ^0} by 5% to account for the contamination; ϕ_{Ξ^0} does not require correction. The effects of scanning, measurement, and fitting losses as well as the effect of precession of Ξ and Λ polarization in the magnetic field of the bubble chamber are negligible at our level of statistical precision. We have increased the errors in (6.4) through (6.7) by 1.1 for $\alpha_{\Xi^-, \Lambda}$ and $\sqrt{2}$ for Φ_{Ξ^-} to account for uncertainties in the fitting procedure which cannot be directly estimated from the likelihood function.[43]

3. Comparison of Experimental Determinations of Ξ Decay Parameters

Table X contains the results of previous measurements of Ξ decay parameters. Only experiments with 100 or more events are included.[44] The line labeled LRL '66 presents the results of a fit to the earlier LRL data using the binning method of Berge et al. and a value of $\alpha_\Lambda = 0.647 \pm 0.020$. The errors have been multiplied by 1.1 and 1.2 for α_{Ξ^-} and Φ_{Ξ^-} respectively. In the last line we have averaged the LRL '68 results with those of LRL '66. Assuming equality of the Ξ^- and Ξ^0 parameters, we obtain

$$\alpha_{\Xi^-} = -0.380 \pm 0.034, \tag{6.8a}$$

$$\Phi_{\Xi^-} = -1 \pm 7 \text{ deg.} \tag{6.8b}$$

Values $\alpha_{\Xi^-} = -0.38$ and $\Phi_{\Xi^-} = 0$ were used in Sec. IV for the production analysis.

The experimental results on Ξ-decay parameters to date may be summarized as follows. The parameters α_{Ξ^-} and Φ_{Ξ^-} for Ξ^- and Ξ^0 are consistent with equality, in agreement with the predictions of the $|\Delta I| = 1/2$ rule. The phase angle Φ_{Ξ^-} is consistent with zero; thus there is no evidence for violation of time-reversal invariance in Ξ decay. Since Φ_{Ξ^-} is inconsistent with ± 90 deg, C invariance in Ξ decay is ruled out unless the $\Lambda\pi$ phase shifts are anomalously large. The decay parameter γ_{Ξ^-} is nearly +1; thus the decay is predominantly s-wave. If we assume on the basis of the $\approx 10^{-3}$ branching ratio of $K_L^0 \to 2\pi$ that T violation in nonleptonic hyperon decay is a small effect, < 0.01 in β,[45] then at the Ξ mass the $\Lambda\pi$ scattering phase shift $(\delta_s - \delta_p) \approx \Delta - \pi = \tan^{-1}(-\beta/\alpha)_{\Xi^-} - \pi$. Experimentally from (6.8), $\Delta = 178 \pm 16$ deg so $(\delta_s - \delta_p) = -2 \pm 16$ deg.

Alternatively we note[46] that if $\beta_{\Xi^0}/\alpha_{\Xi^0} \neq \beta_{\Xi^-}/\alpha_{\Xi^-}$ both time reversal and the $\Delta I = 1/2$ rule are violated, independent of the $\Lambda\pi$ scattering phase shifts. Such a situation might be expected if CP violation occurred in $\Delta I \geq 3/2$ transitions only. The consistency of our results for Ξ^0 and Ξ^- (last line of Table X) provides no evidence of such CP violation.

4. Spin of the Ξ^0

The formalism developed by Byers and Fenster[47] leads to the expression

$$(2J+1) = \frac{\left[\langle \hat{Y}\cdot\hat{p}\sin\theta\rangle^2 + \langle \hat{X}\cdot\hat{p}\sin\theta\rangle^2\right]^{1/2}}{(1-\alpha_{\Xi^-}^2)^{1/2}\,|\langle(\hat{\Lambda}\cdot\hat{p})(\hat{\Lambda}\cdot\hat{n})\rangle|} \quad . \tag{6.9}$$

Table XI shows the results of evaluating (6.9) for several ΞK samples. The value $\alpha_{\Xi^-} = -0.38$ was used and $\hat{n}$ was rotated by 180 deg about the

beam direction for the 1.7-GeV/c $\Xi^0 K^0$ and for the two positive polarization bins of $\Xi^- K^+$. In all cases the results are consistent with $J = 1/2$.

Previous work[7] has indicated that our determination of $\alpha_{\Xi\Lambda}$, $\Phi_{\Xi\Lambda}$ (defined in terms of p- and d-wave amplitudes) would yield nearly identical results in the unlikely case that $J_{\Xi\Lambda} = 3/2$.

VII. UNUSUAL Ξ DECAYS

A. Ξ^- Decays

We have searched for Ξ^- decay modes other than the usual $\Xi^- \to \Lambda\pi^-$ mode. The following modes were considered:

$$\Xi^- \to \Lambda\pi^-\gamma, \quad \text{(A)}$$

$$\Lambda e^- \bar{\nu}, \quad \text{(B)}$$

$$\Lambda\mu^-\bar{\nu}, \quad \text{(C)}$$

$$\Sigma^0 e^-\bar{\nu},\ \Sigma^0 \to \Lambda\gamma, \quad \text{(D)}$$

$$n\pi^-. \quad \text{(E)}$$

1. Modes with $|\Delta S| = 1$

Candidate events for modes (A) through (D), topologically identical to normal Ξ^- decays, fitted Λ decay with the Λ originating at the Ξ^- decay point but failed to fit $\Xi^- \to \Lambda\pi^-$ decay. These candidates were fitted to each production hypothesis followed by the decays (A), (B), (C). Mode (D) is underconstrained and cannot be fitted. Eight candidates fit $\Xi^- \to \Lambda e^- \bar{\nu}$; three of these also fit $\Xi^- \to \Lambda\mu^-\bar{\nu}$ and two of these three fit $\Xi^- \to \Lambda\pi^-\gamma$ as well. Two of the eight have clearly identifiable electrons and are unambiguous examples of Ξ^- beta decay. These two events have been reported previously[48] and are not discussed further here. The negative decay tracks of the three events fitting the muonic

decay mode (C) have ionization consistent with either π^- or μ^-; in one event this track may also be an electron. The other tracks in each event are consistent in their bubble density with Ξ production. The upper limit for the branching fraction of Ξ^- into μ^- is based on these three events, and the limit for the radiative mode (A) on the two events that fit $\Xi^- \rightarrow \Lambda\pi^-\gamma$.

For the electronic decay modes (B) and (D) we have restricted the sample to events with measured negative decay track momentum less than 200 MeV/c, the maximum momentum at which we can distinguish electrons and pions unambiguously by their ionization. The two examples of $\Xi^- \rightarrow \Lambda e^- \bar{\nu}$ are the only events in the sample with identified electrons; there are no serious candidates for $\Xi^- \rightarrow \Sigma^0 e^- \bar{\nu}$.

The branching fractions for the unusual Ξ^- decay modes are based on the restricted sample of 2610 events with visible Λ decay used for the lifetime determination (see Sec. VI. A). We have measured our detection efficiency for each mode by Monte-Carlo-generating a sample of each decay, using a realistic Ξ^- momentum distribution and phase space for the momentum distribution of the decay products in the Ξ^- rest frame. For the pionic mode (A) and the muonic mode (C) the efficiencies are 95% and 90% respectively; events are lost only if they fit the normal decay mode. For the electronic modes (B) and (D), events are also missed if the electron momentum is greater than 200 MeV/c; the efficiencies are 70% and 85%. We obtain the following branching fractions for the $|\Delta S| = 1$ modes:

$$B_A(\Xi^- \to \Lambda\pi^-\gamma) \leq 2/(0.95\times 2610) \approx 0.8\times 10^{-3},$$
$$B_B(\Xi^- \to \Lambda e^- \bar{\nu}) = (1.0 \pm^{1.3}_{0.65}) \times 10^{-3},$$
$$B_C(\Xi^- \to \Lambda\mu^- \bar{\nu}) \leq 3/(0.90\times 2610) \approx 1.3\times 10^{-3},$$
$$B_D(\Xi^- \to \Sigma^0 e^- \bar{\nu}) < 1/(0.85\times 2610) \approx 5\times 10^{-4}.$$

2. Mode with $|\Delta S| = 2$

No decay with a strangeness change of 2 has ever been observed. We have searched for examples of $\Xi^- \to n\pi^-$ (mode E) only among the two-body production events, $K^-p \to \Xi^-K^+$, without a visible Λ decay.

Candidates for mode (E) were required to satisfy the following criteria:

(a) The production vertex had to lie in a restricted fiducial volume, to ensure measurability.

(b) The track length ℓ of the decaying particle had to satisfy $0.5 < \ell < 25.0$ cm. Rejection of events with unusually long decaying tracks greatly reduces background due to K^-p scattering with subsequent K^- decay in the chamber.

(c) The component of momentum of the decay track transverse to the Ξ direction had to be greater than 200 MeV/c. This restriction removes only 25% of the real $\Xi^- \to n\pi^-$ decays, for which the decay momentum q is 303 MeV/c, while excluding all the normal $\Xi^- \to n\pi^-$ decays (q = 139 MeV/c) and nearly all the $\Sigma^- \to n\pi^-$ background (q = 193 MeV/c).

(d) The event must not have fitted elastic scattering or Σ^- production and decay.

(e) Finally, the event had to give a satisfactory fit, consistent with the observed ionization, to Ξ^-K^+ production followed by $\Xi^- \to n\pi^-$ decay.

Of the more than 33 000 topological candidates there is no event that satisfies all criteria. There are 866 $\Xi^- K^+$ events with visible Λ^0 in the sample that satisfy (a) and (b). Criterion (c) would remove 25% of the $|\Delta S| = 2$ decays. Criterion (d) would remove roughly 12%; however, most of these would have been recovered by inspection of the bubble density of the tracks. Our efficiency for detecting $\Xi^- \to n\pi^-$ events that satisfy (a) and (b) is about 70%. Correcting for invisible Λ decays, we find the upper limit for $|\Delta S| = 2$ nonleptonic Ξ^- decay to be

$$B_E(\Xi^- \to n\pi^-) < 1/(0.7 \times 1.53 \times 866) \approx 1.1 \times 10^{-3}.$$

B. Ξ^0 Decays

We have also searched for the following Ξ^0 decay modes:

$$\Xi^0 \to \Sigma^+ e^- \bar{\nu}, \quad \text{(F)}$$
$$\Sigma^+ \mu^- \bar{\nu}, \quad \text{(G)}$$
$$\Sigma^- e^+ \nu, \quad \text{(H)}$$
$$\Sigma^- \mu^+ \nu, \quad \text{(I)}$$
$$p e^- \bar{\nu}, \quad \text{(J)}$$
$$p \mu^- \bar{\nu}, \quad \text{(K)}$$
$$p\pi^-. \quad \text{(L)}$$

The search was limited to two-V^0 events with visible K^0 decay and to $V^0 K^+ \pi^-$ events. This sample includes 890 ± 50 normal Ξ^0 events with a visible Λ decay (correction for unseen Λ decays yields 1360 ± 75 events in the effective denominator).

1. Modes with $|\Delta S| = 1$.

We attempted to find both the $\Delta S = \Delta Q$ decay modes (F) and (G) and the $\Delta S = -\Delta Q$ modes (H) and (I). No serious candidates were discovered.

However, scanners might have missed such events through misidentification of the hyperon decay sequence as $\pi \rightarrow \mu \rightarrow e$. We estimate the scanning efficiency to be 50% and obtain upper limits for the branching ratios:

$$B_{F-I}(\Xi^0 \rightarrow \Sigma^{\pm} \ell^{\mp} \nu) < 1/(0.5 \times 1360) \approx 1.5 \times 10^{-3}.$$

2. Modes with $|\Delta S| = 2$

The $|\Delta S| = 2$ modes (J) through (L) are topologically identical to the normal sequence,

$$\Xi^0 \rightarrow \Lambda \pi^0, \quad \Lambda \rightarrow p\pi^-.$$

Candidates were required to satisfy the criteria

(a) The missing mass for the Ξ^0 had to be within 80 MeV/c^2 of the Ξ^0 mass.

(b) The V which is a candidate for Ξ^0 decay must not have fitted either K^0 or Λ decay, with or without a specified origin.

(c) The event has to fit Ξ^0 production followed by one of decay modes (J), (K), or (L). The observed ionization of all tracks had to be consistent with the hypothesis.

(d) The event had to have measured Ξ^0 length greater than 0.5 cm and satisfy the fiducial volume requirements applied in the lifetime analysis.

For modes (J) and (K) we imposed the additional requirement that the K^+ in the one-V events be unambiguously identified by its ionization or decay in the chamber. Such identification is possible in about 50% of the $\Xi^0 K^+ \pi^-$ events.

After imposition of the above criteria, we were left with only one candidate for $K^- p \rightarrow \Xi^0 K^0$ followed by $\Xi^0 \rightarrow p\mu^-\bar{\nu}$ (K). The negative decay track in this event cannot be unambiguously identified as a muon; we regard

the event as being ambiguous with pionic decay.

The probability that a real example of one of the $|\Delta S| = 2$ decay modes would fail to satisfy the criteria was estimated from Monte Carlo-generated events. The efficiency of the missing-mass selection (a) is 99% for $\Xi^0 K^0$ events and 93% for $\Xi^0 K^+ \pi^-$ events. The net detection efficiency is 55% for the leptonic modes and 85% for the non-leptonic mode. Our upper limits are

$$B_J(\Xi^0 \to p\, e^- \bar{\nu}) < 1/(0.55 \times 1360) \approx 1.3 \times 10^{-3},$$
$$B_K(\Xi^0 \to p \mu^- \bar{\nu}) \leq 1/(0.55 \times 1360) \approx 1.3 \times 10^{-3},$$
$$B_L(\Xi^0 \to p \pi^-) < 1/(0.85 \times 1360) \approx 0.9 \times 10^{-3}.$$

C. Discussion

The only unusual Ξ decay mode observed unambiguously to date is $\Xi^- \to \Lambda e^- \bar{\nu}$. In addition to our two events,[48] one certain event has been found at UCLA,[49] and one unambiguous plus one ambiguous event have been found at Brookhaven.[10] Our branching ratio is $B = \Xi^- \to \Lambda e^- \bar{\nu} / \Xi^- \to \Lambda \pi^- = (1.0 \pm {}^{1.3}_{0.65}) \times 10^{-3}$. This result is consistent with the Cabibbo theory of leptonic decays,[50] in which the weak hadronic currents transform as members of an SU_3 octet. Recent fits to this theory predict $B \approx 0.6 \times 10^{-3}$.[51]

The $\Delta S = 0$ leptonic decay, $\Xi^- \to \Xi^0 e^- \bar{\nu}$, and the other $\Delta S = \Delta Q = 1$ leptonic decays, $\Xi^- \to \Lambda \mu^- \bar{\nu}$ and $\Xi \to \Sigma \ell^- \bar{\nu}$, are also described by the Cabibbo theory. The upper limits for these modes are consistent with the predictions, as shown in Table XII.

Hadronic currents with $\Delta S = -\Delta Q$ cannot be members of an SU_3 octet. If these currents are placed in a single 10, $\overline{10}$, or 27 representation of SU_3,

the rates for $\Xi^0 \to \Sigma^- \ell^+ \nu$ are related to those for $\Sigma^+ \to n\ell^+\nu$.[52] Three possible $\Sigma^+ \to n\ell^+\nu$ events have been reported.[53] The theoretical estimates in Table XII for $\Xi^0 \to \Sigma^-\ell^+\nu$ are based on these three events.[52]

The $\Delta S = 2$ leptonic decays, $\Xi \to N\ell^-\bar{\nu}$, could be related to the $\Delta S = -\Delta Q$ leptonic decays if the two currents belong to the same SU_3 representation.[52, 54] The theoretical upper limits in Table XII assume such currents coupled with equal weight to the current of leptons.

Glashow has shown that nonleptonic $\Delta S = 2$ decays, $\Xi \to N\pi$, might arise even in the absence of first-order contributions to the $K_1^0 - K_2^0$ mass difference.[55] A branching ratio of $\approx 10^{-4}$ to 10^{-6} could then be expected.[56]

The three-body radiative decay rates $\Xi \to \Lambda\pi\gamma$ have been calculated from inner brehmsstrahlung;[57] the $\Sigma^- \to n\pi^-\gamma$ results[58] are consistent with these calculations. The current-algebra calculations of Gupta et al.[59] yield a large branching ratio for $\Xi^0 \to \Lambda\pi^0\gamma$; however, the rate predicted for $\Sigma^- \to n\pi^-\gamma$ is 100 times the experimental value.[58] The branching ratio for $\Xi^- \to \Lambda\pi^-\gamma$ with π^- momentum in the Ξ rest frame smaller than 125 MeV/c would be $\approx 10^{-3}$ from inner brehmsstrahlung.

All these predictions are compared with the experimental results for Ξ decays in Table XII.

ACKNOWLEDGMENTS

We wish to thank Dr. Frank T. Solmitz, Professor Arthur H. Rosenfeld, Professor M. Lynn Stevenson, and Professor Robert D. Tripp for helpful comments on this work. We appreciate the extensive contributions of Dr. Janice Button-Shafer to the preliminary analyses of these data. The early work of Dr. Gerald A. Smith and Dr. James S. Lindsey on $\Xi^*(1815)$ and $\Xi^*(1930)$ is also much appreciated. Discussions with Professor J. D. Jackson, Dr. Christoph Schmid, and Dr. Charles Wohl were highly informative. We are grateful to Dr. Tom Trippe for making his data available prior to publication. We are indebted to our scanning and measuring staff; the contribution of Miss Jo Canada Cochran is particularly appreciated.

We are indebted to Dr. Joseph J. Murray for the design of the K^- beam. The bubble chamber and Bevatron crews are thanked for their untiring efforts.

The support and encouragement of Professor Luis W. Alvarez is gratefully acknowledged.

APPENDIX: CORRECTION FOR LOSS OF SMALL-ANGLE Ξ^- DECAYS

The loss of small-angle Ξ^- decays was estimated by using a Monte Carlo technique to correct the $\hat{\Lambda}$ (Ξ rest frame) $\cdot$ $\hat{\Xi}$ (lab) distribution to isotropy. (Isotropy of this distribution is a consequence of the absence of longitudinal Ξ polarization in the two-body events and the fact that we average over all other angular variables in the multibody events.) A large number of Ξ^- decays were generated in the Ξ rest frame and Lorentz-transformed into the laboratory frame by using the observed Ξ^- momentum spectrum. Various models of the loss at small projected angles were constructed, and the effect of each on the $\hat{\Lambda} \cdot \hat{\Xi}$ distribution of the Monte Carlo events was checked against the $\hat{\Lambda} \cdot \hat{\Xi}$ distribution of the real events (Fig. 20). It was found that a sharp cutoff of the projected angle at 3 deg gives an acceptable fit to the data as shown by the curve in Fig. 20(a). This assumed 3-deg cutoff was used to obtain detection probabilities, P_D, for 20 bins of $\hat{\Lambda} \cdot \hat{\Xi}$ and 11 bins of the Ξ^- momentum, which ranges from 0.5 to 2.9 GeV/c. These probabilities are independent of the sharp-cutoff model; very similar results were obtained by using a smooth fall-off of detection probability with projected angle. The model is also approximate in the sense that it fails to account properly for the fact that the scanner sees the event projected in three different planes. It was found that the detection probability for a Ξ^- decay due to the small-angle effect is $90 \pm 3\%$ averaged over $\hat{\Lambda} \cdot \hat{\Xi}$ and over Ξ^- momentum, with a variation from 95% to 84% with increasing momentum. P_D varies from a maximum of 98% to as little as 31% for fast Ξ^- with $\hat{\Lambda} \cdot \hat{\Xi} < -0.9$.

Table I. Path lengths.

P_{K^-} (GeV/c)	$\mathcal{L}_{K^-}$ (ev/μb)	$\frac{\mathcal{L}_{\pi^-}}{\mathcal{L}_{\pi^-}+\mathcal{L}_{K^-}}$ (%)
1.70 ± 0.02	3.34 ± 0.06	4.6 ± 1.8
2.10 ± 0.03	5.86 ± 0.09	3.3 ± 1.2
2.47 ± 0.03	1.80 ± 0.05	$6.9^{+5.3}_{-3.3}$
2.64 ± 0.08	13.11 ± 0.16	16.8 ± 2.4

Table II. Total cross sections.

Reaction	P_{K^-} (GeV/c)	Events	σ (μb)
$K^-p \to \Xi^-K^+$	1.70	329	175 ± 16
	2.10	376	112 ± 10
	2.47	78	87 ± 14
	2.64	388	58 ± 6
$K^-p \to \Xi^0K^0$	1.70	51	100 ± 23
	2.10	34	25 ± 7
	2.47	7	24 ± 11
	2.64	44	15 ± 4
$K^-p \to \Xi^-K^+\pi^0$	1.70	38	16 ± 4
	2.10	120	36 ± 5
	2.47	55	58 ± 10
	2.64	307	40 ± 4
$K^-p \to \Xi^-K^0\pi^+$	1.70	119	54 ± 7
	2.10	379	97 ± 9
	2.47	92	70 ± 11
	2.64	612	67 ± 5
$K^-p \to \Xi^0K^+\pi^-$	1.70	65 ± 11[a]	34 ± 7
	2.10	200 ± 19[a]	60 ± 9
	2.47	56 ± 9[a]	57 ± 12
	2.64	452 ± 42[a]	65 ± 9
$K^-p \to \Xi^-K^+\pi^+\pi^-$	2.64	79	11 ± 2
$K^-p \to \Xi^-K^0\pi^+\pi^0$	2.64	42	12 ± 3
$K^-p \to \Xi^0K^0\pi^+\pi^-$	2.64	25 ± 5[a]	10 ± 3

[a] Corrected for contamination and loss due to fitting ambiguities.

Table III. Polarization in $K^- p \to \Xi K$. The average polarization along the production normal $\hat{n} = (\hat{K}_{in} \times \hat{K}_{out})/|\hat{K}_{in} \times \hat{K}_{out}|$ in each bin of momentum and production angle was calculated as a moment of the distribution function (6.2).

P_{K^-} (GeV/c)	Interval of $\hat{K}_{in} \cdot \hat{K}_{out}$	Events	$\langle P_\Xi \rangle$
$K^- p \to \Xi^- K^+$			
1.70	-1.0 → -0.95	39	0.34 ± 0.39
	-0.95 → -0.8	85	-0.43 ± 0.26
	-0.8 → -0.5	81	-0.24 ± 0.27
	-0.5 → 0.0	30	-0.13 ± 0.45
	0.0 → 0.5	38	-1.01 ± 0.36
	0.5 → 1.0	39	-0.51 ± 0.38
	-1.0 → 1.0	313	-0.35 ± 0.14
2.10	-1.0 → -0.95	34	0.16 ± 0.42
	-0.95 → -0.8	89	-0.22 ± 0.26
	-0.8 → -0.5	82	-0.16 ± 0.27
	-0.5 → 0.0	45	0.07 ± 0.37
	0.0 → 0.5	40	-1.18 ± 0.34
	0.5 → 1.0	67	-0.03 ± 0.30
	-1.0 → 1.0	357	-0.24 ± 0.13
2.47	-1.0 → 0.0	41	-0.83 ± 0.36
	0.0 → 1.0	36	-1.28 ± 0.35
	-1.0 → 1.0	77	-1.06 ± 0.25
2.64	-1.0 → -0.95	69	-0.01 ± 0.30
	-0.95 → -0.8	88	-0.31 ± 0.26
	-0.8 → 0.5	81	-0.53 ± 0.27
	-0.5 → 0.1	59	-0.44 ± 0.31
	0.1 → 1.0	66	-0.48 ± 0.30
	-1.0 → 1.0	373	-0.35 ± 0.13

Table III. (continued)

$K^- p \to \Xi^0 K^0$			
1.70	-1.0 → 0.0	33	0.50 ± 0.42
	0.0 → 1.0	18	0.97 ± 0.53
	-1.0 → 1.0	51	0.67 ± 0.33
2.10	-1.0 → 0.0	14	0.56 ± 0.64
	0.0 → 1.0	20	-1.41 ± 0.45
	-1.0 → 1.0	34	-0.60 ± 0.41
2.6[a]	-1.0 → 0.0	30	-0.39 ± 0.44
	0.0 → 1.0	21	-0.25 ± 0.54
	-1.0 → 1.0	51	-0.33 ± 0.34

[a] The data at 2.47 and 2.64 GeV/c have been combined.

Table IV. Legendre polynomial expansion coefficients of $\Xi^- K^+$ differential cross section. The expansion is of the form $d\sigma/d\Omega = \sigma/4\pi \Sigma_{\ell=0} (A_\ell/A_0) P_\ell(\cos\Theta)$, where $A_0 = \sigma/4\pi\lambda^2$, $\cos\Theta = \hat{K}^- \cdot \hat{K}^+$, and λ is $\hbar$ divided by the initial-state c.m. momentum. The A_ℓ/A_0 are shape parameters independent of the total cross section.

P_{K^-} in (GeV/c) =	1.7	2.1	2.47	2.64
$10^3 \times A_0$ =	20.8±1.9	17.2 ± 1.5	16.3 ± 2.6	11.9 ± 1.2
ℓ		(A_ℓ/A_0)		
0	1	1	1	1
1	-1.22 ± 0.11	-1.05 ± 0.11	-1.29 ± 0.19	-1.64 ± 0.09
2	1.55 ± 0.14	1.50 ± 0.13	1.02 ± 0.31	1.60 ± 0.15
3	-1.08 ± 0.18	-0.79 ± 0.18	-1.25 ± 0.33	-1.82 ± 0.18
4	0.37 ± 0.21	0.24 ± 0.20	0.70 ± 0.36	1.54 ± 0.22
5	-0.15 ± 0.24	-0.17 ± 0.22	-0.12 ± 0.43	-0.84 ± 0.25
6	0.16 ± 0.26	0.34 ± 0.24	-0.50 ± 0.47	0.84 ± 0.27
7	-0.38 ± 0.28	0.08 ± 0.27	0.92 ± 0.52	-1.00 ± 0.30
8	-0.18 ± 0.30	-0.38 ± 0.29	-1.30 ± 0.55	0.70 ± 0.32
9	0.09 ± 0.30	-0.04 ± 0.31	0.78 ± 0.57	-0.27 ± 0.34
10	0.05 ± 0.32	-0.09 ± 0.33	-0.02 ± 0.60	-0.21 ± 0.36
11	-0.01 ± 0.34	-0.14 ± 0.34	0.51 ± 0.63	0.18 ± 0.38
12	0.20 ± 0.36	0.28 ± 0.35	-0.16 ± 0.64	-0.09 ± 0.39

Table V. Legendre polynomial expansion coefficients of $\Xi^0 K^0$ differential cross section.

P_{K^-} in (GeV/c)	1.7	2.1	2.6[a]
$10^3 \times A_0$ =	11.7 ± 2.7	3.8 ± 1.1	3.2 ± 0.8
ℓ		(A_ℓ/A_0)	
0	1	1	1
1	-0.86 ± 0.30	0.36 ± 0.47	-0.42 ± 0.35
2	0.95 ± 0.41	2.48 ± 0.46	1.36 ± 0.43
3	0.27 ± 0.51	-0.68 ± 0.81	-1.45 ± 0.47
4	0.63 ± 0.55	2.26 ± 0.79	1.05 ± 0.56
5	1.14 ± 0.58	0.07 ± 0.96	-1.40 ± 0.61
6	0.20 ± 0.63	2.20 ± 0.99	-0.42 ± 0.66
7	0.98 ± 0.65	-0.09 ± 1.13	0.06 ± 0.67

[a] The data at 2.47 and 2.64 GeV/c have been combined.

Table VI. Cross sections for $\Xi^*(1530)$ and $K^*(890)$ production in $K^- p \to \Xi K \pi$.

Final State	Ξ^* Fraction (%)	σ_{Ξ^*}[a] (μb)	K^* Fraction (%)	σ_{K^*}[a] (μb)
$\Xi^- K^+ \pi^0$				
1.7 GeV/c	64 ± 11	10 ± 3	——	——
2.1 GeV/c	20 ± 5	7 ± 2	23 ± 7	8 ± 3
2.6 GeV/c	11 ± 2	4.6 ± 1.0	32 ± 4	13 ± 2
$\Xi^- K^0 \pi^+$				
1.7 GeV/c	88 ± 4	47 ± 6	——	——
2.1 GeV/c	55 ± 5	53 ± 7	10 ± 5	18 ± 3
2.6 GeV/c	24 ± 2	16 ± 2	33 ± 3	22.1 ± 2.6
$\Xi^0 K^+ \pi^-$				
1.7 GeV/c	51 ± 9[b]	18 ± 5	——	——
2.1 GeV/c	31 ± 4[b]	21 ± 4	23 ± 5[c]	16 ± 4
2.6 GeV/c	12 ± 2[b]	11.0 ± 2.5	22 ± 6[c]	14 ± 4

Reaction	σ[d] (μb)	Reaction	σ[d] (μb)
$K^- p \to \Xi^{*0} K^0$		$K^- p \quad \Xi^0 K^{*0}$	
1.7 GeV/c	70 ± 9		
2.1 GeV/c	80 ± 11	2.1 GeV/c	24 ± 6
2.6 GeV/c	24 ± 3	2.6 GeV/c	21 ± 6
$K^- p \quad \Xi^{*-} K^+$		$K^- p \quad \Xi^- K^{*+}$	
1.7 GeV/c	28 ± 6		
2.1 GeV/c	28 ± 4	2.1 GeV/c	26 ± 5
2.6 GeV/c	16 ± 3	2.6 GeV/c	35.5 ± 3.5

a. Uncorrected for other Ξ^*, K^* decay modes.
b. Fractions in the nearly complete but contaminated samples. To correct for contamination the fractions should be multiplied by 1.05, 1.15, and 1.45 for the respective momenta.
c. The sample is contaminated but the non-Ξ^0 events include real K^* production. We have doubled the error to account for this effect.
d. Final states combined and cross sections corrected for unobserved decay modes.

Table VII. Cross sections for $\Xi^*(1530)$ and $K^*(890)$ production in $K^- p \to \Xi K \pi\pi$.[a]

Reaction	σ[b] (μb)
$K^- p \to \Xi^{*0} K^{*0}$[c]	3 ± 2
$\Xi^{*-} K^{*+}$[c]	12 ± 4
$\Xi^{*0} K^+ \pi^-$	9 ± 2
$\Xi^{*0} K^0 \pi^0$	3 ± 3
$\Xi^{*-} K^0 \pi^+$	6 ± 3
$\Xi^- K^{*0} \pi^+$	1 ± 1
$\Xi^- K^{*+} \pi^0$	1 ± 2
$\Xi^0 K^{*+} \pi^-$	2 ± 2

a. The momentum range covered is 2.4 to 2.7 GeV/c.
b. Fully corrected for unseen decay modes.
c. The $\Xi^* K^*$ events are not included in the $\Xi^* K\pi$ and $\Xi K^* \pi$ cross sections.

Table VIII. Comparison of Ξ lifetime determinations.

Experiment	Ref.	N_{Ξ^-}	τ_{Ξ^-} ($\times 10^{-10}$ sec)	N_{Ξ^0}	τ_{Ξ^0} ($\times 10^{-10}$ sec)
BNL-SYR	10	311	1.80 ± 0.16		
EP +	11	273	$1.86 \pm {}^{0.15}_{0.14}$	24	$3.8 \, {}^{+1.0}_{-0.7}$
UCLA	9	246	1.70 ± 0.12	80	3.0 ± 0.5
Schneider	13	62	1.55 ± 0.31		
LRL'64	6	794	1.69 ± 0.07	101	$2.5 \, {}^{+0.4}_{-0.3}$
This experiment		2610	1.61 ± 0.04	340	$3.07 \, {}^{+0.22}_{-0.20}$

Table IX. Summary of maximum-likelihood fits for Ξ decay parameters.

Quantity	Value
Ξ^- events	2781
Ξ^0 events	739
$\alpha_\Lambda \alpha_{\Xi^-}$ fitted separately	-0.267 ± 0.032
$\alpha_\Lambda \alpha_{\Xi^0}$ fitted separately	-0.235 ± 0.063
$W = \ell n \mathcal{L}$; Ξ^-, Ξ^0 independent	88.6 , 25.5
α_Λ obtained with constraint; see text	0.650 ± 0.019
α_{Ξ^-}	-0.391 ± 0.041
Φ_{Ξ^-} (deg)	-14 ± 8
α_{Ξ^0}	-0.410 ± 0.083
Φ_{Ξ^0} (deg)	38 ± 14
$W = \ell n \mathcal{L}$; Ξ^-, Ξ^0 parameters equal	113.5
α_Ξ	-0.398 ± 0.036
Φ_Ξ (deg)	-5 ± 7
$C(\alpha_\Lambda \alpha_\Xi)$[a]	0.125
$C(\alpha_\Lambda \Phi_\Xi)$[a]	0.016
$C(\alpha_\Xi \Phi_\Xi)$[a]	-0.001
α_Λ determined independently	0.669 ± 0.054

[a] Correlation coefficients which are the off-diagonal elements of the normalized error matrix.

Table X. Comparison of determinations of Ξ decay parameters.

Experiment	Ref.	N_{Ξ^-}	α_{Ξ^-}	Φ_{Ξ^-}-(deg)	N_{Ξ^0}	α_{Ξ^0}	Φ_{Ξ^0} (deg)
EP+	11	517	-0.44 ± 0.11[a]	-16 ± 37			
UCLA'64	8	356	-0.62 ± 0.12[a]	54 ± 25			
BNL-SYR	10	364	-0.47 ± 0.12[a]	0 ± 17			
LRL'66	7	1004	-0.365 ± 0.068[b]	0 ± 12	201	-0.13 ± 0.17	-8 ± 30
LRL'68		2781	-0.391 ± 0.045[b]	-14 ± 11	739	-0.43 ± 0.09	38 ± 19
LRL'66 + '68		3785	-0.383 ± 0.038[b]	-8 ± 8	940	-0.36 ± 0.08	25 ± 16

[a] Assumed value of $\alpha_\Lambda = 0.62 \pm 0.07$

[b] Assumed value of $\alpha_\Lambda = 0.647 \pm 0.020$

Table XI. Ξ spin determination.

Sample	(2 J + 1)	Standard deviations discrimination against J = 3/2
1.7-GeV/c $\Xi^0 K^0$	4.7 ±4.5	----
$\gtrsim$2.1-GeV/c $\Xi^0 K^0$	1.61± 1.09	2.2
Combined $\Xi^0 K^0$	2.34 ± 1.25	1.3
$\Xi^- K^+$	2.23 ± 1.08	1.6

Table XII. Unusual Ξ decay modes.

Mode	B_{expt} ($\times 10^{-3}$)	B_{theor} ($\times 10^{-3}$)	Theoretical reference
$\Delta S = 0$ leptonic			
$\Xi^- \to \Xi^0 e^- \bar{\nu}$	< 0.5	3×10^{-7}	51
$\Delta S = \Delta Q$ leptonic			
$\Xi^- \to \Lambda e^- \bar{\nu}$	$1.0^{+1.3}_{-0.65}$	0.56	51
$\Lambda \mu^- \bar{\nu}$	≤ 1.3	0.16	51
$\Sigma^0 e^- \bar{\nu}$	< 0.5	0.07[a]	51
$\Sigma^0 \mu^- \bar{\nu}$	---	8×10^{-4}[b]	51
$\Xi^0 \to \Sigma^+ e^- \bar{\nu}$	< 1.5	0.28	51
$\Sigma^+ \mu^- \bar{\nu}$	< 1.5	0.002[b]	51
$\Delta S = -\Delta Q$ leptonic			
$\Xi^0 \to \Sigma^- e^+ \nu$	< 1.5	10^{-3}	52
$\Sigma^- \mu^+ \nu$	< 1.5	10^{-6}	52
$\Delta S = 2$ leptonic			
$\Xi^- \to n e^- \bar{\nu}$	---	<0.1	52
$\Xi^0 \to p e^- \bar{\nu}$	< 1.3	<0.1	52
$p \mu^- \bar{\nu}$	≤ 1.3	<0.1	52
$\Delta S = 2$ nonleptonic			
$\Xi^- \to n \pi^-$	< 1.1	$\lesssim 0.1$	56
$\Xi^0 \to p \pi^-$	< 0.9	$\lesssim 0.1$	56
Radiative three-body			
$\Xi^- \to \Lambda \pi^- \gamma$	≤ 0.8	≈ 1	57
$\Xi^0 \to \Lambda \pi^0 \gamma$	---	≈ 1	57

a. Carlson [51] used an incorrect form, $(1/\sqrt{2})\, F \sin\theta$, for the axial-vector coupling in the reaction $\Xi^- \to \Sigma^0 \ell \nu$. The entry here corresponds to the correct form, $(1/\sqrt{2})(D+F)\sin\theta$.

b. The branching ratios for the muonic decays were obtained from those of the corresponding electronic decays, reduced by the phase-space dependence on the lepton mass. [See M. Deutsch and O. Kofoed-Hansen in Part XI of Experimental Nuclear Physics, Vol. III, edited by E. Segrè (John Wiley & Sons, Inc., New York, 1959)].

FOOTNOTES AND REFERENCES

*Work done under the auspices of the U. S. Atomic Energy Commission.

†Present address: Nuclear Physics Laboratory, University of Oxford, Oxford, England.

‡Present address: Departement de Physique des Particules Elémentaires, CEN, Saclay, France.

**Supported in part by the National Science Foundation.

1. J. Murray, J. Button-Shafer, F. Shively, G. Trilling, J. Kadyk, A. Rittenberg, D. Siegel, J. Lindsey, and D. Merrill, in Proceedings of the International Conference on High Energy Physics, Dubna, 1964 (Atomizdat, Moscow, 1966), Vol. II, p. 541; and Lawrence Radiation Laboratory Report UCRL-11426, 1964 (unpublished).

2. G. A. Smith, J. S. Lindsey, J. J. Murray, J. Button-Shafer, A. Barbaro-Galtieri, O. I. Dahl, P. Eberhard, W. E. Humphrey, G. R. Kalbfleisch, R. R. Ross, F. T. Shively, and R. D. Tripp, Phys. Rev. Letters 13, 61 (1964); G. A. Smith, J. S. Lindsey, J. Button-Shafer, and J. J. Murray, Phys. Rev. Letters 14, 25 (1965).

3. J. Button-Shafer, J. S. Lindsey, J. J. Murray, and G. A. Smith, Phys. Rev. 142, 883 (1966).

4. Deane W. Merrill (Ph.D. Thesis), Lawrence Radiation Laboratory Report UCRL-16455, 1966 (unpublished).

5. Deane W. Merrill and J. Button-Shafer, Phys. Rev. 167, 1202 (1968).

6. J. R. Hubbard, J. P. Berge, G. R. Kalbfleisch, J. B. Shafer, F. T. Solmitz, M. L. Stevenson, S. G. Wocjicki, and P. G. Wohlmut, Phys. Rev. 135, B183 (1964).

7. J. P. Berge, P. Eberhard, J. R. Hubbard, D. W. Merrill, J. Button-Shafer, F. T. Solmitz, and M. L. Stevenson, Phys. Rev. 147, 945 (1966).

8. D. D. Carmony, G. M. Pjerrou, P. E. Schlein, W. E. Slater, D. H. Stork, and H. K. Ticho, Phys. Rev. Letters 12, 482 (1964).

9. G. M. Pjerrou (Ph. D. Thesis), University of California, Los Angeles, 1965 (unpublished).

10. G. W. London, R. R. Rau, N. P. Samios, S. S. Yamamoto, M. Goldberg, S. Lichtman, M. Primer, and J. Leitner, Phys. Rev. 143, 1034 (1966).

11. L. Jauneau et al. in Proceedings of the Sienna International Conference on Elementary Particles, Sienna, Italy, 1963 (Società Italiana di Fisica, Bologna, Italy, 1963) v.I, p.1; and L. Jauneau et al., ibid., p. 4. (Ξ's observed in heavy liquid bubble chamber)

12. L. Jauneau et al., Phys. Letters 4, 49 (1963) and L. Jauneau et al., Phys. Letters 5, 261 (1963).

13. H. Schneider, Phys. Letters 4, 360 (1963).

14. See references in the compilation by A. H. Rosenfeld, N. Barash-Schmidt, A. Barbaro-Galtieri, L. R. Price, P. Söding, C. G. Wohl, M. Roos, and W. J. Willis, Rev. Mod. Phys. 40, 77 (1968).

15. Gerald R. Lynch, Lawrence Radiation Laboratory Report UCRL-10335, 1962 (unpublished).

16. O. I. Dahl, L. M. Hardy, R. I. Hess, J. Kirz, D. H. Miller, and J. A. Schwartz, Phys. Rev. 163, 1430 (1967), and O. I. Dahl et al., ibid. 1377.

17. The loss is somewhat reduced because of the large ionization differences between decay π^- and slow Ξ^-.

18. We assume the separate detection probabilities to be statistically independent. Small correlations may exist between P_D and Ξ^- length or position in the chamber. We have not been able to detect such effects.

19. P. Davis, Alvarez Group Internal Memo No. 656, 1968 (unpublished).

20. T. G. Trippe and P. E. Schlein, Phys. Rev. 158, 1334 (1967).

21. J. Badier, M. Demoulin, J. Goldberg, B. Gregory, C. Pelletier, A. Rouge, M. Ville, R. Barloutaud, A. Leveque, C. Louedec, J. Meyer, P. Schlein, A. Verglas, D. Holthuizen, W. Hoogland, and A. Tenner, Phys. Letters 16, 171 (1965). See also J. Badier et al., Sections Efficaces K^-p à 3 GeV/c, Saclay Internal Report No. CEA-N532.

22. The possibility of $Y_0^*(2100)$ decay into ΞK was first suggested on the basis of the data in Ref. 7 alone by R. Tripp, D. Leith, A. Minten, R. Armenteros, M. Ferro-Luzzi, R. Levi-Setti, H. Filthuth, V. Hepp, E. Kluge, H. Schneider, R. Barloutaud, P. Granet, J. Meyer, and J. Porte, in Nucl. Phys. B3, 10 (1967).

23. Aachen-Berlin-CERN-London (Imperial College)-Vienna collaboration, Nucl. Phys. B4, 326 (1968).

24. J. T. Donohue (Ph. D. Thesis), University of Illinois, 1967 (unpublished).

25. Trippe and Schlein point out that the presence of nonnegligible I = 1 exchange could lead to fortuitous agreement of their partial-wave amplitudes with the calculations of Donohue, due to cancellation of I = 0 and I = 1 contributions. However, this could not occur for $\Xi^0 K^0$ production.

26. R. L. Cool, G. Giacomelli, T. F. Kycia, B. A. Leontić, K. K. Li, A. Lundby, and J. Teiger, Phys. Rev. Letters 16, 1228 (1966).

27. G. Burgun, J. Meyer, E. Pauli, B. Tallini, J. Vrana, A. de Bellefon, A. Berthon, K. L. Rangan, J. Beany, M. U. Deen, C. M. Fischer, and J. R. Smith, Resonance Formation in the Reactions $K^- p \to \Xi^- K^+$ and $K^- p \to \Xi^0 K^0$ in the Mass Region from 1915 to 2168 MeV (preprint), submitted to Nucl. Phys. Sept. 1968.

28. R. J. Abrams, R. L. Cool, G. Giacomelli, T. F. Kycia, B. A. Leontić, K. K. Li, and D. N. Michael, Phys. Rev. Letters 19, 678 (1967).

29. J. Friedman, Alvarez Group Programming Note No. P-156, 1966 (unpublished).

30. P. E. Schlein, in Lectures in Theoretical Physics, 1965 (University of Colorado Press, 1966). Vol. VIII-B, p. 111. The data are those of Ref. 9.

31. T. Trippe (Ph. D. Thesis), University of California, Los Angeles, 1968 (unpublished).

32. G. A. Smith and J. S. Lindsey, Final State Interactions Involving Hyperons, in Proceedings of the Second Topical Conference on Resonant Particles, Athens, Ohio, June 1965, p. 251.

33. See the discussion of the κ by A. H. Rosenfeld, A. Barbaro-Galtieri, W. J. Podolsky, L. R. Price, P. Söding, C. G. Wohl, M. Roos, and W. J. Willis, Rev. Mod. Phys. 39, 1 (1967). Explanations of κ in terms of singularities in triangle diagrams have been offered previously [(e.g., M. Month, Phys. Rev. 139, B1093 (1965)]. Such an explanation is not appropriate for $K^- p \to \Xi K \pi$ in the 2-GeV/c K^- momentum region because the final state kaon is too energetic in the center-of-mass frame for the pion from Ξ^* decay to be able to catch and rescatter off it. Coleman and Norton [Nuovo Cimento 38, 438 (1965)] have shown that the triangle singularity occurs for physical M(Kπ) only if this classical space-time interpretation is possible.

34. G. Wolsky (Ph. D. Thesis), University of Maryland, 1967 (unpublished).

35. Models involving exchange of several baryons have been constructed by M. E. Ebel and P. B. James [Phys. Rev. 153, 1694 (1967)] to explain the previously available $K^- p \to \Xi^- K^+$ data. The authors concluded that their formulation was not an adequate representation of baryon exchange.

36. This value, taken from Ref. 14, was obtained from experiments that are in rather poor agreement.

37. Based on measurements of $\sigma_{\Lambda p}$ by Margaret Alston (Lawrence Radiation Laboratory, private communication) and by D. Bassano, C. Y. Chang, M. Goldberg, T. Kikuchi, and J. Leitner, Phys. Rev. 160, 1239 (1967).

38. A total of 9 Ξ^0 decays in our sample of 934 identified Ξ^0 events made Dalitz pairs. This number implies a branching fraction of π^0 into the $e^+e^-\gamma$ mode of 0.010±.003, in agreement with the accepted value of 0.0117 (Ref. 14).

39. The likelihood method for determination of the Ξ^0 lifetime is described in Ref. 6, and in somewhat more detail by Hubbard in his Ph. D. thesis, Lawrence Radiation Laboratory Report UCRL-11510, 1966 (unpublished). We have also calculated the Ξ^0 mean life from the join length and hyperon momenta alone, assuming the Ξ^0 decays to be colinear, which is a good approximation at our momenta. The likelihood function in that case has a maximum at $\tau_{\Xi^0} = (2.86^{+0.26}_{-0.22}) \times 10^{-10}$ sec using $\tau_\Lambda = 2.52 \times 10^{-10}$ sec. The difference in the relative errors for the two methods, which is roughly a factor of $\sqrt{2}$, demonstrates the importance of using the calculated Ξ^0 length.

40. For example, measurements of the I = 1 π-p phase shifts at 37 MeV (equivalent to the Λ mass) has yielded $\delta_s - \delta_p = 6.5° \pm 1.5°$. See S. W. Barnes, H. Winick, K. Miyake and K. Kinsey, Phys. Rev. 117, 238 (1960) and O. E. Overseth and R. F. Roth, Phys. Rev. Letters 19, 391 (1967).

41. The coefficient of the polarization in Eq. (6.2) reduces to $C(\xi\eta\phi) = [(\alpha_{\Xi} \xi + \alpha_\Lambda \xi\eta - \alpha_\Lambda(1 - \alpha_{\Xi}^2)^{1/2}(1-\xi^2)^{1/2}(1 - \eta^2)^{1/2} \cos(\Phi_{\Xi} + \phi)]$. This term is an odd function of the configuration variables ξ, η, ϕ in the sense that $\int C(\xi\eta\phi)\, d\Omega = 0$. This enables us to estimate $\langle P_{\Xi} \rangle$ and the expansion coefficients B_ℓ of (4.2) from $\langle P_{\Xi} \rangle = \frac{1}{D} \langle C(\xi\eta\phi) \rangle$; $B_\ell = \frac{2\ell+1}{\ell(\ell+1)} \frac{1}{D} \langle C(\xi\eta\phi) P_\ell'(\cos\Theta) \rangle$, where $D = \int C^2 d\Omega$.

42. The restriction of the $\Xi^0 K^+ \pi^-$ sample to events in which the Λ does not point back to the production vertex leads to a bias of the $\hat{\Lambda} \cdot \hat{n}$ distribution. Events with small $|\hat{\Lambda} \cdot \hat{n}|$ are lost preferentially due to the discrimination against events having $|\hat{\Lambda}$ (Ξ rest frame) $\cdot \hat{\Xi}$(lab)$| \approx 1$. This effect is unmeasurably small for the experimental $\hat{\Lambda} \cdot \hat{n}$ distribution; study of Monte-Carlo-generated events indicates that it should lead to an increase of $\langle \hat{\Lambda} \cdot \hat{n} \rangle$ of less than 5%. The bias against $|\hat{\Lambda} \cdot \hat{\Xi}| \approx 1$ does not affect the distribution of $\hat{\Lambda} \cdot \hat{p}$ and ϕ. Since the statistical relative uncertainty in α_{Ξ^0} from the $\Xi^0 K^+ \pi^-$ events alone is only 25%, and most of this precision arises from the $\hat{\Lambda} \cdot \hat{p}$ distribution, we are justified in ignoring the bias. The above reasoning also guarantees that the loss of events having $\hat{\Lambda} \cdot \hat{\Xi}^-$ (lab) ≈ -1, which arises because of the difficulty in detecting forward pions from Ξ^- decay (see Sec. II. B), does not significantly affect the Ξ^- polarization or α_{Ξ^-} determinations. The latter loss in $\hat{\Lambda} \cdot \hat{\Xi}^-$ amounts to $\leq 1/2$ of that in $\hat{\Lambda} \cdot \hat{\Xi}^0$ due to Ξ^0 purification, so that the effect on $\langle \hat{\Lambda} \cdot \hat{n} \rangle$ is only a few percent. We have checked this argument by calculating values of $\langle \hat{\Lambda} \cdot \hat{n} \rangle$, using the weights discussed in Sec. II. B, and have found no significant departures from the unweighted results.

43. Sources of error considered were (a) uncertainty in the maximum order of expansion coefficients to use (variations typically change α_{Ξ} by < 0.01 and ϕ_{Ξ} by < 3 deg, and (b) uncertainty in the coefficients themselves (uncertainty in Φ_{Ξ^0} of about 5 to 10 deg is indicated by manipulation of the A_ℓ, B_ℓ).

44. A reanalysis of the data of Ref. 8 has yielded the same result as reported by the UCLA group, $\Phi_{\Xi} \approx 1$ radian.

45. Albright [C. H. Albright, Phys. Rev. Letters 21, 1216 (1968)] has recently calculated the effect of CP nonconservation in nonleptonic hyperon decay according to the theory of Oakes [R. J. Oakes, Phys. Rev. Letters 20, 1539 (1968)]. His results, obtained by using p-wave amplitudes that do not obey the $|\Delta I| = 1/2$ rule, are $\beta/\alpha(\Xi^-) \approx -0.00003$ and $\beta/\alpha(\Xi^0) \approx 0.00014$.

46. O. E. Overseth (University of Michigan) and S. Pakvasa (University of Hawaii), preprint, 1968.

47. N. Byers and S. Fenster, Phys. Rev. Letters 11, 52 (1963).

48. J. R. Hubbard, J. P. Berge, and P. M. Dauber, Phys. Rev. Letters 20, 465 (1968).

49. D. D. Carmony and G. M. Pjerrou, Phys. Rev. Letters 10, 381 (1963).

50. N. Cabibbo, Phys. Rev. Letters 10, 531 (1963).

51. C. Carlson, Phys. Rev. 152, (1433 (1966); L. K. Gershwin, M. Alston-Garnjost, R. O. Bangerter, A. Barbaro-Galtieri, F. T. Solmitz, and R. D. Tripp, Phys. Rev. Letters 20, 1270 (1968).

52. E. de Rafael and M. Goldhaber, Phys. Rev. Letters 20, 522 (1968).

53. A. Barbaro-Galtieri, W. Barkas, H. Heckman, J. Patrick and F. Smith, Phys. Rev. Letters 9, 26 (1962); U. Nauenberg, P. Schmidt, J. Steinberger, S. Marateck, R. Plano, H. Blumenfeld, and L. Seidlitz, Phys. Rev. Letters 12, 679 (1964); F. Eisele,

R. Engelmann, H. Filthuth, W. Föhlisch, V. Hepp, E. Kluge, E. Leitner, P. Lexa, P. Mokry, W. Presser, H. Schneider, M. Stevenson, and G. Zech, Z. Physik 205, 409 (1967). See also N. Baggett, T. Day, R. Glasser, B. Kehoe, R. Knop, B. Sechi-Zorn, and G. A. Snow, Phys. Rev. Letters 19, 1458 (1967).

54. B. d'Espagnat and M. K. Gaillard, Nuovo Cimento (10) 42A, 1035 (1966).

55. S. L. Glashow, Phys. Rev. Letters 6, 196 (1961); R. E. Behrends and Sirlin, Phys. Rev. Letters 8, 221 (1962).

56. L. B. Okuń, Yadern. Fiz. 1, 1132 (1965) [English transl: Soviet J. Nucl. Phys. 1, 806 (1965)].

57. K. Tanaka, Phys. Rev. 153, 1519 (1967); S. Barshay, U. Nauenberg, and J. Schultz, Phys. Rev. Letters 12, 76 and 156 (1964).

58. M. Bazin, H. Blumenfeld, U. Nauenberg, L. Seidlitz, R. J. Plano, S. Marateck, and P. Schmidt, Phys. Rev. 140, B1358 (1965).

59. K. C. Gupta, Rabi Majumdar, and K. C. Tripathy, Phys. Rev. 157, 1306 (1967).

FIGURE CAPTIONS

Fig. 1. Total cross section divided by $4\pi\lambda^2$ for $K^-p \to \Xi^-K^+$ (solid symbols) and $K^-p \to \Xi^0K^0$ (open symbols) as a function of beam momentum. The data have not been fitted; the curves are intended only to guide the eye.

Fig. 2. $d\sigma/d\Omega$ and $P_\Xi d\sigma/d\Omega$ for $K^-p \to \Xi^-K^+$ at 1.7, 2.1, 2.47, and 2.64 GeV/c. The production plane normal is taken along $\hat{K}^- \times \hat{K}^+$. The solid curves are calculated from Legendre function moments of the distributions with $\ell_{max} = 7$, 6, 8, and 8 at the respective momenta. Dashed curves corresponding to $\ell_{max} = 3$ are also plotted. The errors on each point are statistical only.

Fig. 3. $d\sigma/d\Omega$ and $P_\Xi d\sigma/d\Omega$ for $K^-p \to \Xi^0K^0$ at 1.7, 2.1, and 2.6 GeV/c. The production plane normal is taken along $\hat{K}^- \times \hat{K}^0$. The solid curves are calculated from Legendre function moments of the distributions with $\ell_{max} = 5$; the dashed curves correspond to $\ell_{max} = 3$.

Fig. 4. Legendre polynomial expansion coefficients of Ξ^-K^+ differential cross section plotted as a function of total center-of-mass energy. The solid symbols represent our data. The open symbols represent LRL and UCLA data at adjacent momenta. The zeroth-order term is plotted in Fig. 1.

Fig. 5. Dalitz plots of $M^2(K\pi)$ vs $M^2(\Xi\pi)$ for the $\Xi K\pi$ final states at 1.7, 2.1, and 2.6 GeV/c. The 2.6-GeV/c plot includes data at 2.47 and 2.64 ± 0.08 GeV/c. Reactions (2.3) through (2.5) have been combined in making these plots, which introduces some non-Ξ contamination, as explained in the text.

Fig. 6. ($\Xi\pi$) mass squared projections for each three-body final state and momentum. The shaded events in plots (g), (h), and (i) are purified Ξ^0 for which the decay Λ does not fit with the production vertex taken as the origin, as discussed in the text. The curves were calculated by using $\Xi^*(1530)$ and $K^*(890)$ resonance fractions obtained in maximum-likelihood fits. See Table II for numbers of events and reaction cross sections.

Fig. 7. (ΞK) mass squared projections for each three-body final state and momentum. The shaded events in plots (g), (h), and (i) are purified Ξ^0 for which the decay Λ does not fit with the production vertex taken as the origin, as discussed in the text. The curves were calculated by using $\Xi^*(1530)$ and $K^*(890)$ resonance fractions obtained in maximum-likelihood fits.

Fig. 8. ($K\pi$) mass squared projections for each three-body final state and momentum. The shaded events in plots (g), (h), and (i) are purified Ξ^0 for which the decay Λ does not fit with the production vertex taken as the origin, as discussed in the text. The curves were calculated by using $\Xi^*(1530)$ and $K^*(890)$ resonance fractions obtained in maximum-likelihood fits.

Fig. 9. Total cross section divided by $4\pi\lambda^2$ for (a) $K^-p \to \Xi K^*$, and (b) $K^-p \to \Xi^* K$, as a function of beam momentum. The Ξ^* production cross sections of Ref. 6 are the mean of the $\Xi^{*0}K^0$ and $\Xi^{*-}K^+$ charge states. The curves in (b) are intended solely to guide the eye.

Fig. 10. ($\Xi\pi$) mass squared for the highest-momentum events, $P_{K^-} > 2.63$ GeV/c. Figures 10(a), 10(b), and 10(c) show the events of reactions (2.3), (2.4), and (2.5) purified. Figure 10(d) contains the events of

plots (a) and (c). The cross-hatched region contains only events outside the K^* band, $860 < M(K\pi) < 930$ MeV/c^2. The solid curves show the result of fits to the Dalitz plots for these events, including $\Xi^*(1530)$, $K^*(890)$, and $\Xi^*(1930)$. The dashed curve in (d) results from the exclusion of $\Xi^*(1930)$ from the fit.

Fig. 11. (ΞK) mass squared spectra at 2.1 and 2.6 GeV/c. Events in the K^* band, $0.86 < M(K\pi) < 0.93$ GeV/c^2, and in the Ξ^* band, $1.51 < M(\Xi\pi) < 1.57$ GeV/c^2, have been removed. The curves were calculated from the fits assuming $\Xi^*(1530)$, K^*, $\Xi^*(1930)$ and phase space.

Fig. 12. ($K\pi$) mass squared spectra for the 2.1- and 2.6-GeV/c data combined (upper histograms) and 2.1 GeV/c separately (cross-hatched). Plot (a) contains only events inside the Ξ^* band, $1.51 < M(\Xi\pi) < 1.57$ GeV/c^2, and plot (b) contains only events outside this band. The curves were calculated from the fits assuming only $\Xi^*(1530)$, K^* and unmodified phase space.

Fig. 13. $\Xi^*(1530)$ production angular distributions. Plots (a), (b), and (c) include events of reaction (2.4); the cross-hatched histograms represent a sample purified by removing events in the Ξ^* - K^* overlap region of the Dalitz plot. Plots (d), (e), and (f) include events of reactions (2.3) and (2.5). The darkened histograms contain only purified Ξ^0 events outside the K^* band; the cross-hatched events are those of reaction (2.3) outside the K^* band.

Fig. 14. Ξ^* decay alignment with the beam direction. No purification has been carried out beyond selection of events in the Ξ^* band. The cross-hatched events are those in the backward hemisphere of Ξ^*

production, $\hat{K}_{in} \cdot \hat{K}_{out} < 0$. The curves show the expected decay distribution of a spin 3/2 Ξ^* for pure population of either the $m = \pm 1/2$ or $m = \pm 3/2$ substates. The purity of the samples is given in Fig. 13.

Fig. 15. K^* production angular distributions. Only purified Ξ^0 events are included in plots (a) and (b). Plots (c) and (d) contain events of both reactions (2.3) and (2.4).

Fig. 16. Scatter diagrams of $M(\Xi\pi)$ vs (a) $M(K\pi)$ and (b) $M(\Xi\pi\pi)$ for $K^- p \rightarrow \Xi K\pi\pi$ events with beam momenta 2.4 to 2.7 GeV/c. The three $\Xi K\pi\pi$ charge states have been combined, but only $\Xi\pi$ and $K\pi$ charge combinations with $I_z = \pm 1/2$ have been plotted.

Fig. 17. $(\Xi\pi)$, $(K\pi)$, and $(\Xi\pi\pi)$ mass projections for $K^- p \rightarrow \Xi K\pi\pi$. The three $\Xi K\pi\pi$ charge states have been combined, but only $\Xi\pi$ and $K\pi$ charge combinations with $I_z = \pm 1/2$ have been plotted. The solid curves were calculated from the fits allowing $\Xi^*(1530)$, $K^*(890)$, and phase space. The darkened events in (c) are those inside the Ξ^* band, $1500 < M(\Xi\pi)^{\overline{0}} < 1560$ MeV/c^2, and outside the K^* band, $840 < M(K\pi)^{\overline{0}}_{\dagger} < 940$ MeV/c^2; the cross-hatched events are those inside both bands. The dotted (dashed) curve represents the original fit with the same cuts applied as in the darkened (cross-hatched) histograms.

Fig. 18. Differential lifetime distributions of Ξ^- and Ξ^0. The upper points represent the Ξ^0 data with the scale on the right; the proper times of the Ξ^- beyond the 0.5-cm minimum-length cutoff are represented by the lower points, with the scale on the left. Only events with Ξ produced 80 cm or more from the down-stream end

wall of the chamber are included; average Ξ^- lengths are $\approx$ 6 cm, average Ξ^0 lengths $\approx$ 9 cm. Since escape losses from the side, top and bottom walls are small, the decay curves fit the uncorrected data well. The slopes of the lines plotted correspond to the best-fit values for Ξ^- and Ξ^0 from likelihood functions without correction for interactions, energy loss, or kinematic fitting biases. These uncorrected values are 1.60 and 2.97×10^{-10} sec for Ξ^- and Ξ^0 respectively. The lines have been normalized to the $t = 1.5 \times 10^{-10}$ sec points.

Fig. 19. Distributions of $\Lambda \cdot p$ for Ξ^- (upper histogram) and Ξ^0 (cross-hatched histogram). The straight lines are based on maximum likelihood fits to the distribution function $(1 + \alpha_\Lambda \alpha_\Xi \hat{\Lambda} \cdot \hat{p})$. The corresponding values of the slope are $\alpha_\Lambda \alpha_{\Xi^-} = -0.267 \pm 0.032$ and $\alpha_\Lambda \alpha_{\Xi^0} = -0.235 \pm 0.063$.

Fig. 20. Distribution of $\hat{\Lambda}_\Xi \cdot \hat{\Xi}_{lab}$ for (a) Ξ^- and (b) Ξ^0. The Λ direction is evaluated in the Ξ rest frame and the Ξ direction is that in the laboratory frame. The Ξ^- sample includes all fitted Ξ^- events. The Ξ^0 sample contains all $\Xi^0 K^0$ events and those $\Xi^0 K^+ \pi^-$ events for which the decay Λ does not fit with the production vertex as the origin.

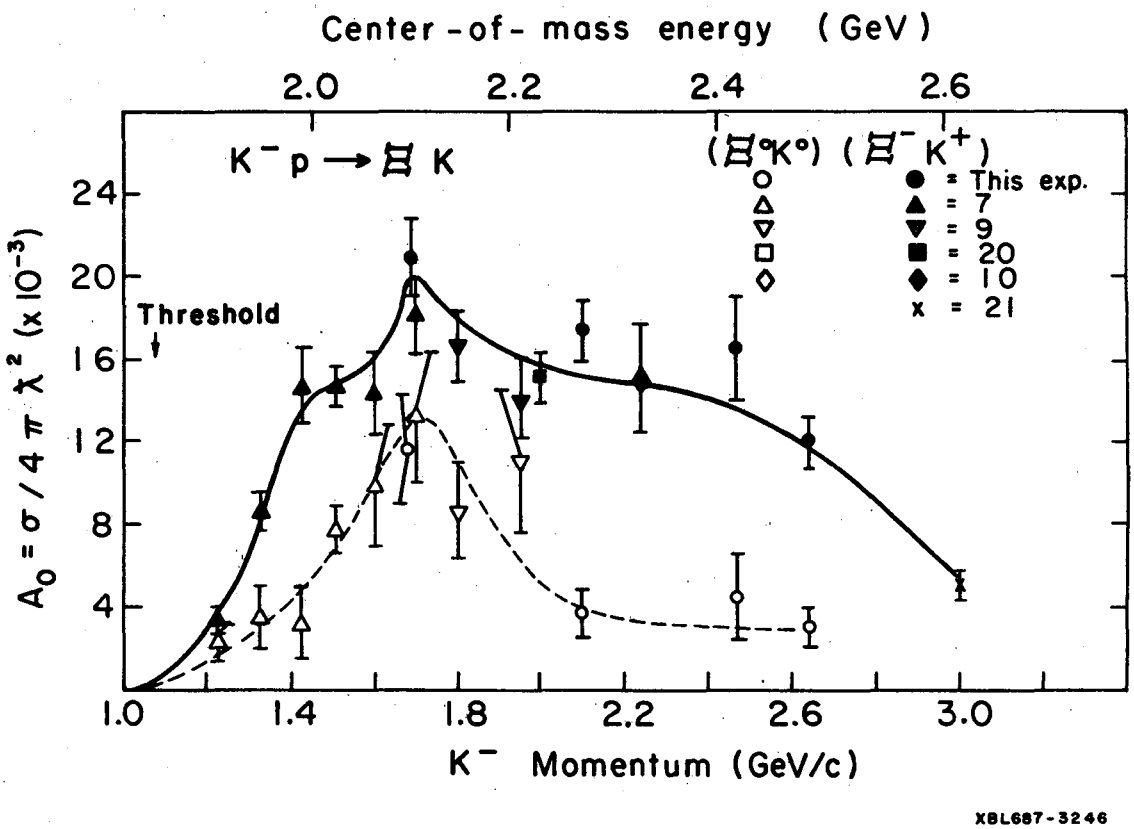
Center-of-mass energy (GeV)
2.0
2.2
2.4
2.6
$K^- p \rightarrow \Xi K$
$(\Xi^0 K^0)$ $(\Xi^- K^+)$
● = This exp.
▲ = 7
▼ = 9
■ = 20
◆ = 10
x = 21
Threshold
$A_0 = \sigma / 4\pi\lambda^2$ (x 10^{-3})
24
20
16
12
8
4
1.0
1.4
1.8
2.2
2.6
3.0
K^- Momentum (GeV/c)
XBL687-3246

Fig. 1

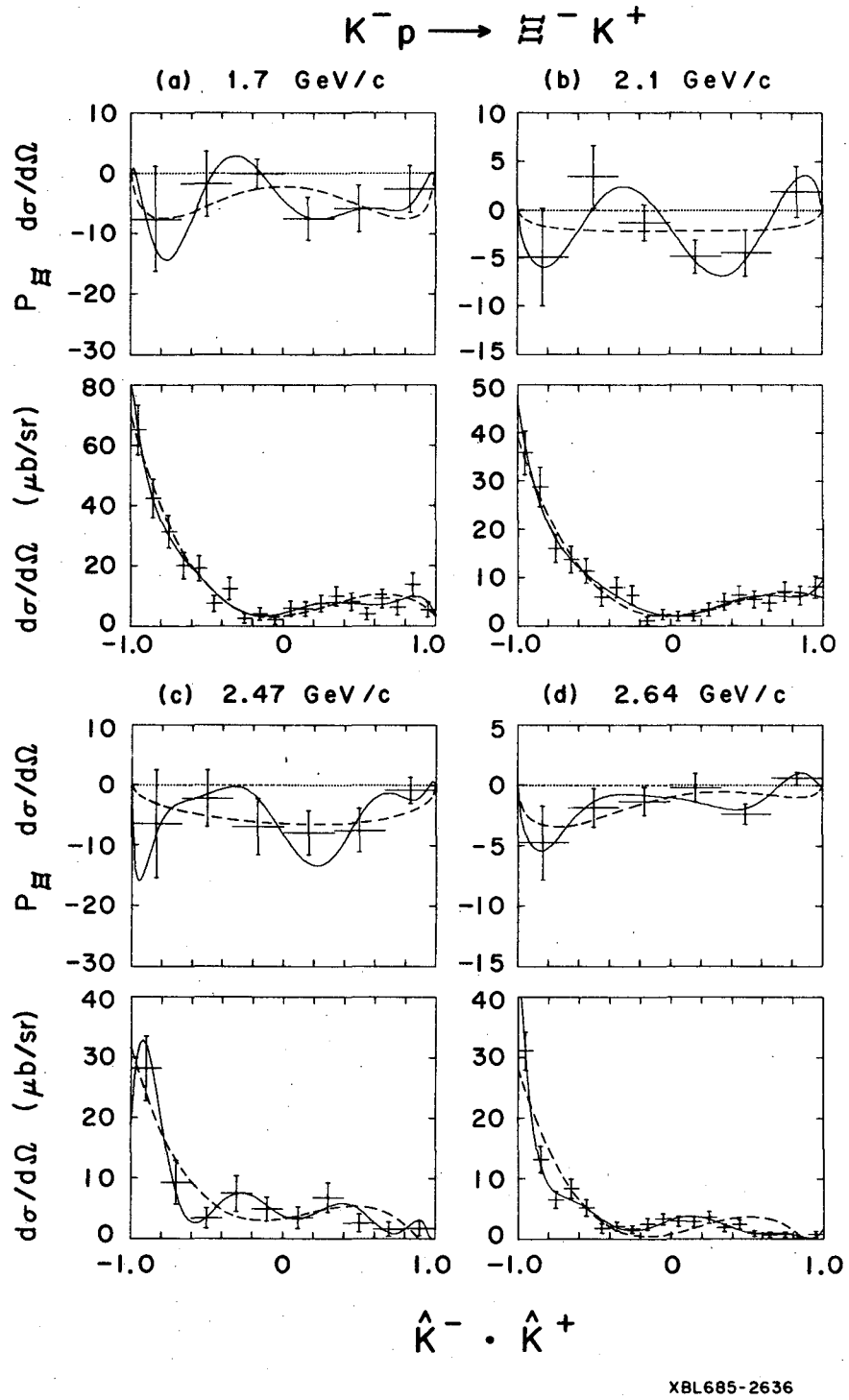
K⁻p ⟶ Ξ⁻K⁺
(a) 1.7 GeV/c
(b) 2.1 GeV/c
(c) 2.47 GeV/c
(d) 2.64 GeV/c
P_Ξ dσ/dΩ
dσ/dΩ (μb/sr)
K̂⁻ · K̂⁺
XBL685-2636

Fig. 2

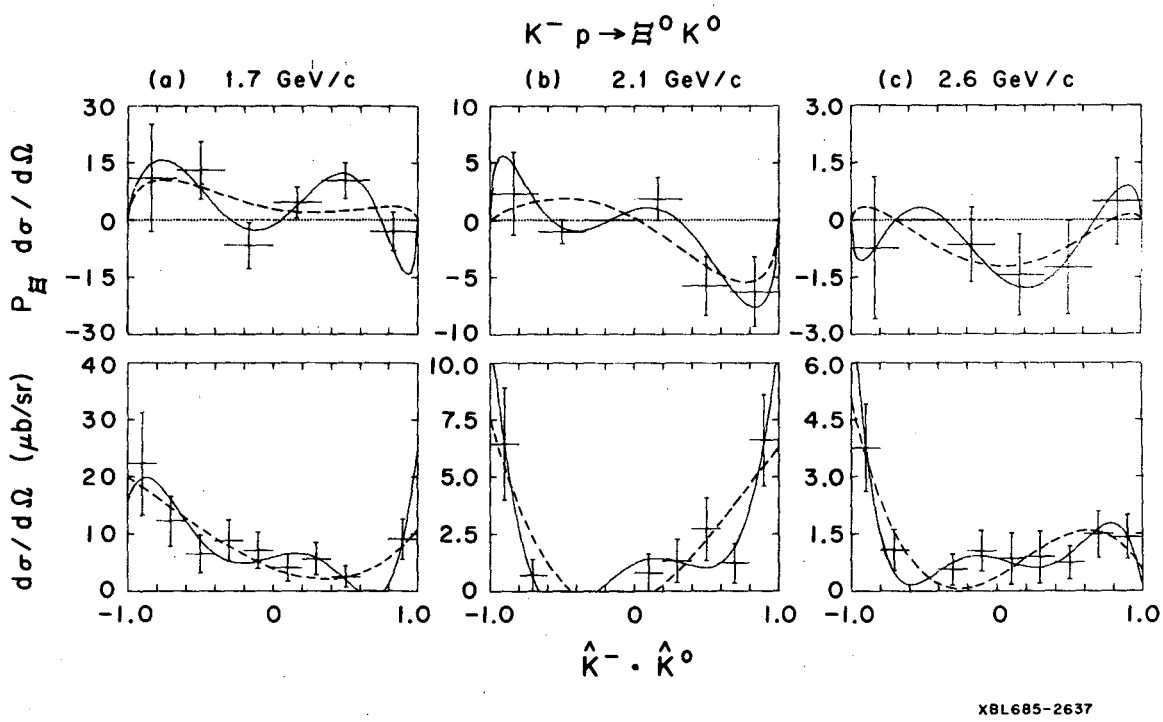
K⁻ p → Ξ⁰ K⁰
(a) 1.7 GeV/c
(b) 2.1 GeV/c
(c) 2.6 GeV/c
P_Ξ dσ/dΩ
dσ/dΩ (μb/sr)
K̂⁻ · K̂⁰
X8L685-2637

Fig. 3

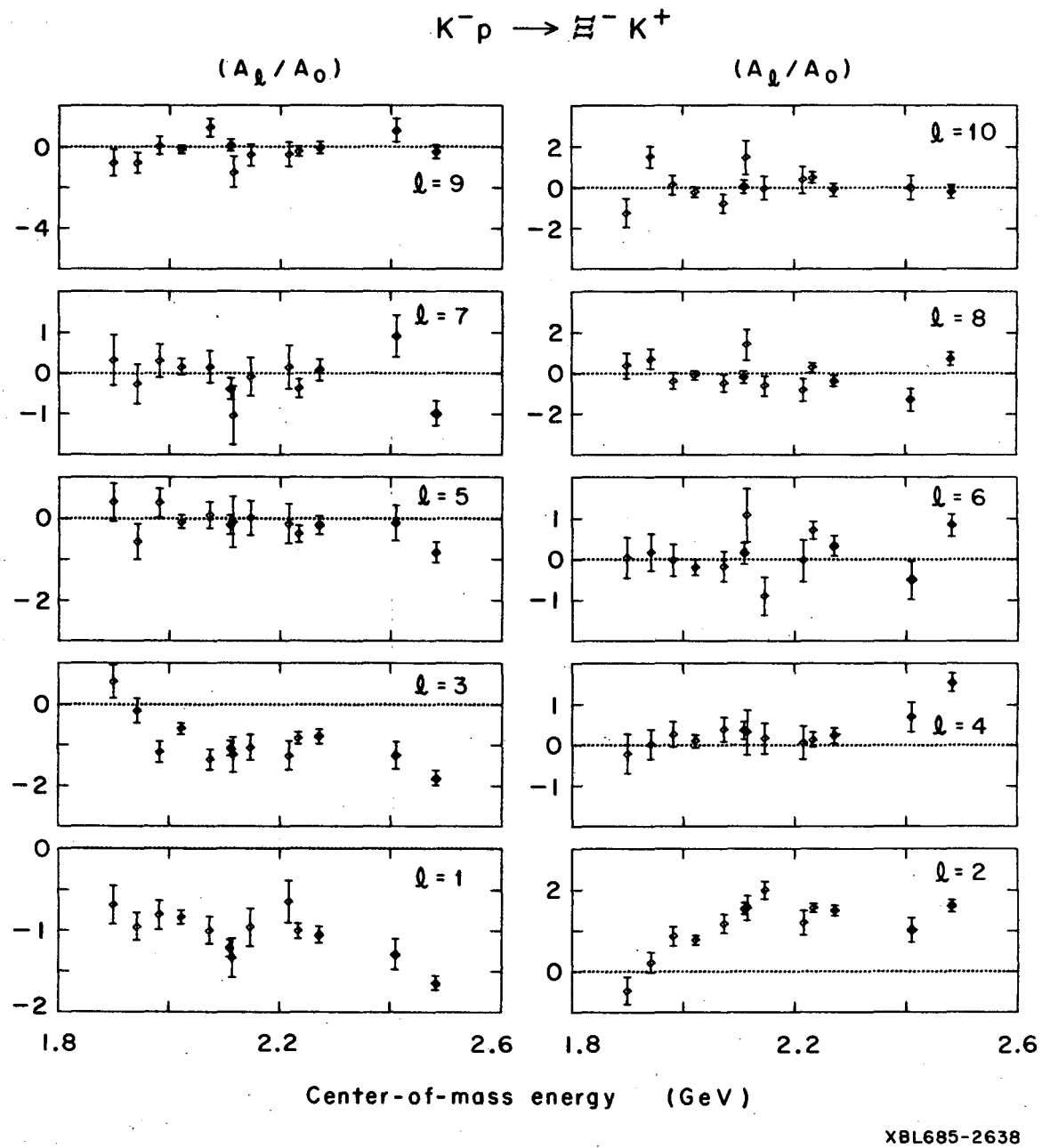
$K^- p \longrightarrow \Xi^- K^+$
(A_ℓ / A_0)
(A_ℓ / A_0)
$\ell = 9$
$\ell = 10$
$\ell = 7$
$\ell = 8$
$\ell = 5$
$\ell = 6$
$\ell = 3$
$\ell = 4$
$\ell = 1$
$\ell = 2$
1.8
2.2
2.6
1.8
2.2
2.6
Center-of-mass energy (GeV)
XBL685-2638

Fig. 4

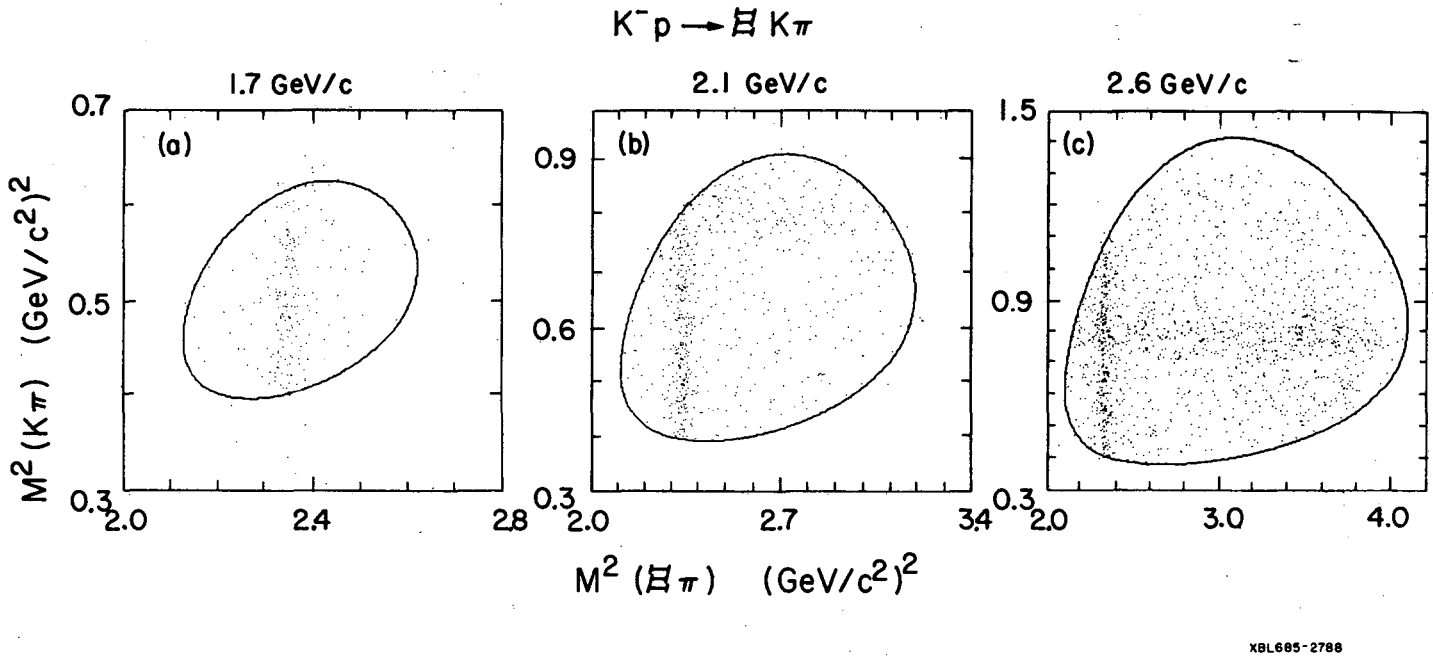
K⁻p → Ξ Kπ
1.7 GeV/c
2.1 GeV/c
2.6 GeV/c
(a)
(b)
(c)
M² (Kπ) (GeV/c²)²
M² (Ξπ) (GeV/c²)²
0.7
0.5
0.3
2.0
2.4
2.8
0.9
0.6
0.3
2.0
2.7
3.4
1.5
0.9
0.3
2.0
3.0
4.0
XBL685-2788

Fig. 5

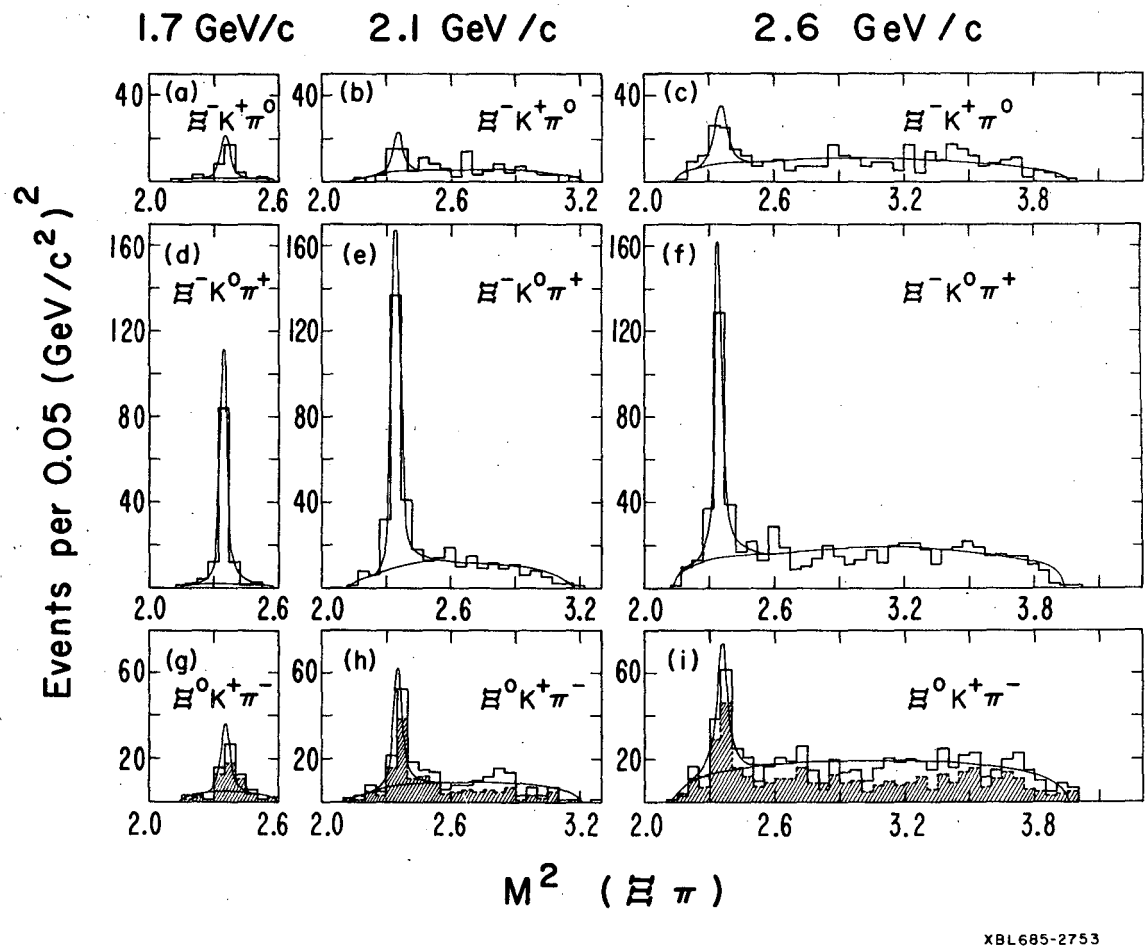
1.7 GeV/c
2.1 GeV/c
2.6 GeV/c
(a) Ξ⁻K⁺π⁰
(b) Ξ⁻K⁺π⁰
(c) Ξ⁻K⁺π⁰
(d) Ξ⁻K⁰π⁺
(e) Ξ⁻K⁰π⁺
(f) Ξ⁻K⁰π⁺
(g) Ξ⁰K⁺π⁻
(h) Ξ⁰K⁺π⁻
(i) Ξ⁰K⁺π⁻
Events per 0.05 (GeV/c²)²
M² (Ξπ)
XBL685-2753

Fig. 6

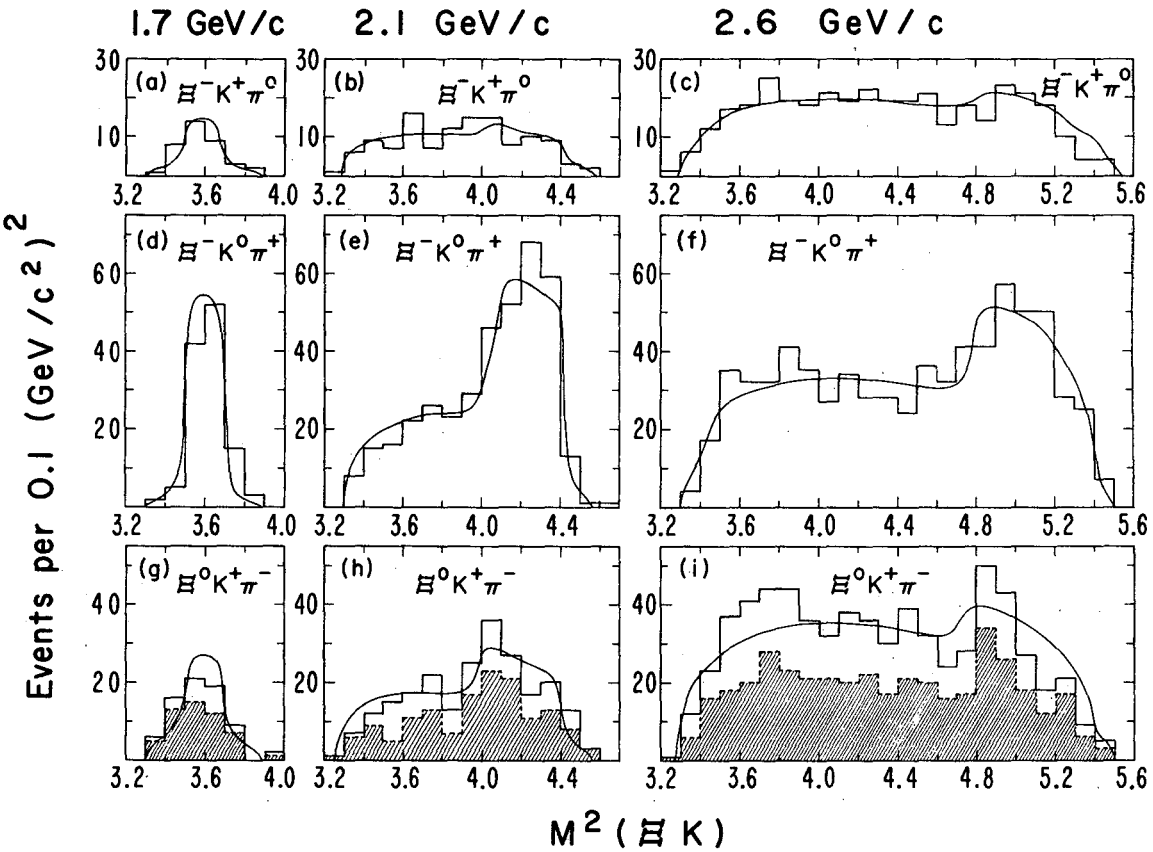
1.7 GeV/c
2.1 GeV/c
2.6 GeV/c
(a) Ξ⁻K⁺π⁰
(b) Ξ⁻K⁺π⁰
(c) Ξ⁻K⁺π⁰
(d) Ξ⁻K⁰π⁺
(e) Ξ⁻K⁰π⁺
(f) Ξ⁻K⁰π⁺
(g) Ξ⁰K⁺π⁻
(h) Ξ⁰K⁺π⁻
(i) Ξ⁰K⁺π⁻
Events per 0.1 (GeV/c²)²
M²(ΞK)
XBL685-2751

Fig. 7

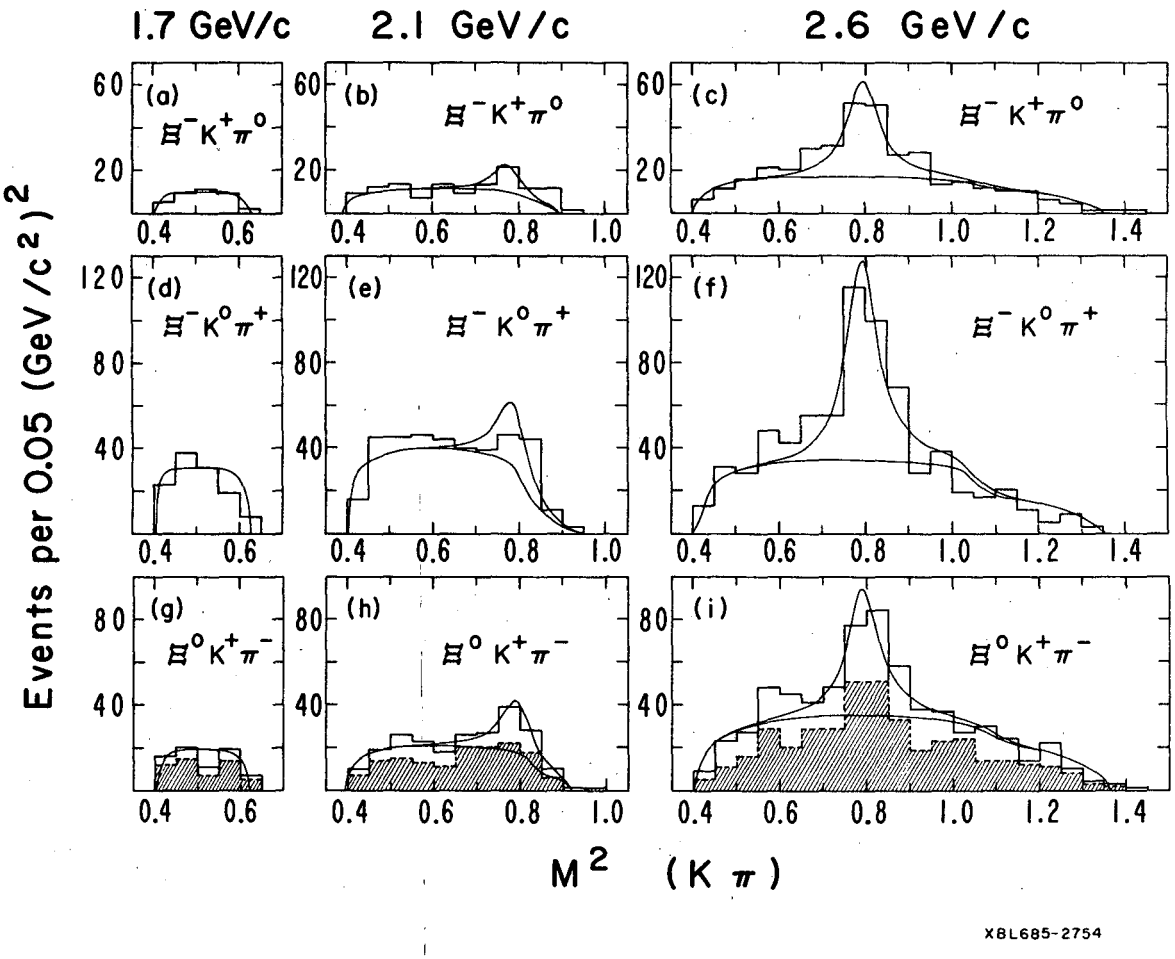
1.7 GeV/c
2.1 GeV/c
2.6 GeV/c
(a) Ξ⁻K⁺π⁰
(b) Ξ⁻K⁺π⁰
(c) Ξ⁻K⁺π⁰
(d) Ξ⁻K⁰π⁺
(e) Ξ⁻K⁰π⁺
(f) Ξ⁻K⁰π⁺
(g) Ξ⁰K⁺π⁻
(h) Ξ⁰K⁺π⁻
(i) Ξ⁰K⁺π⁻
Events per 0.05 (GeV/c²)²
M² (Kπ)
X8L685-2754

Fig. 8

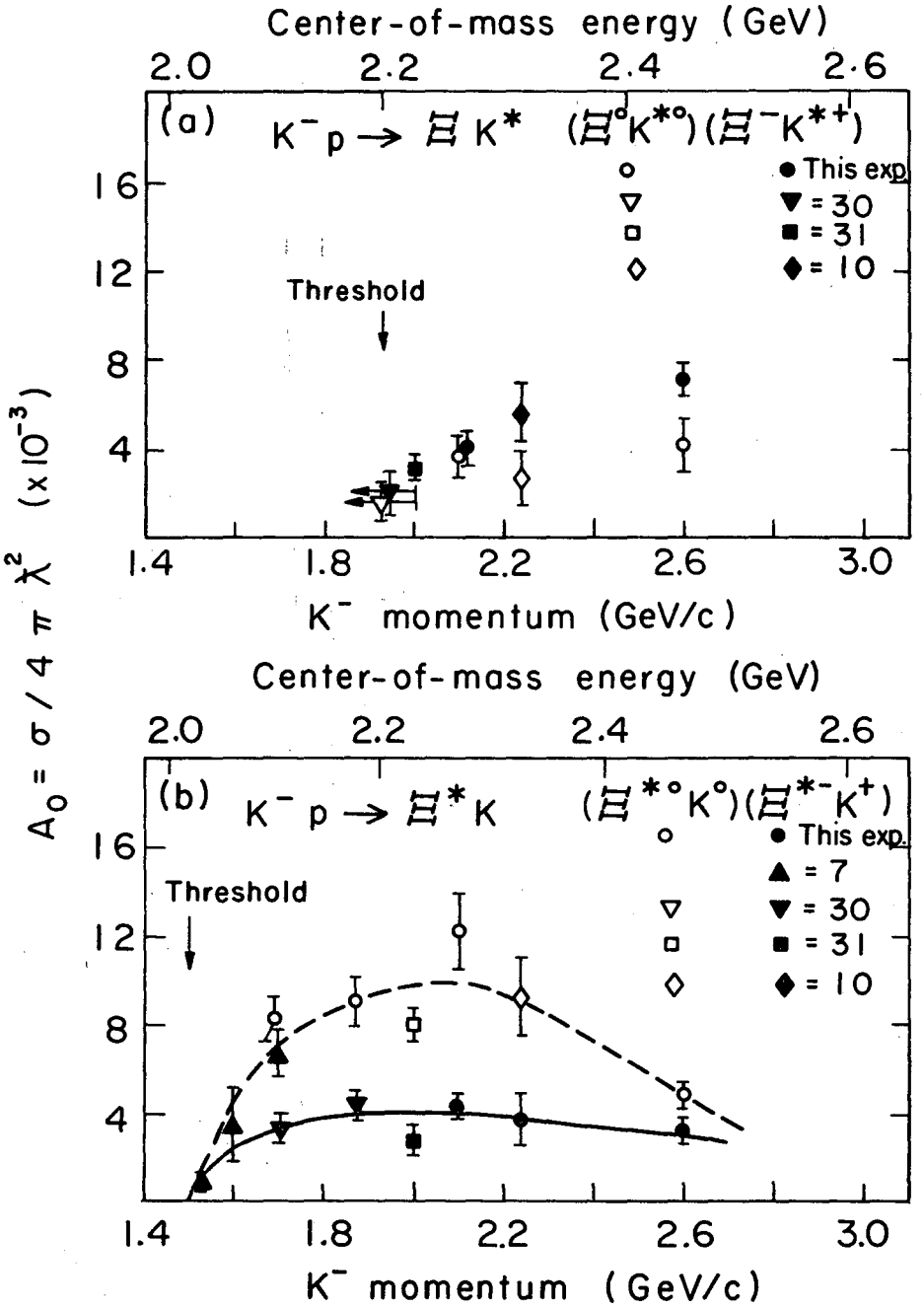

XBL687-3245

Fig. 9

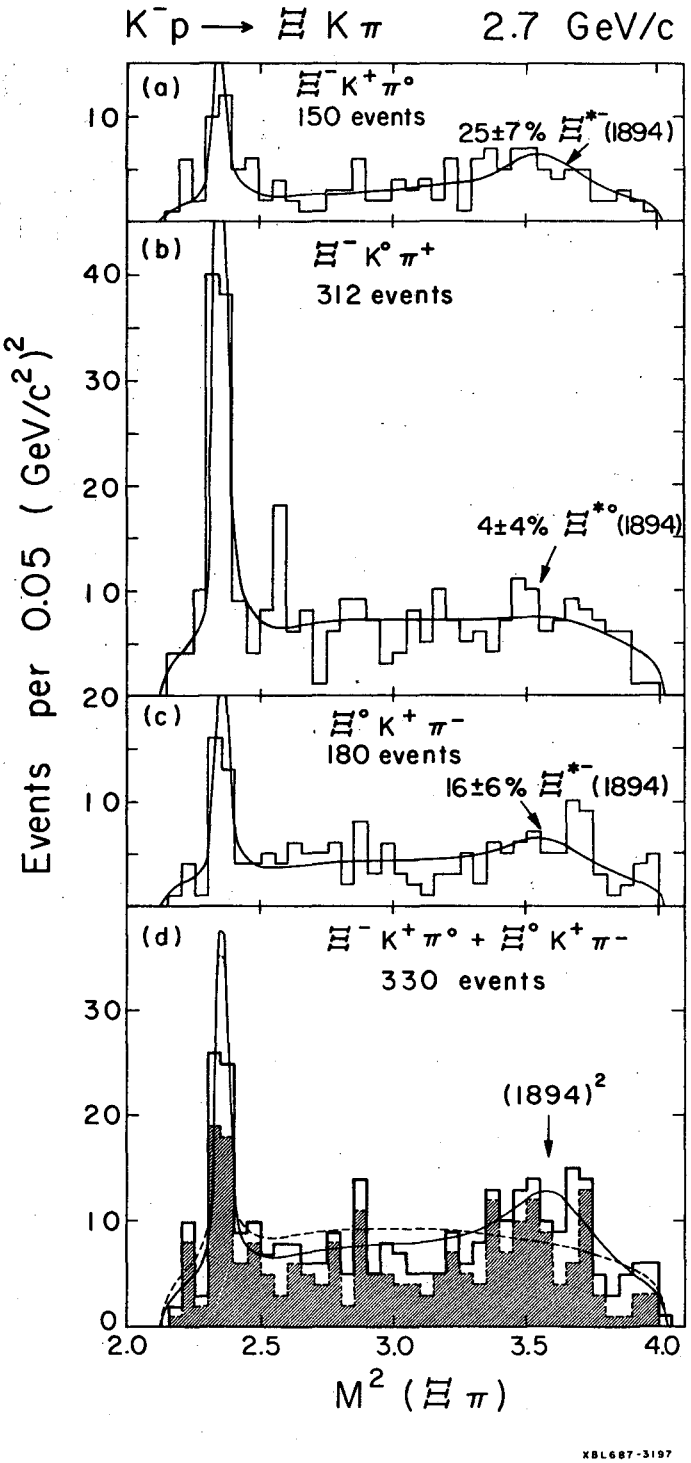
K⁻p → Ξ K π 2.7 GeV/c
(a) Ξ⁻ K⁺ π°
150 events
25±7% Ξ*⁻(1894)
(b) Ξ⁻ K° π⁺
312 events
4±4% Ξ*°(1894)
(c) Ξ° K⁺ π⁻
180 events
16±6% Ξ*⁻(1894)
(d) Ξ⁻ K⁺ π° + Ξ° K⁺ π⁻
330 events
(1894)²
Events per 0.05 (GeV/c²)²
M² (Ξ π)
XBL687-3197

Fig. 10

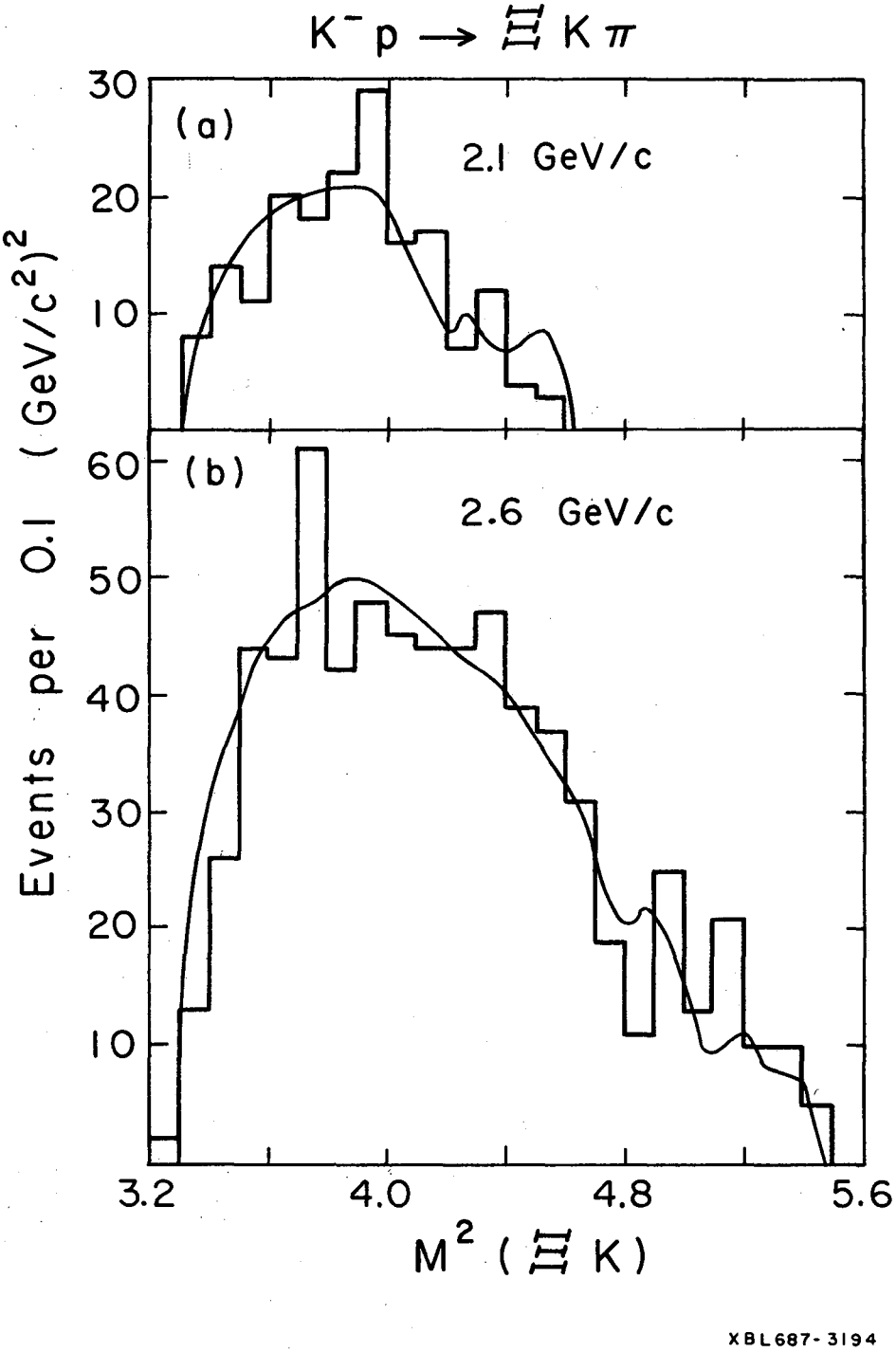
K⁻p → Ξ K π
(a)
2.1 GeV/c
(b)
2.6 GeV/c
Events per 0.1 (GeV/c²)²
M² (Ξ K)
3.2
4.0
4.8
5.6
10
20
30
40
50
60
XBL687-3194

Fig. 11

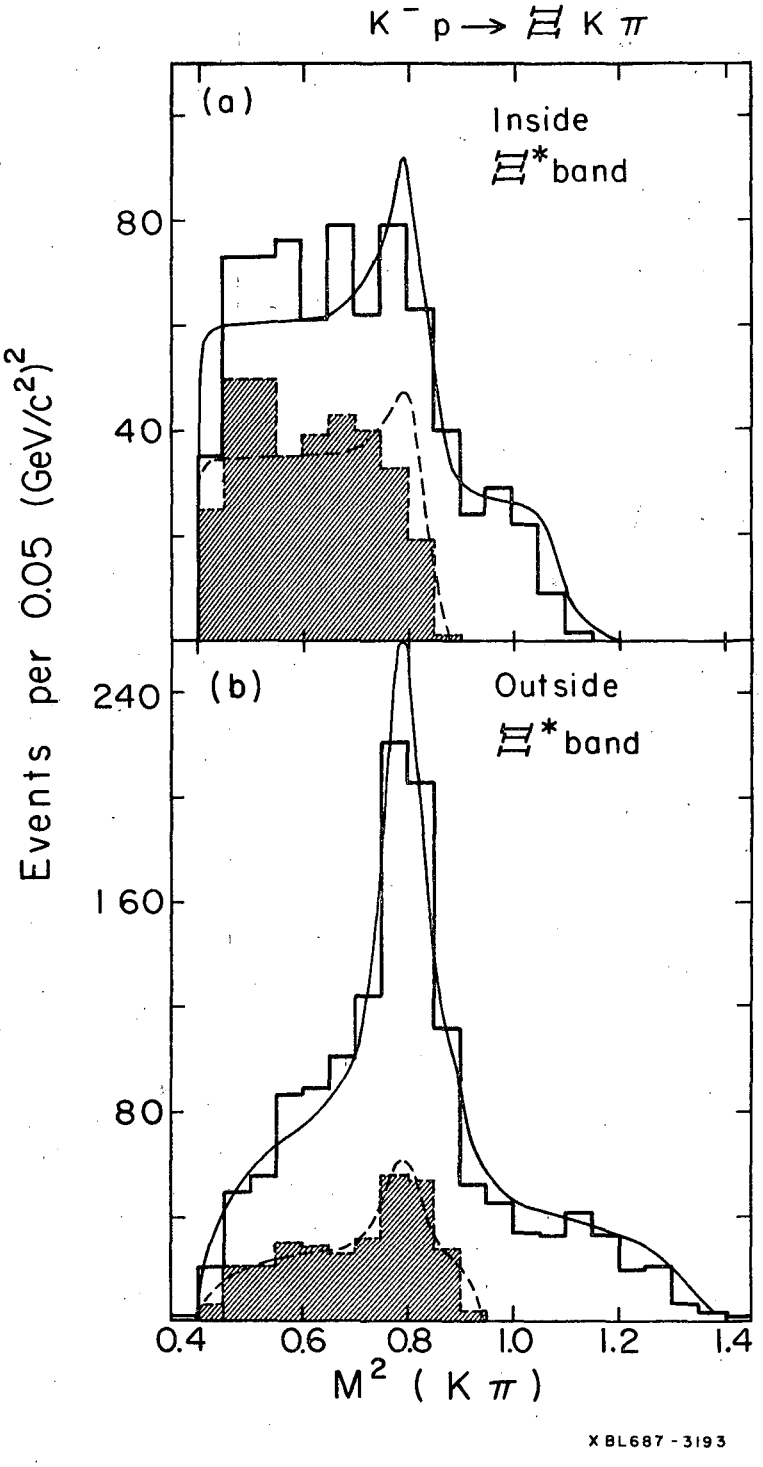
K⁻ p → Ξ K π
(a)
Inside
Ξ* band
80
40
(b)
Outside
Ξ* band
240
160
80
Events per 0.05 (GeV/c²)²
0.4
0.6
0.8
1.0
1.2
1.4
M² (K π)
XBL687-3193

Fig. 12

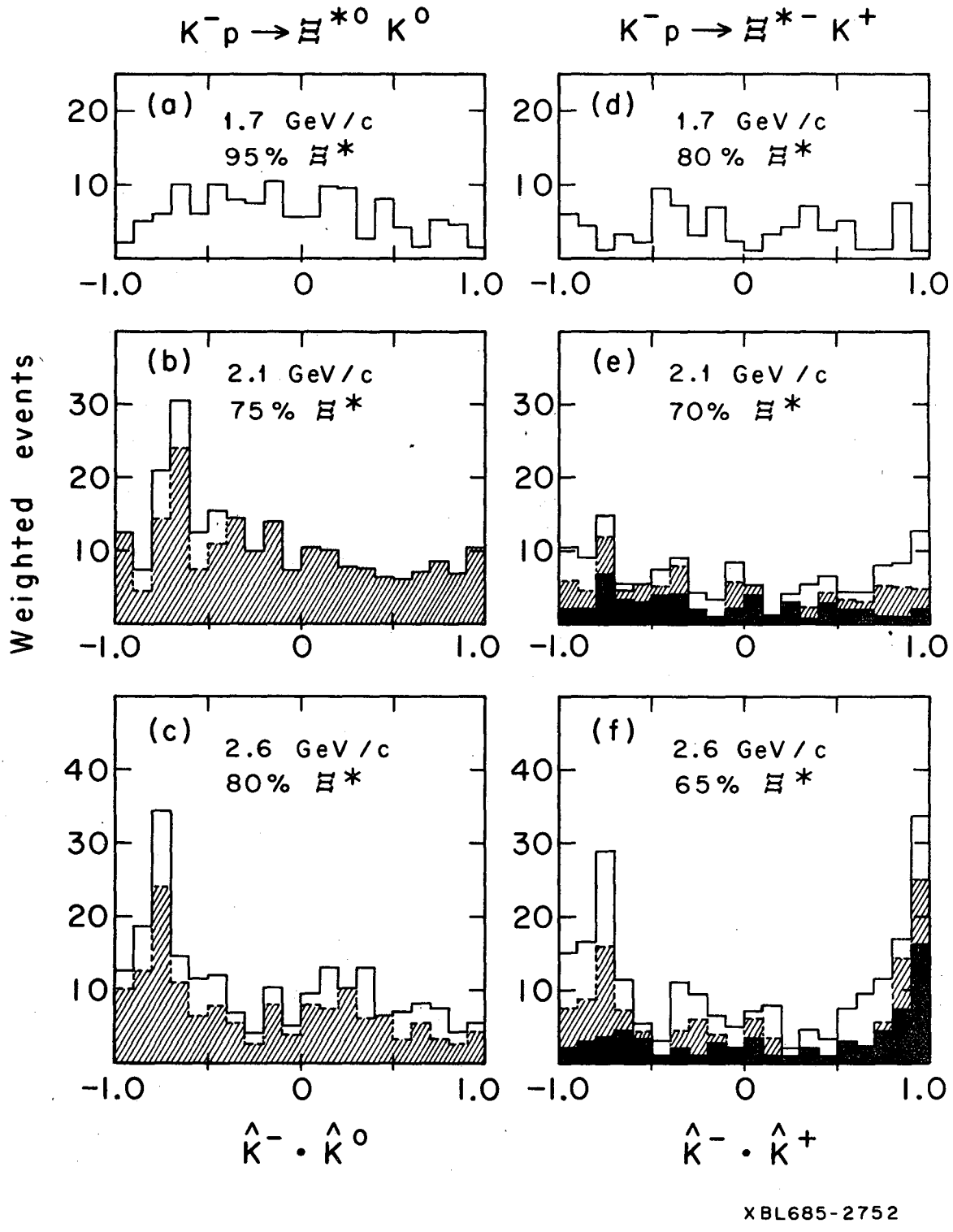
$K^- p \to \Xi^{*0} K^0$
$K^- p \to \Xi^{*-} K^+$
(a) 1.7 GeV/c 95% Ξ*
(b) 2.1 GeV/c 75% Ξ*
(c) 2.6 GeV/c 80% Ξ*
(d) 1.7 GeV/c 80% Ξ*
(e) 2.1 GeV/c 70% Ξ*
(f) 2.6 GeV/c 65% Ξ*
Weighted events
$\hat{K}^- \cdot \hat{K}^0$
$\hat{K}^- \cdot \hat{K}^+$
XBL685-2752

Fig. 13

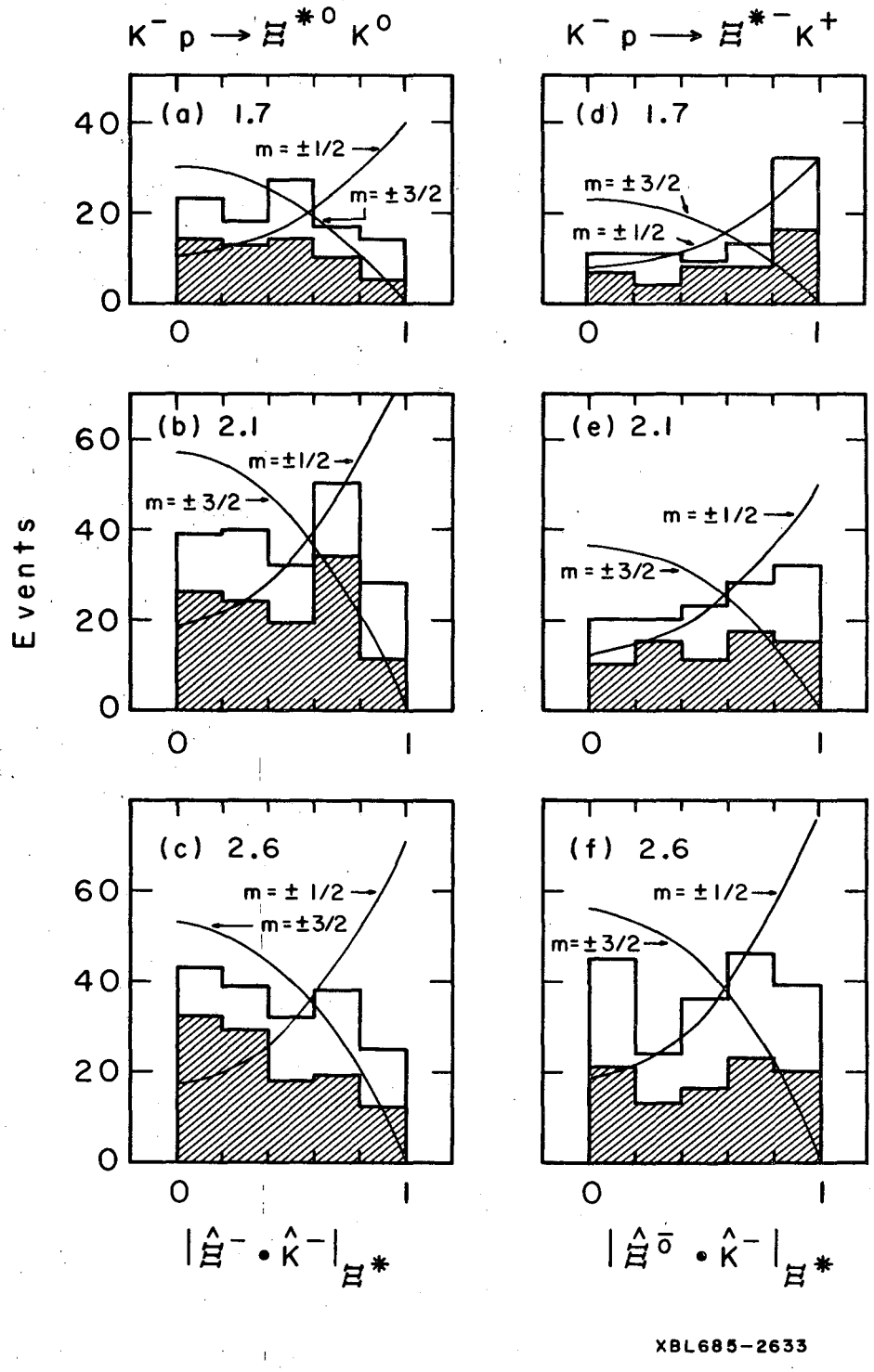
K⁻ p → Ξ*⁰ K⁰
K⁻ p → Ξ*⁻ K⁺
(a) 1.7
(b) 2.1
(c) 2.6
(d) 1.7
(e) 2.1
(f) 2.6
m = ±1/2
m = ±3/2
Events
|Ξ̂⁻ • K̂⁻|Ξ*
|Ξ̂⁰̄ • K̂⁻|Ξ*
XBL685-2633

Fig. 14

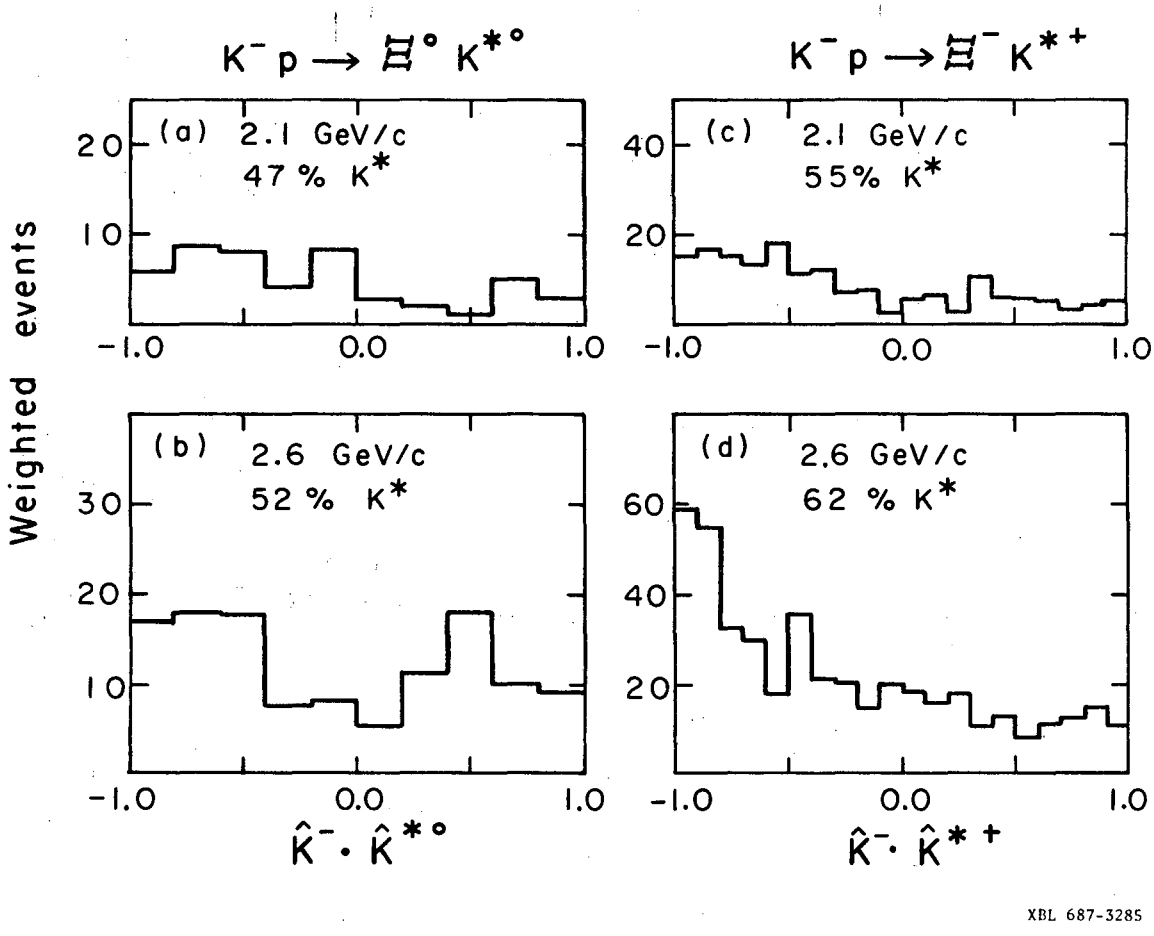
$K^- p \rightarrow \Xi^\circ K^{*\circ}$
$K^- p \rightarrow \Xi^- K^{*+}$
(a) 2.1 GeV/c
47 % K*
(c) 2.1 GeV/c
55% K*
(b) 2.6 GeV/c
52 % K*
(d) 2.6 GeV/c
62 % K*
Weighted events
$\hat{K}^- \cdot \hat{K}^{*\circ}$
$\hat{K}^- \cdot \hat{K}^{*+}$
XBL 687-3285

Fig. 15

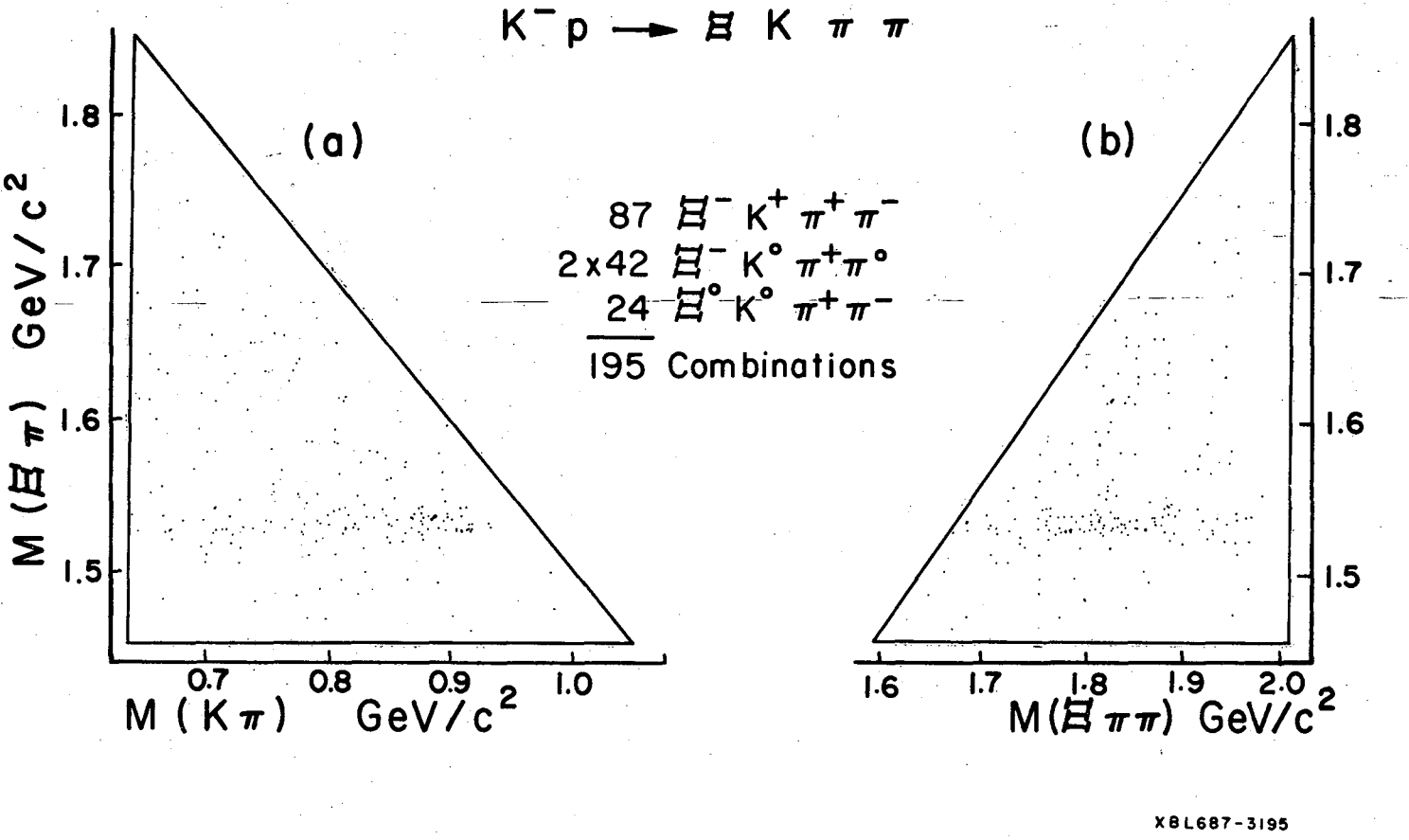
$K^- p \longrightarrow \Xi K \pi \pi$
(a)
(b)
87 $\Xi^- K^+ \pi^+ \pi^-$
2x42 $\Xi^- K^\circ \pi^+ \pi^\circ$
24 $\Xi^\circ K^\circ \pi^+ \pi^-$
195 Combinations
$M(\Xi\pi)$ GeV/c^2
1.8
1.7
1.6
1.5
0.7
0.8
0.9
1.0
$M(K\pi)$ GeV/c^2
1.6
1.7
1.8
1.9
2.0
$M(\Xi\pi\pi)$ GeV/c^2
XBL687-3195

Fig. 16

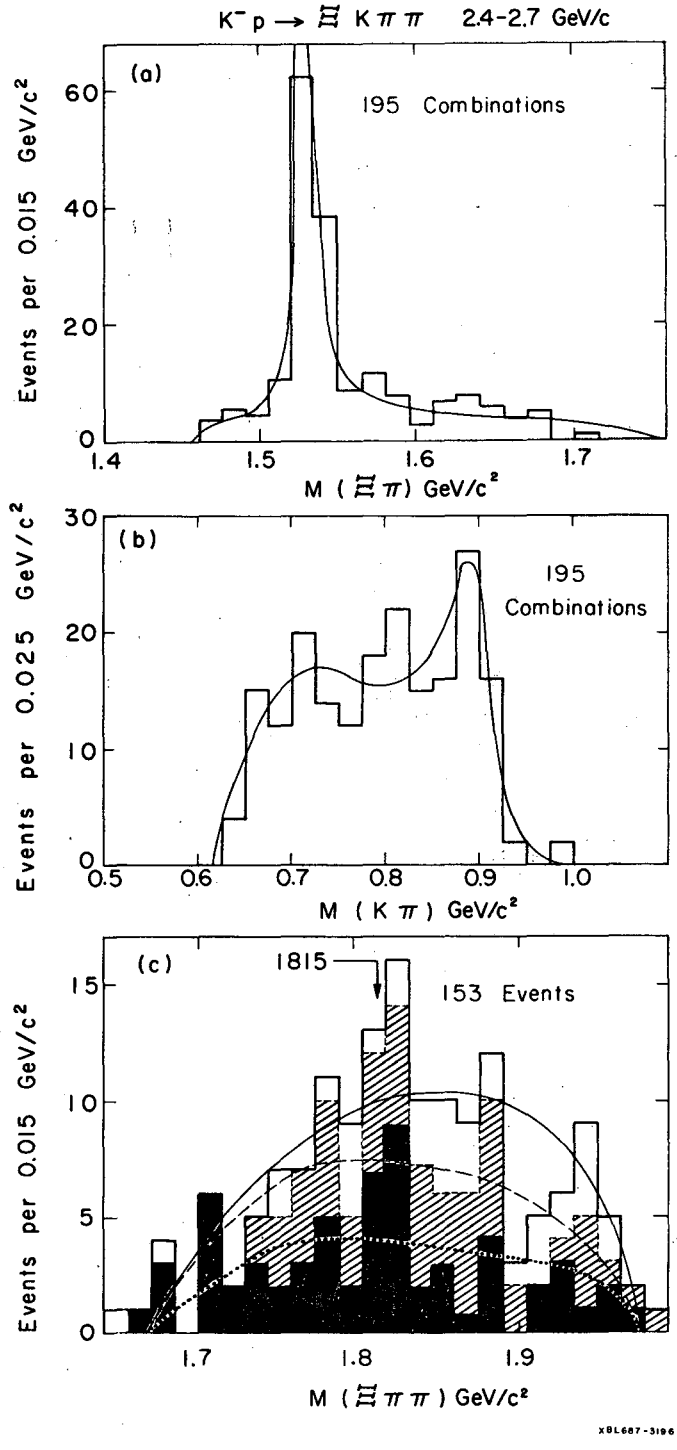
$K^- p \rightarrow \Xi K\pi\pi$ 2.4-2.7 GeV/c
(a)
195 Combinations
Events per 0.015 GeV/c²
M (Ξπ) GeV/c²
(b)
195
Combinations
Events per 0.025 GeV/c²
M (Kπ) GeV/c²
(c)
1815
153 Events
Events per 0.015 GeV/c²
M (Ξππ) GeV/c²
XBL687-3196

Fig. 17

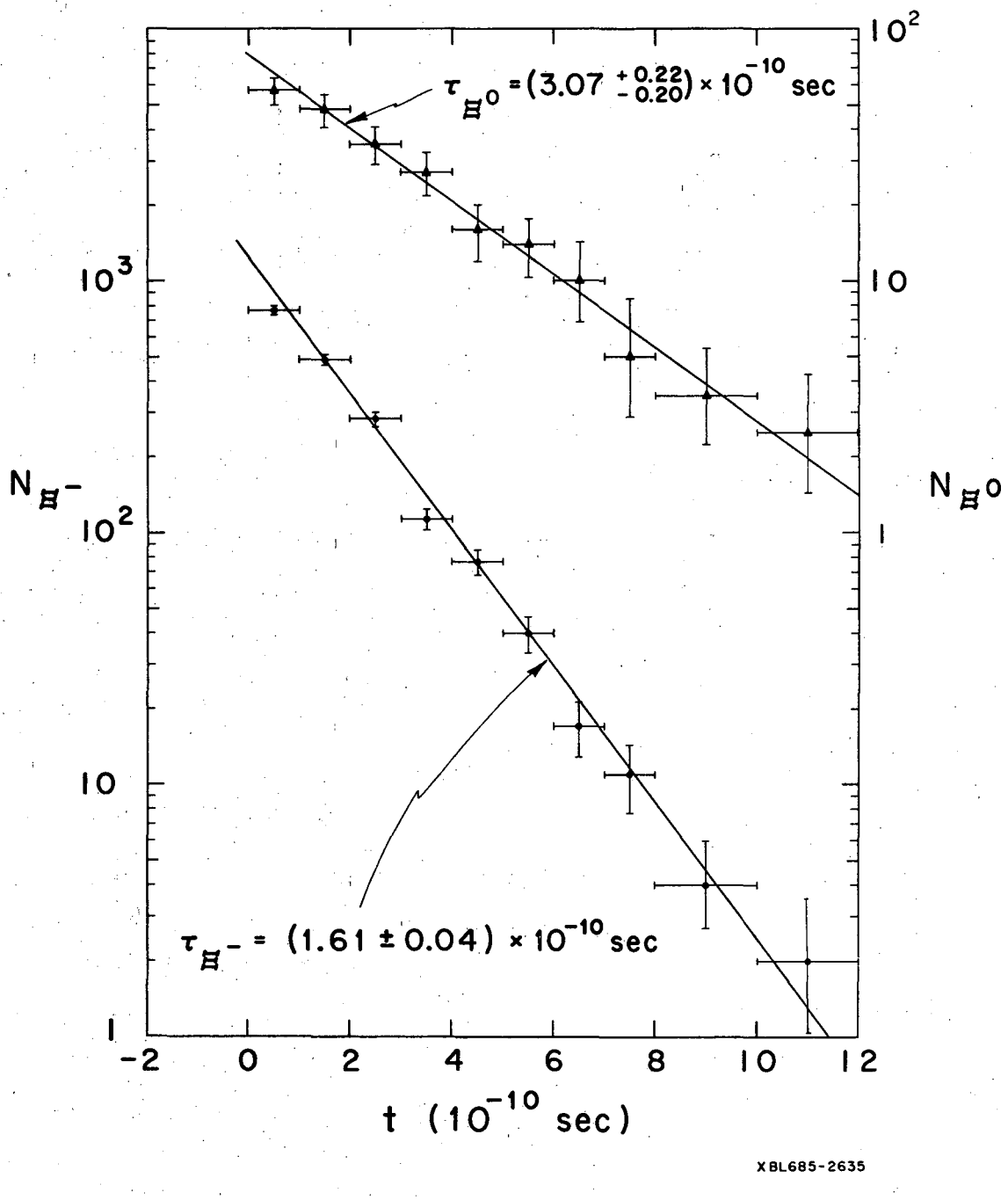
$\tau_{\Xi^0} = (3.07 \pm^{0.22}_{0.20}) \times 10^{-10}$ sec
$\tau_{\Xi^-} = (1.61 \pm 0.04) \times 10^{-10}$ sec
N_{Ξ^-}
N_{Ξ^0}
10^3
10^2
10
1
10^2
10
1
-2
0
2
4
6
8
10
12
t (10^{-10} sec)
XBL685-2635

Fig. 18

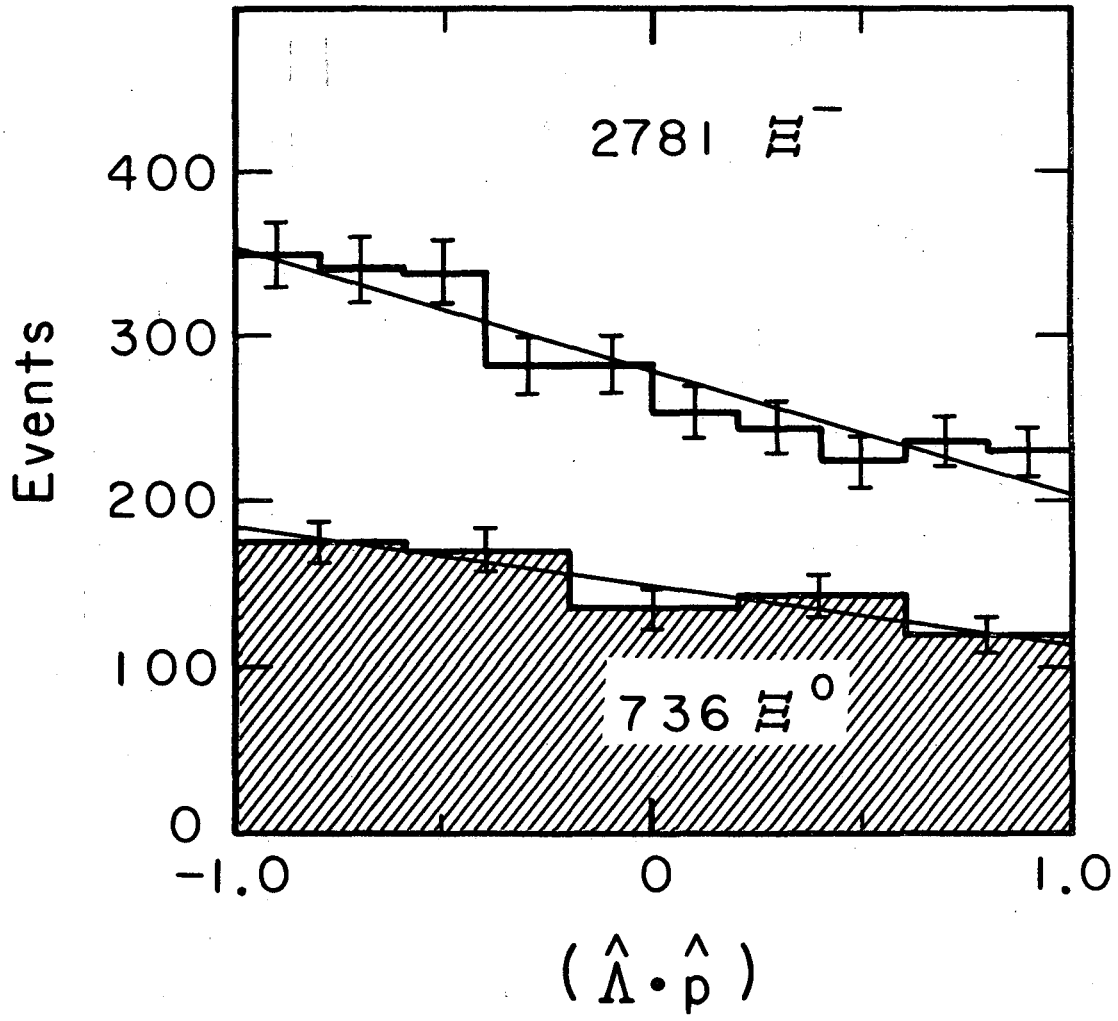

Fig. 19

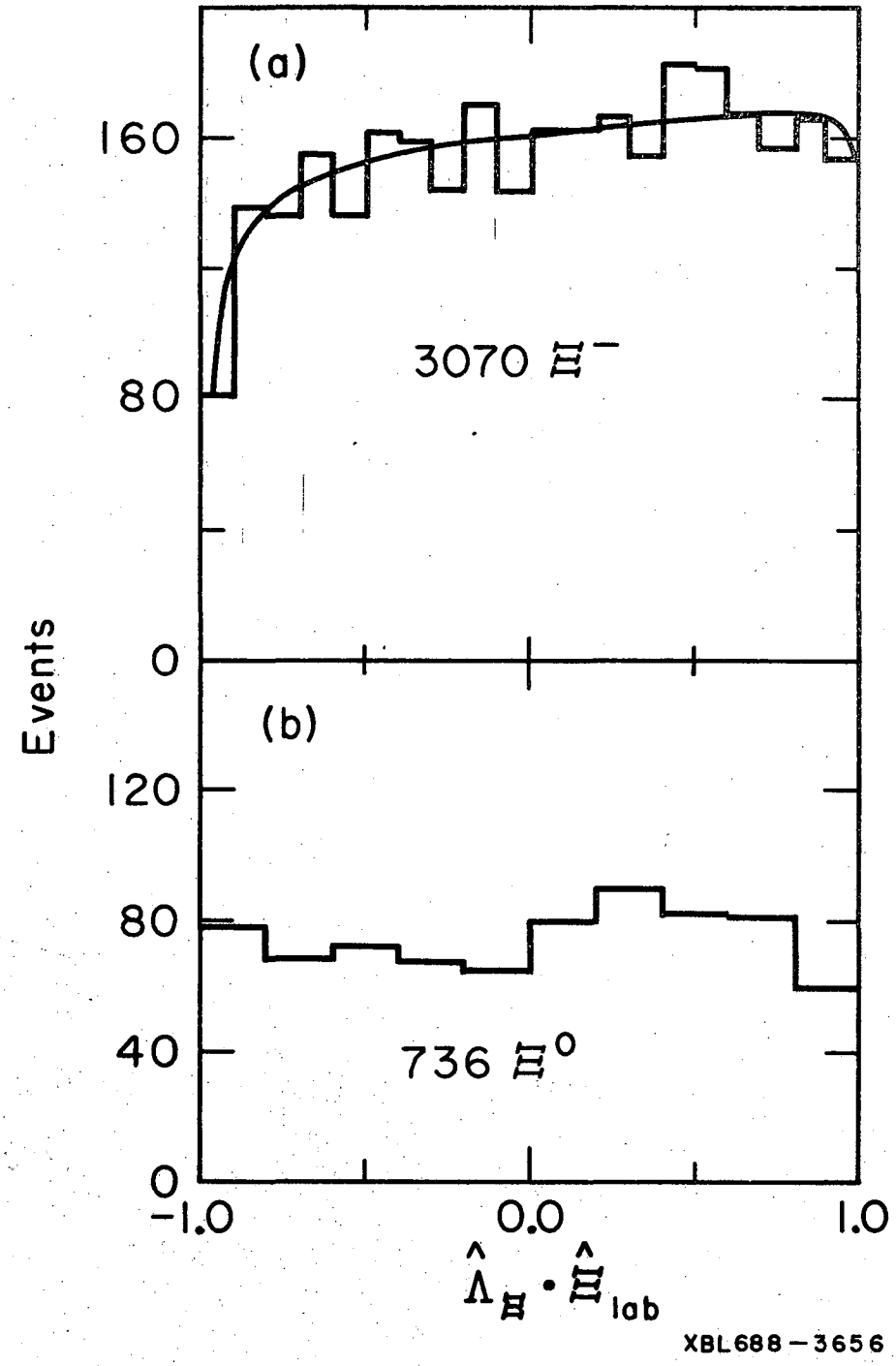
(a)
160
80
0
3070 Ξ⁻
Events
(b)
120
80
40
0
736 Ξ⁰
-1.0
0.0
1.0
$\hat{\Lambda}_{\Xi} \cdot \hat{\Xi}_{lab}$
XBL688-3656

Fig. 20

TECHNICAL INFORMATION DIVISION
LAWRENCE RADIATION LABORATORY
UNIVERSITY OF CALIFORNIA
BERKELEY, CALIFORNIA 94720